Supporting Information

Pillar[5]arene-Derived *endo*-Functionalized Molecular Tube for Mimicking Protein-Ligand Interactions

Zhuo Wang[1,2,3],Tao Chen[1,2], Hua Liu[3], Yahu A. Liu[4], Xiao-Li Zhao[5], Wei-Bo Hu*[,1], Hui Yang*[,1,3] and Ke Wen*[,1,3]

[1]Shanghai Advanced Research Institute, Chinese Academy of Sciences, Shanghai 201210, China
[2]University of Chinese Academy of Sciences, Beijing 100049, China
[3]School of Physical Science and Technology, ShanghaiTech University, Shanghai 201210, China
[4]Medicinal Chemistry, ChemBridge Research Laboratories, San Diego, CA 92127, USA
[5]Shanghai Key Laboratory of Green Chemistry and Chemical Processes, Department of Chemistry, East China Normal University, Shanghai 200062, China.

*Corresponding Authors

Wei-Bo Hu, PhD
E-Mail: huwb@sari.ac.cn

Hui Yang, PhD
E-Mail: yangh@sari.ac.cn

Ke Wen, PhD
E-Mail: wenk@sari.ac.cn

Table of Contents

Job Plots Deriving from a 1:1 Complexation of *endo*-[P4-BPO(1-OH)] and Guests

Nonlinear Curve Fitting of NMR Titrations

2D NOSEY Spectra

Single-Crystal X-ray Crystallography

Calculation of Mulliken charges

Methods and Synthetic Procedures

General

Unless otherwise noted, all commercial reagents and solvents were used without purification. Separation by flash column chromatography was performed on silica gel (200-300 mesh). 1H and 13C NMR spectra were recorded on Bruker AVANCE NEO 400 NMR spectrometer in CDCl3 at 298K. Atmospheric pressure chemical ionization (APCI) mass spectra were recorded on a Thermo Scientific Q Exactive Focus (UltiMate 3000 HPLC) mass spectrometer. Single crystal X-ray diffraction data were collected at 100 K on a Rigaku-Oxford Diffraction SuperNova dual source diffractometer (Cu at Zero equipped with an AtlasS2 CCD using Cu Kα radiation). The data were collected and processed using CrysAlisPro. The structures were solved by direct methods using Olex2 software, and the non-hydrogen atoms were refined anisotropically with SHELXL-2018 using a full-matrix least-squares procedure based on F^2. The weighted R factor, wR and goodness-of-fit S values were obtained based on F^2.The hydrogen atom positions were fixed geometrically at the calculated distances and allowed to ride on their parent atoms. Crystallographic data for the structures disclosed in this paper have been deposited at the Cambridge Crystallographic Data Center (CCDC).

Synthesis of [P4-(OH)BPO]

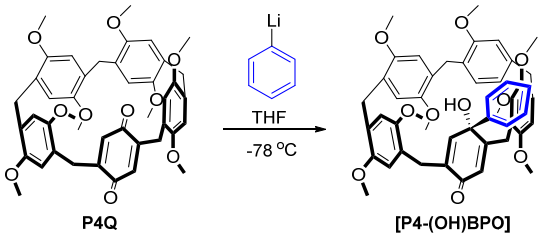

To a solution of **P4Q**[S1] (1.44 g, 2 mmol) in THF (200 mL) was added a solution of phenyllithium in ether (2.0 mL, 1.0 M) at -78 ℃ under nitrogen. The resulting mixture which was warmed to 0 ℃, and stirred at 0 ℃ for 2 h, and poured into saturated NH_4Cl solution (300 mL). The aqueous phase was extracted with EtOAc (3 × 100 mL). The combined organic extracts were concentarted under redcued pressure to result in a residue which was subjected to column chromatography to afford **[P4-(OH)BPO]** as white solid (1.44 g, 90%). ^{1}H NMR (400 MHz, CD_2Cl_2, 298K) δ 7.57 (s, 1H), 7.46 (t, 2H), 7.39 (s, 1H), 7.31 (d, 2H), 6.99 (d, 2H), 6.98 (s, 1H), 6.93 (s, 2H), 6.91 (t, 3H), 6.74 (s, 1H), 6.65 (s, 1H), 3.85 (s, 3H), 3.83 (s, 3H), 3.81 (t, 14H), 3.77 (s, 3H), 3.74 (s, 3H), 3.73 (s, 3H), 3.68 (s, 2H), 3.55 (s, 3H); ^{13}C NMR (400 MHz, CD_2Cl_2, 298K) δ 152.1, 151.9, 151.0, 150.8, 150.7, 148.9, 148.6, 148.1, 144.7, 139.4, 129.7, 129.2, 128.9, 128.8, 128.4, 128.3, 128.0, 127.9, 127.3, 127.0, 125.0, 56.9, 56.7, 56.1, 55.9, 31.3, 30.1, 29.6, 29.3, 25.6. ACPI-MS (ESI): calcd for $C_{49}H_{50}O_{10}$ [M+NH_4^+] m/z 798.3404, found 796.4582.

NMR experiments

All ^{1}H NMR spectra were recorded at a Bruker Avance III HD 400 MHz spectrometer. ^{1}H NMR experiments were performed on all of the host–guest pairs at a 1:1 ratio, and the peak shifts of the complexed host and guest relative to the free species were used to access complexation. Job plots [S2] showing the 1:1 stoichiometry of the complex between **[P4-(OH)BPO]** and **G** (**G** = **1**–**42**) in CDCl3 were obtained by plotting the chemical shift (Δδ) of the guest's proton in ^{1}H NMR spectra against the mole fraction of complex ([host] + [guest] = 20.0 mM). In the determination of binding constants of complexes **G⊂[P4-(OH)BPO]** (**G** = **1**–**41**), ^{1}H NMR titrations were performed in $CDCl_3$ with the host concentration of 10.0 mM and varying concentrations of the guest (0, 2.0, 6.0, 10.0, 20.0, 40.0, 80.0, 120.0, 160.0, 320.0, and 640.0 mM)[S3]. The nonlinear curve fitting was calculated by the following equation:

$$\Delta\delta = (\Delta\delta_\infty/[\text{host}]_0)\,(0.5[\text{guest}]_0 + 0.5([\text{host}]_0+1/Ka)-(0.5$$
$$([\text{guest}]_0^2+(2[\text{guest}]_0(1/Ka-[\text{host}]_0)) + (1/Ka + [\text{host}]_0)^2)^{0.5}))$$

Where Δδ is the chemical shift change of H_α (Figure S1) of the host at the total concentration of the guest $[\text{guest}]_0$, $\Delta\delta_\infty$ is the chemical shift change of H_α when host is completely complexed, $[\text{host}]_0$ is the fixed initial concentration of the host, and $[\text{guest}]_0$ is the varying total concentration of the guest.

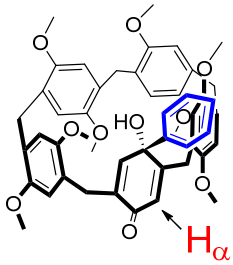

Figure S1. Structure of **[P4-(OH)BPO]**.

Calculations

Quantum chemical calculations were performed using Gaussian 16[S4]. Fragment library compounds and designed "drug molecules" were calculated by RMO62X 6-311G (d,p) level of theory, and vibrational frequency calculations have be carried out to verify that all optimized geometries are true minima. Molecular volume (*V*) and surface area (*S*) of guest moleculars were calculated using Marching Tetrahedron algorithm via Multiwfn program[S5]. Dipol momnet values were calculated using Gaussian 09 at the RB3LYP/6-31++G level of calcualtion.

Asphericity(Ω_a) was defined as $\Omega_a = \frac{(I_A-I_B)^2+(I_A-Ic)^2+(I_B-Ic)^2}{2(I_A+I_B+I_C)^2}$, I_A, I_B and I_C are the principal moments of inertia of a molecule[S6]. Mulliken charges were calculated by Gaussian 09 at PM6-D3 level. Molecular docking of **G⊂[P4-(OH)BPO]** (**G** = **39** or **40**) was performed with AutoDock Vina[S7].

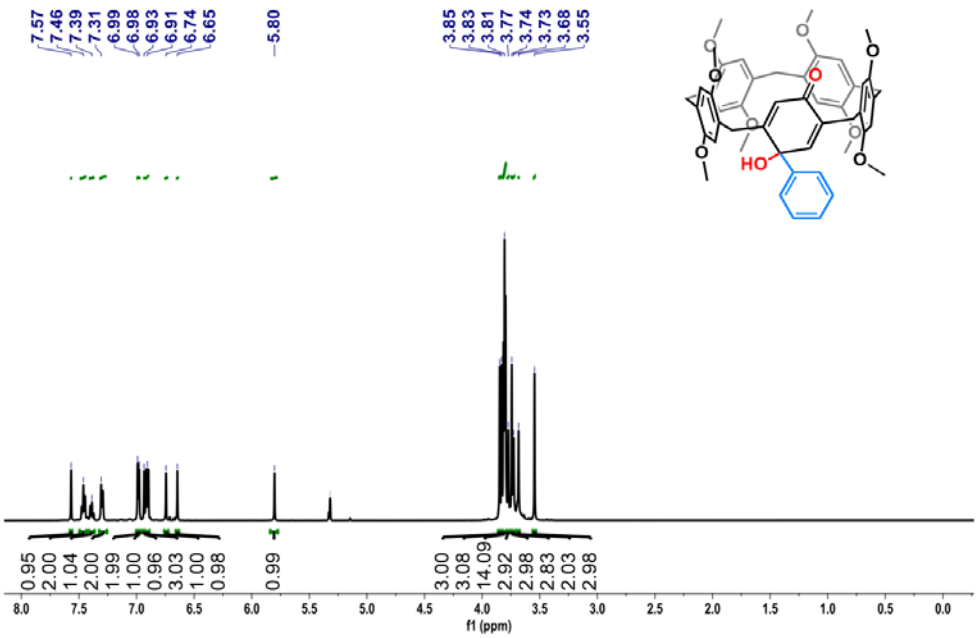

Figure S2. ^{1}H NMR of **[P4-(OH)BPO]** in CD_2Cl_2.

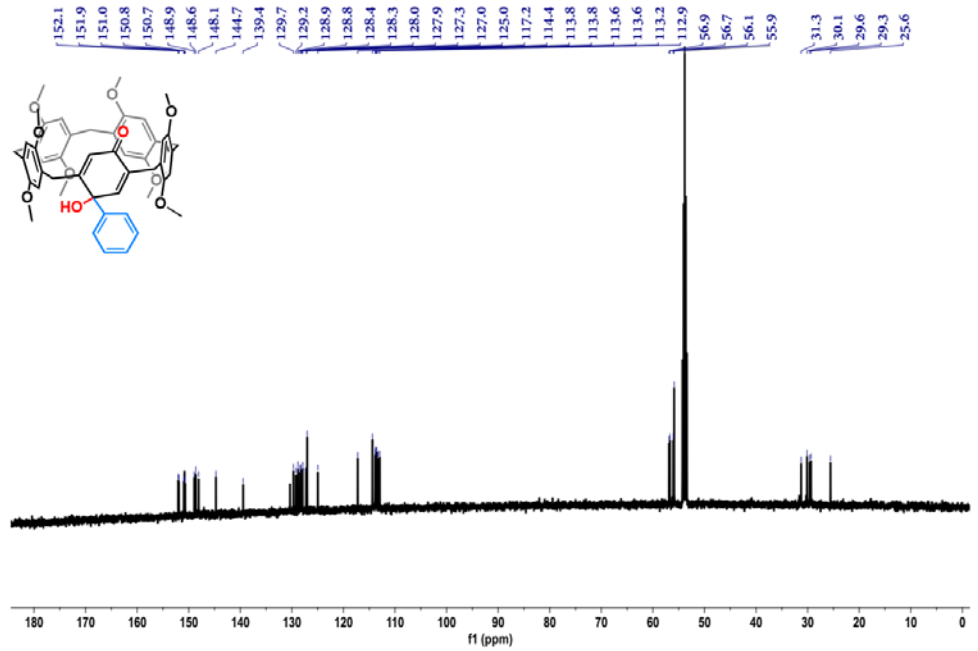

Figure S3. ^{13}C NMR of **[P4-(OH)BPO]** in CD_2Cl_2.

NMR Spectra of [P4-(OH)BPO]–Guest Complexation

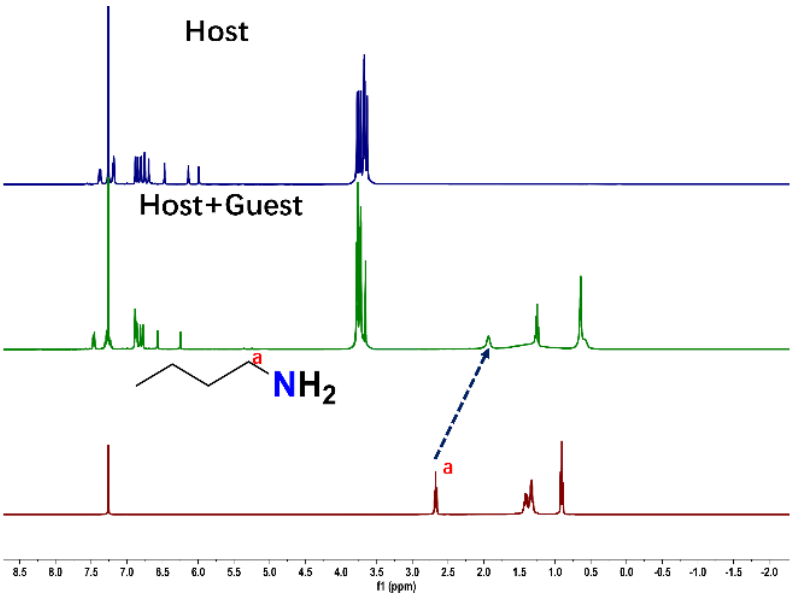

Figure S6. ^{1}H NMR spectra (400 MHz, $CDCl_3$, 298 K) of *n*-butylamine (**1**), **[P4-(OH)BPO]** (10.0 mM), and an equimolar mixture of **1** and **[P4-(OH)BPO]**.

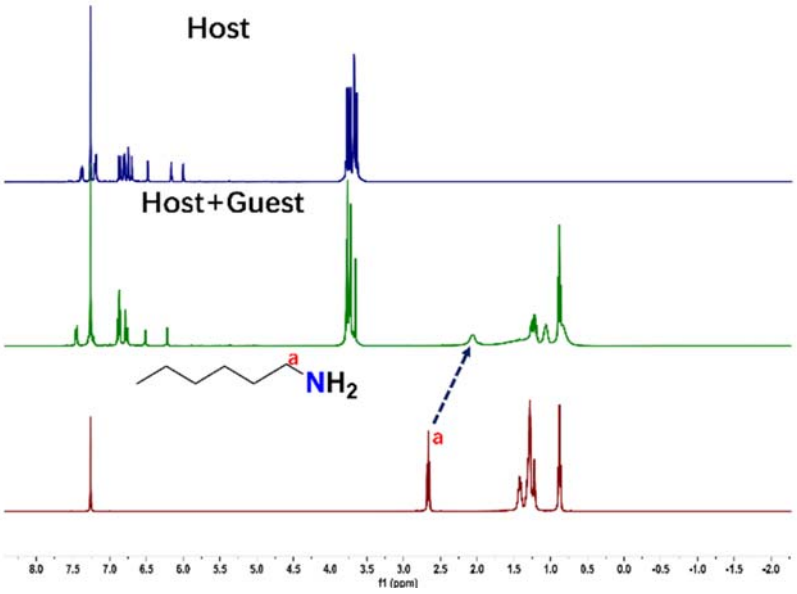

Figure S7. ^{1}H NMR spectra (400 MHz, $CDCl_3$, 298 K) of *n*-hexylamine (**2**), **[P4-(OH)BPO]** (10.0 mM), and an equimolar mixture of **2** and **[P4-(OH)BPO]**.

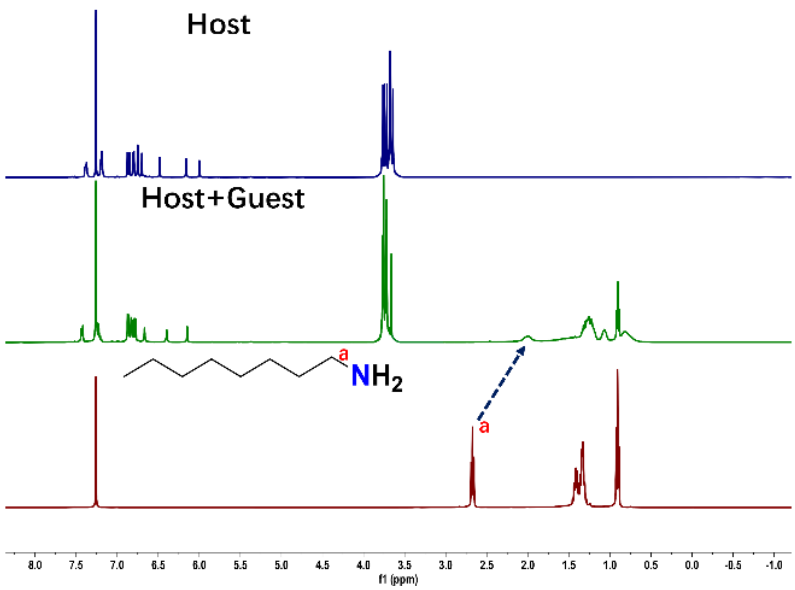

Figure S8. ^{1}H NMR spectra (400 MHz, $CDCl_3$, 298 K) of *n*-octylamine (**3**), **[P4-(OH)BPO]** (10.0 mM), and an equimolar mixture of **3** and **[P4-(OH)BPO]**.

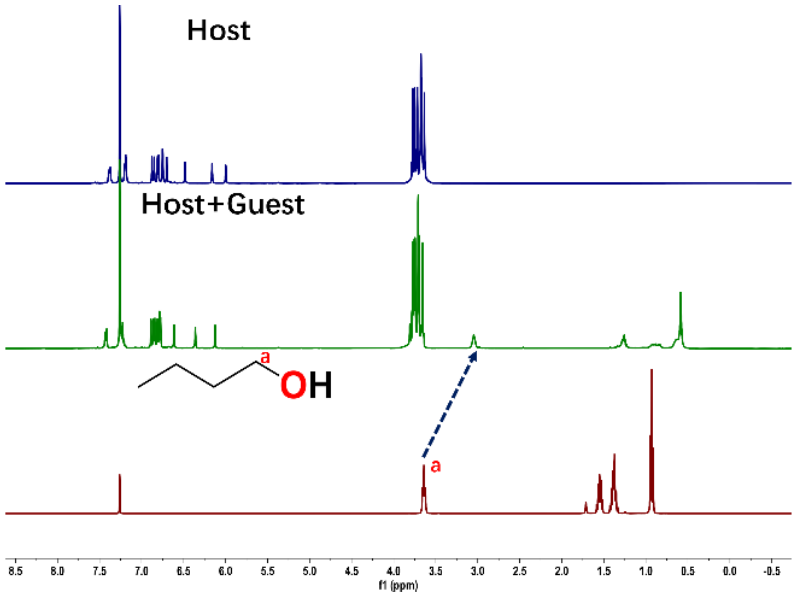

Figure S9. ^{1}H NMR spectra (400 MHz, $CDCl_3$, 298 K) of *n*-butanol (**4**), **[P4-(OH)BPO]** (10.0 mM), and an equimolar mixture of **4** and **[P4-(OH)BPO]**.

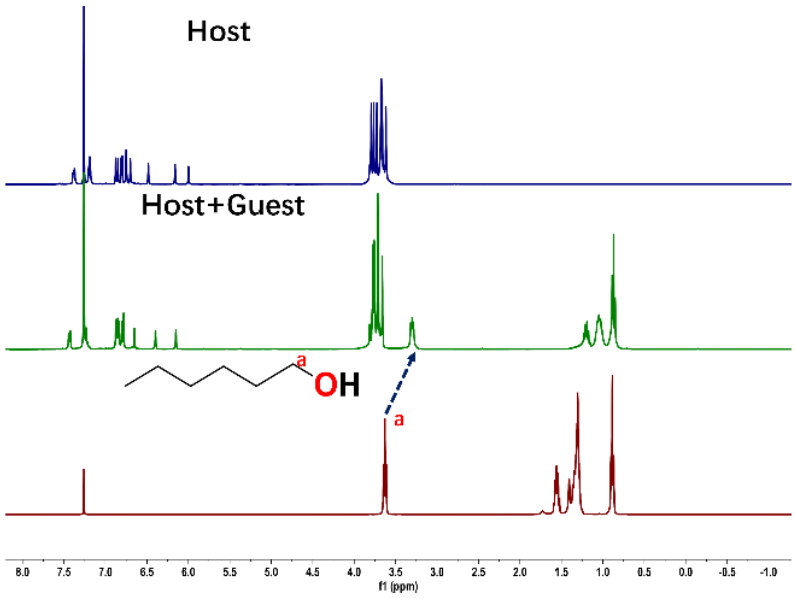

Figure 10. ^{1}H NMR spectra (400 MHz, $CDCl_3$, 298 K) of *n*-hexanol (**5**), **[P4-(OH)BPO]** (10.0 mM), and an equimolar mixture of **5** and **[P4-(OH)BPO]**.

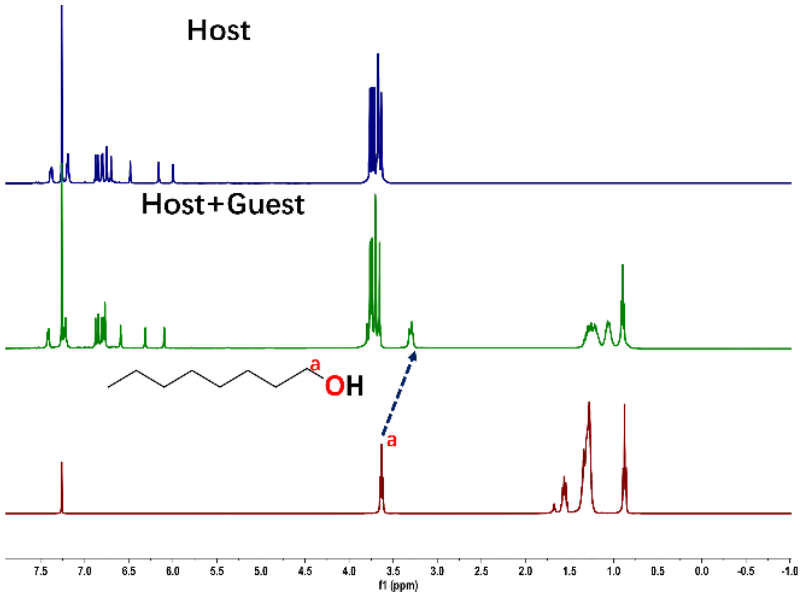

Figure 11. ^{1}H NMR spectra (400 MHz, $CDCl_3$, 298 K) of *n*-octanol (**6**), **[P4-(OH)BPO]** (10.0 mM), and an equimolar mixture of **6** and **[P4-(OH)BPO]**.

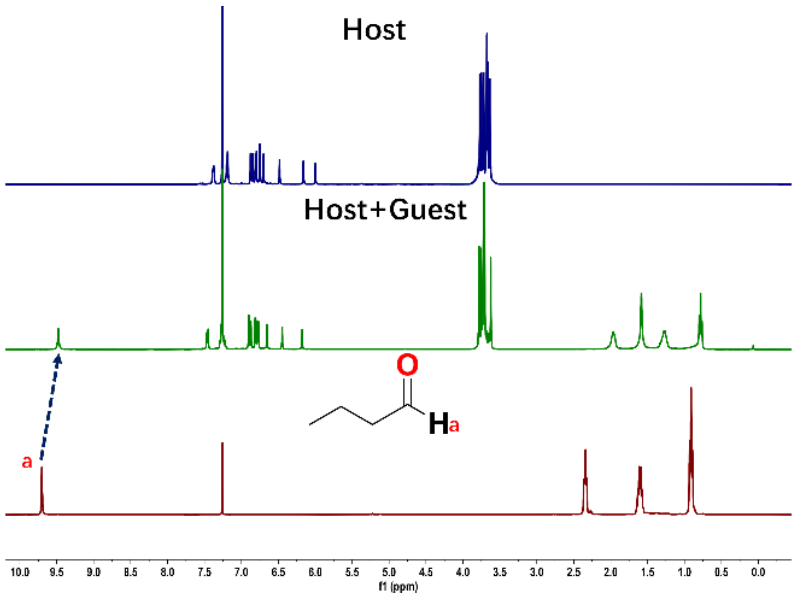

Figure S12. ^{1}H NMR spectra (400 MHz, $CDCl_3$, 298 K) of *n*-butyraldehyde (7), **[P4-(OH)BPO]** (10.0 mM), and an equimolar mixture of **7** and **[P4-(OH)BPO]**.

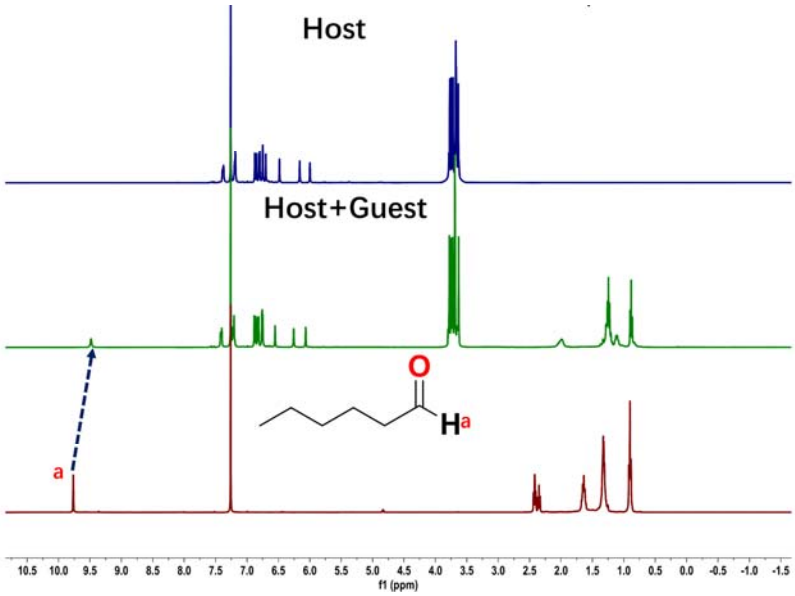

Figure S13. ^{1}H NMR spectra (400 MHz, $CDCl_3$, 298 K) of *n*-hexanaldehyde (**8**), **[P4-(OH)BPO]** (10.0 mM), and an equimolar mixture of **8** and **[P4-(OH)BPO]**.

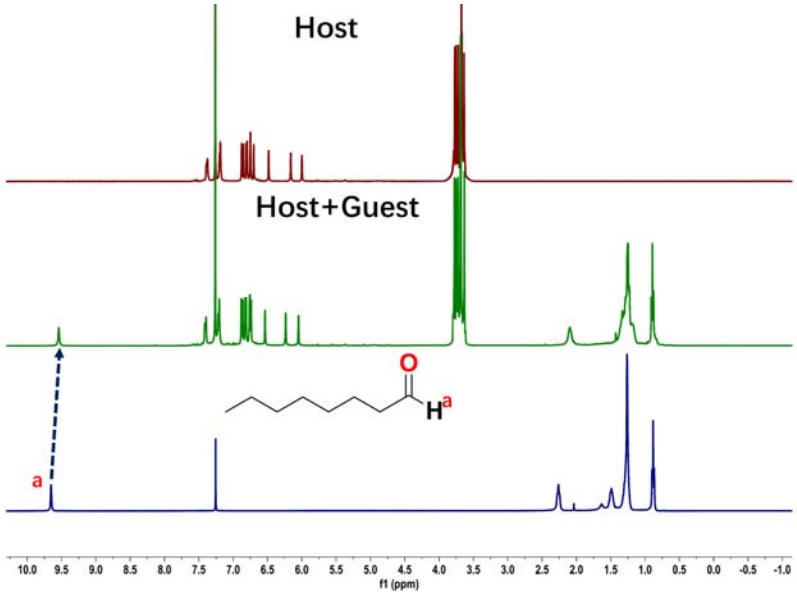

Figure S14. ^{1}H NMR spectra (400 MHz, $CDCl_3$, 298 K) of *n*-octanaldehyde (**9**), **[P4-(OH)BPO]** (10.0 mM), and an equimolar mixture of **9** and **[P4-(OH)BPO]**.

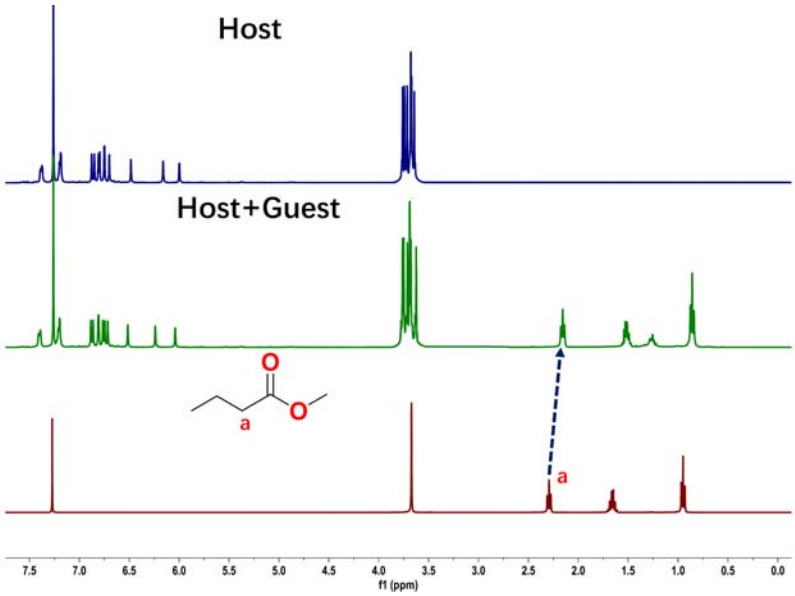

Figure S15. ^{1}H NMR spectra (400 MHz, $CDCl_3$, 298 K) of methyl butyrate (**10**), **[P4-(OH)BPO]** (10.0 mM), and an equimolar mixture of **10** and **[P4-(OH)BPO]**.

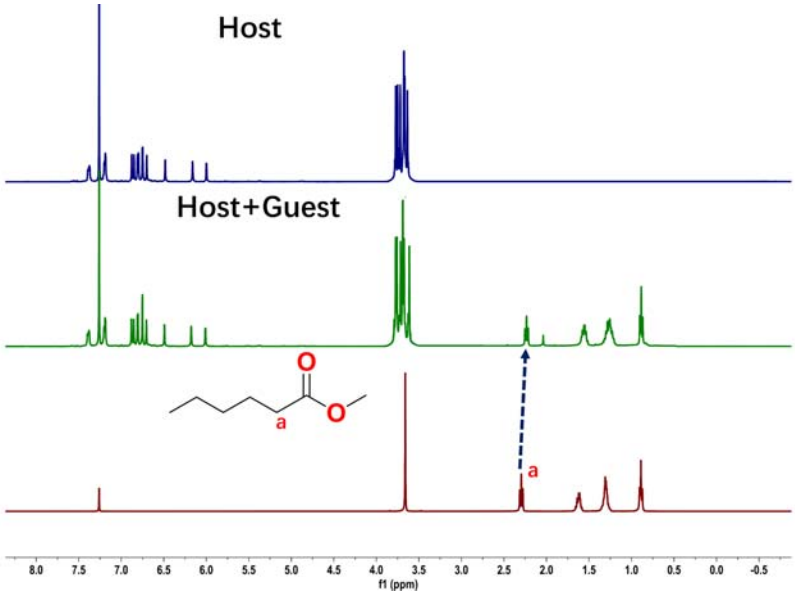

Figure S16. ^{1}H NMR spectra (400 MHz, $CDCl_3$, 298 K) of methyl hexanoate (**11**), **[P4-(OH)BPO]** (10.0 mM), and an equimolar mixture of **11** and **[P4-(OH)BPO]**.

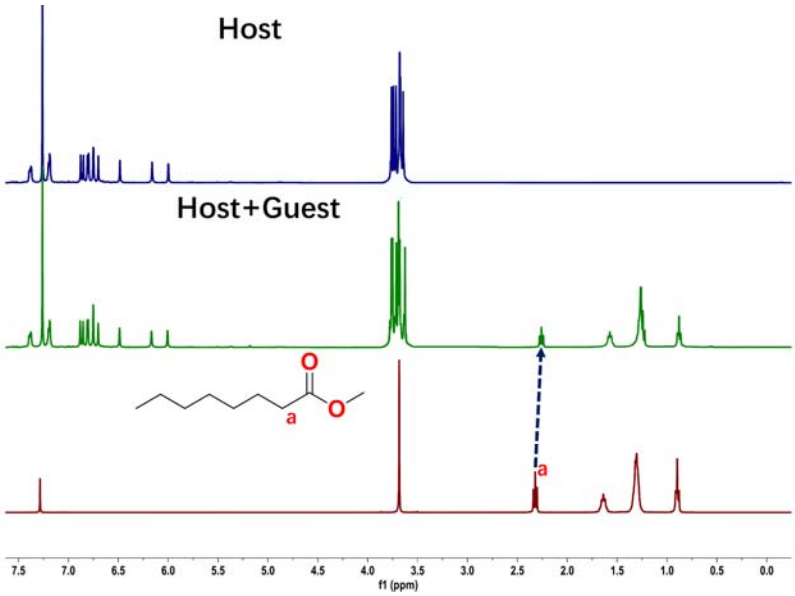

Figure S17. ^{1}H NMR spectra (400 MHz, $CDCl_3$, 298 K) of methyl octanoate (**12**), **[P4-(OH)BPO]** (10.0 mM), and an equimolar mixture of **12** and **[P4-(OH)BPO]**.

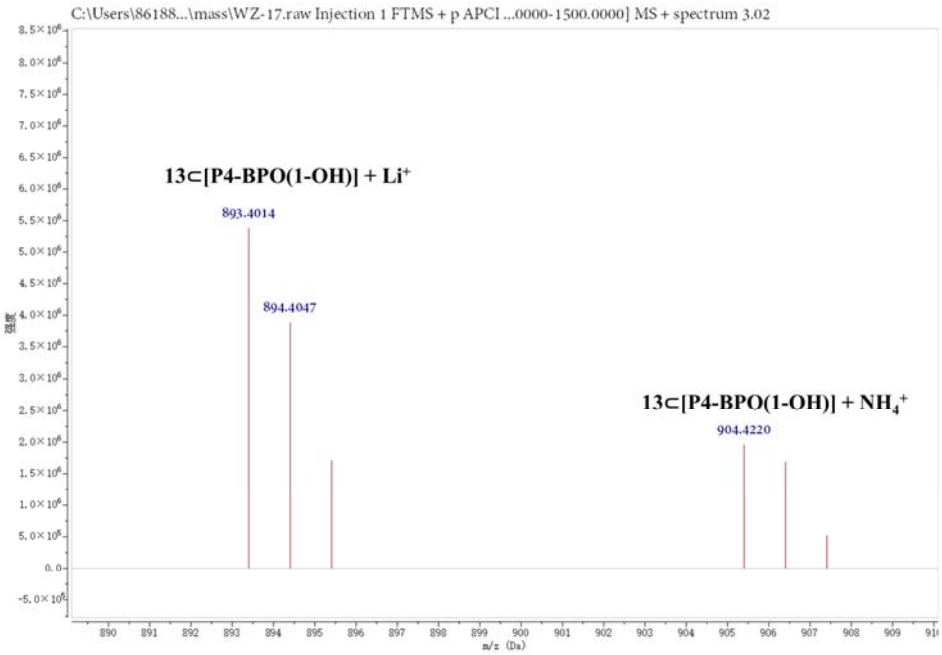

Figure S18. APCI-MS spectrum of **13⊂ [P4-(OH)BPO]**

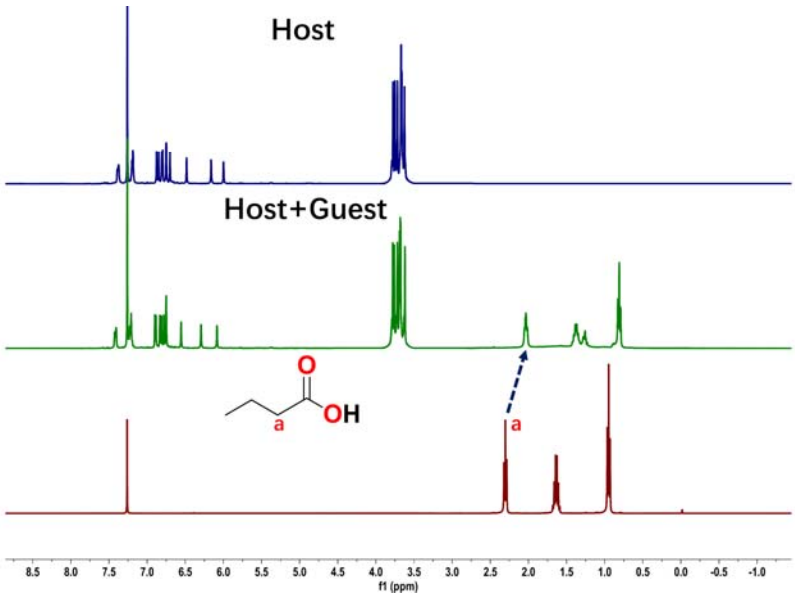

Figure S19. ^{1}H NMR spectra (400 MHz, $CDCl_3$, 298 K) of *n*-butanoic acid (**13**), **[P4-(OH)BPO]** (10.0 mM), and an equimolar mixture of **13** and **[P4-(OH)BPO]**.

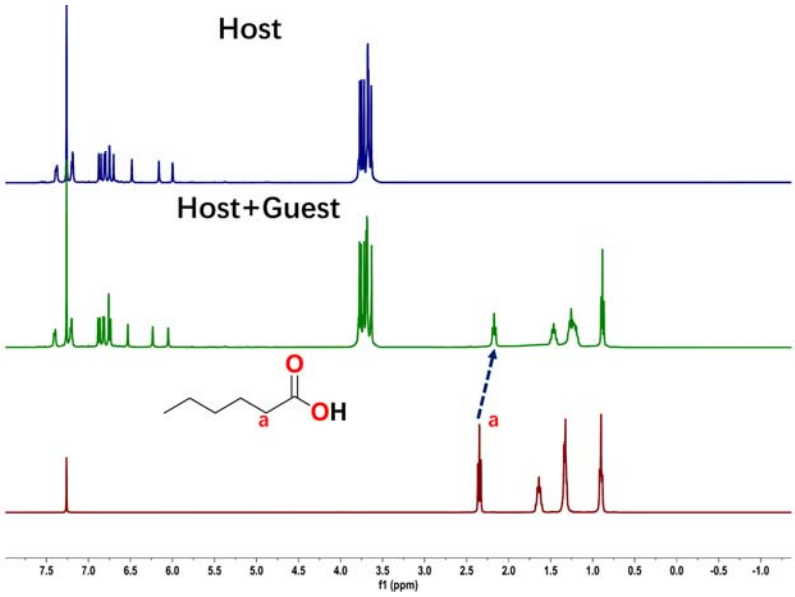

Figure S20. ^{1}H NMR spectra (400 MHz, $CDCl_3$, 298 K) of *n*-hexanoic acid (**14**), **[P4-(OH)BPO]** (10.0 mM), and an equimolar mixture of **14** and **[P4-(OH)BPO]**.

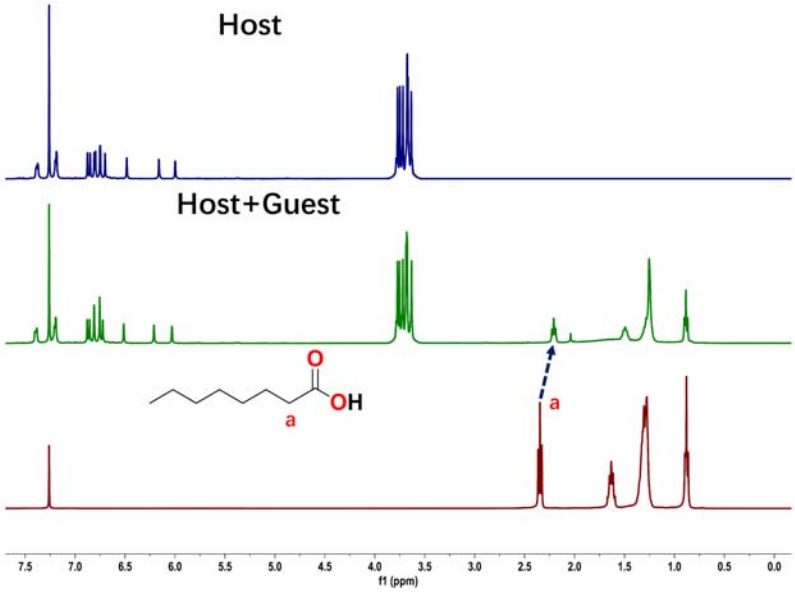

Figure S21. ^{1}H NMR spectra (400 MHz, $CDCl_3$, 298 K) of *n*-octanoic acid (**15**), **[P4-(OH)BPO]** (10.0 mM), and an equimolar mixture of **15** and **[P4-(OH)BPO]**.

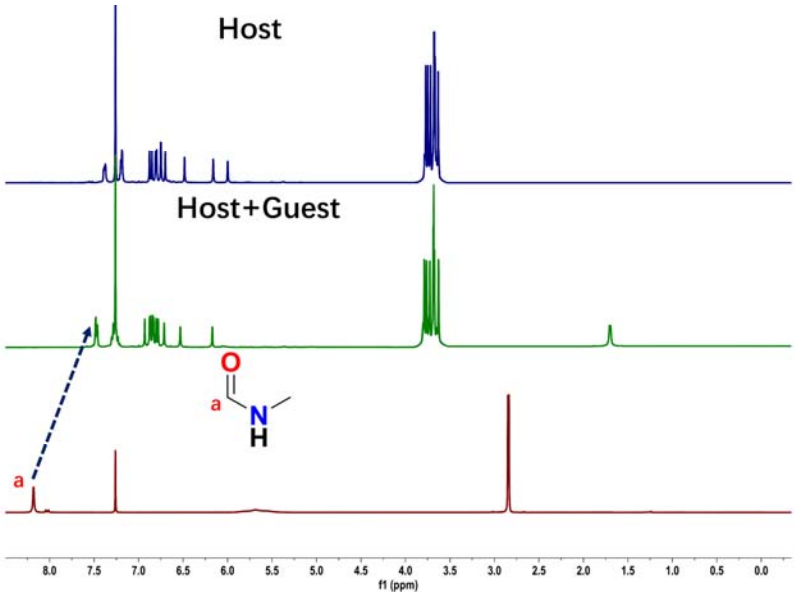

Figure S22. ^{1}H NMR spectra (400 MHz, $CDCl_3$, 298 K) of *N*-methylformamide (**16**), **[P4-(OH)BPO]** (10.0 mM), and an equimolar mixture of **16** and **[P4-(OH)BPO]**.

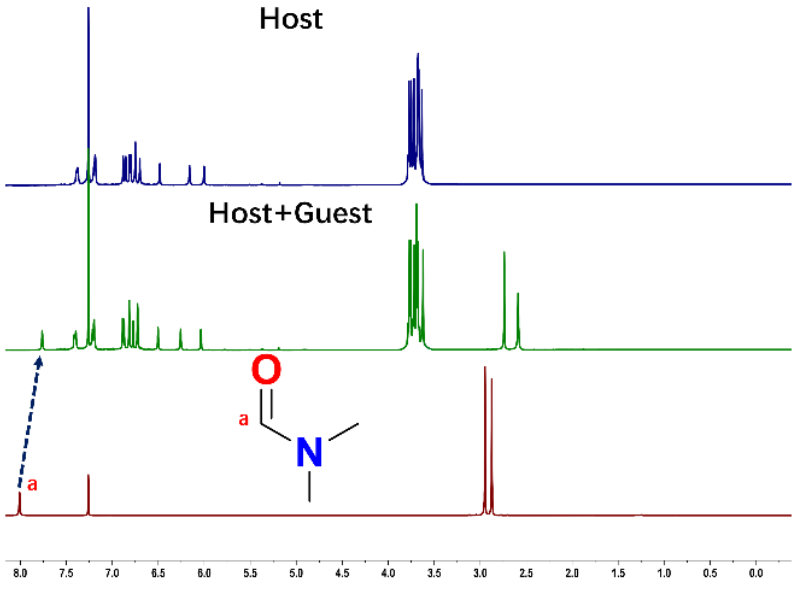

Figure S23. ^{1}H NMR spectra (400 MHz, $CDCl_3$, 298 K) of *N*,*N*-dimethylformamide (**17**), **[P4-(OH)BPO]** (10.0 mM), and an equimolar mixture of **17** and **[P4-(OH)BPO]**.

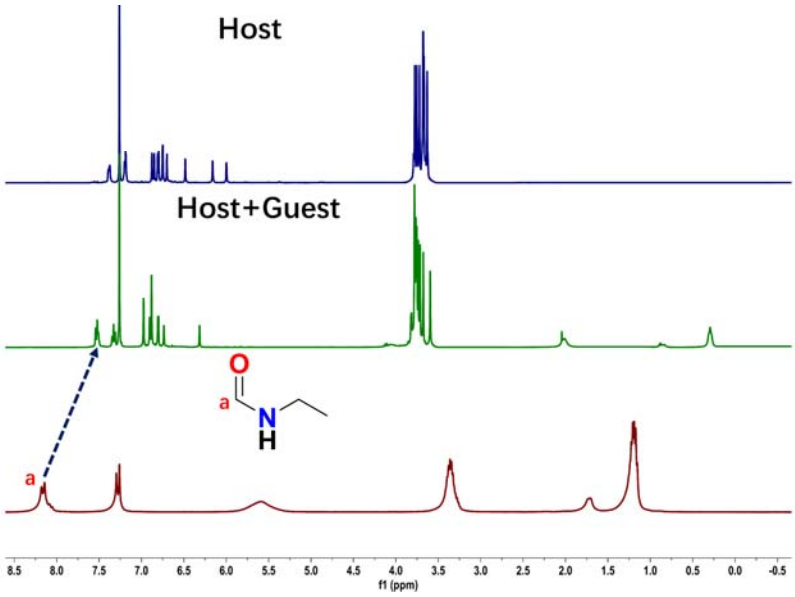

Figure S24. ^{1}H NMR spectra (400 MHz, $CDCl_3$, 298 K) of *N*-ethylformamide (**18**), **[P4-(OH)BPO]** (10.0 mM), and an equimolar mixture of **18** and **[P4-(OH)BPO]**.

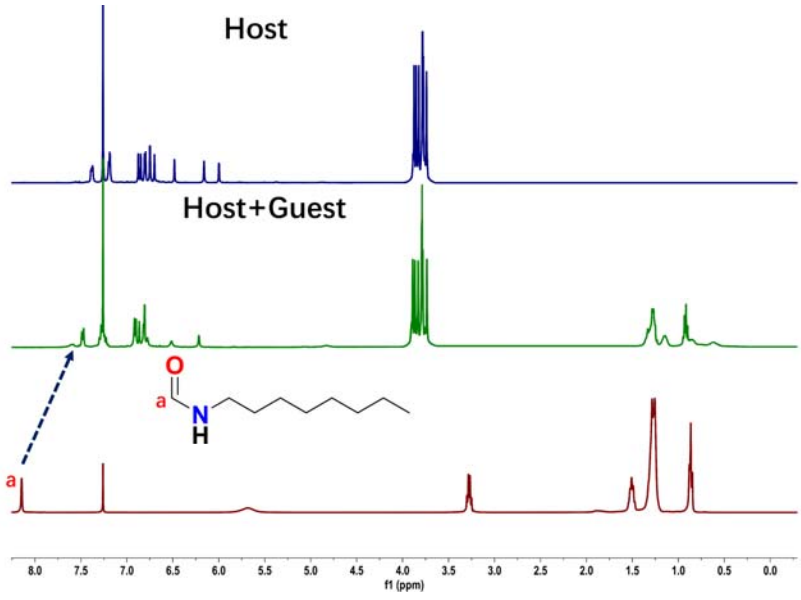

Figure S25. ^{1}H NMR spectra (400 MHz, $CDCl_3$, 298 K) of *N*-octylformamide (**19**), **[P4-(OH)BPO]** (10.0 mM), and an equimolar mixture of **19** and **[P4-(OH)BPO]**.

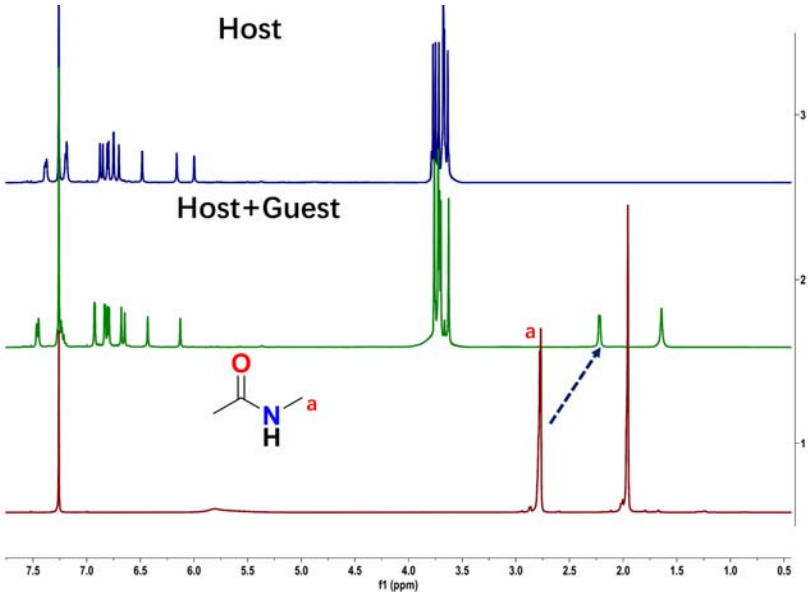

Figure S26. ^{1}H NMR spectra (400 MHz, $CDCl_3$, 298 K) of *N*-methylacetamide (**20**), **[P4-(OH)BPO]** (10.0 mM), and an equimolar mixture of **20** and **[P4-(OH)BPO]**.

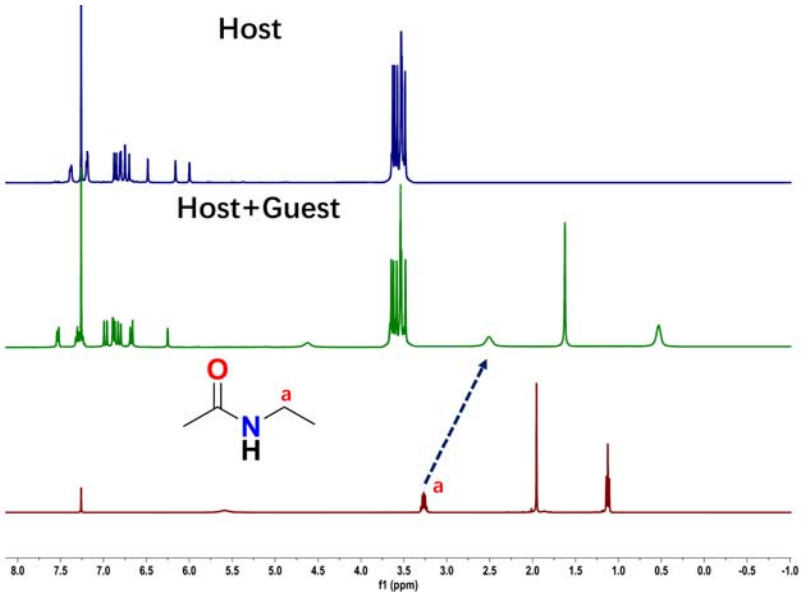

Figure S27. ^{1}H NMR spectra (400 MHz, $CDCl_3$, 298 K) of *N*-ethylacetamide (**21**), **[P4-(OH)BPO]** (10.0 mM), and an equimolar mixture of **21** and **[P4-(OH)BPO]**.

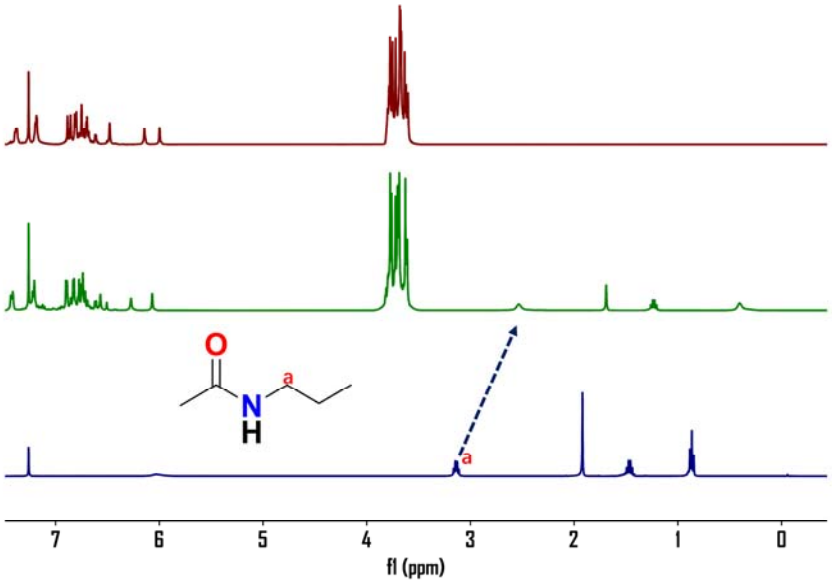

Figure S28. ^{1}H NMR spectra (400 MHz, $CDCl_3$, 298 K) of *N*-propylacetamide (**22**), **[P4-(OH)BPO]** (10.0 mM), and an equimolar mixture of **22** and **[P4-(OH)BPO]**.

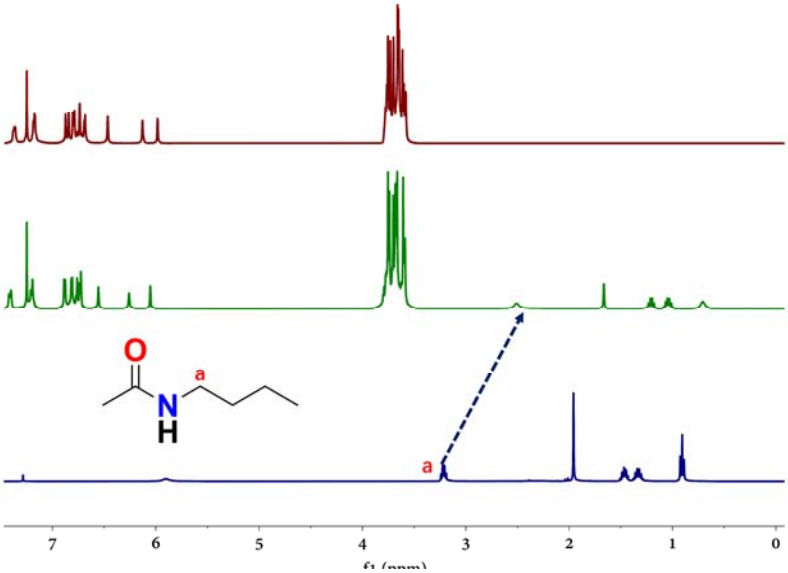

Figure S29. ^{1}H NMR spectra (400 MHz, $CDCl_3$, 298 K) of *N*-butylacetamide (**23**), **[P4-(OH)BPO]** (10.0 mM), and an equimolar mixture of **23** and **[P4-(OH)BPO]**.

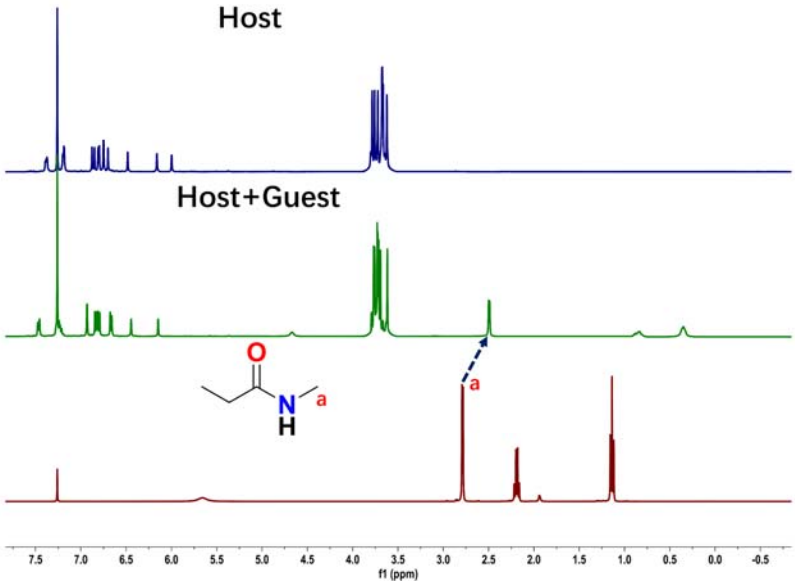

Figure S30. ^{1}H NMR spectra (400 MHz, $CDCl_3$, 298 K) of *N*-methylpropionamide (**24**), **[P4-(OH)BPO]** (10.0 mM), and an equimolar mixture of **24** and **[P4-(OH)BPO]**.

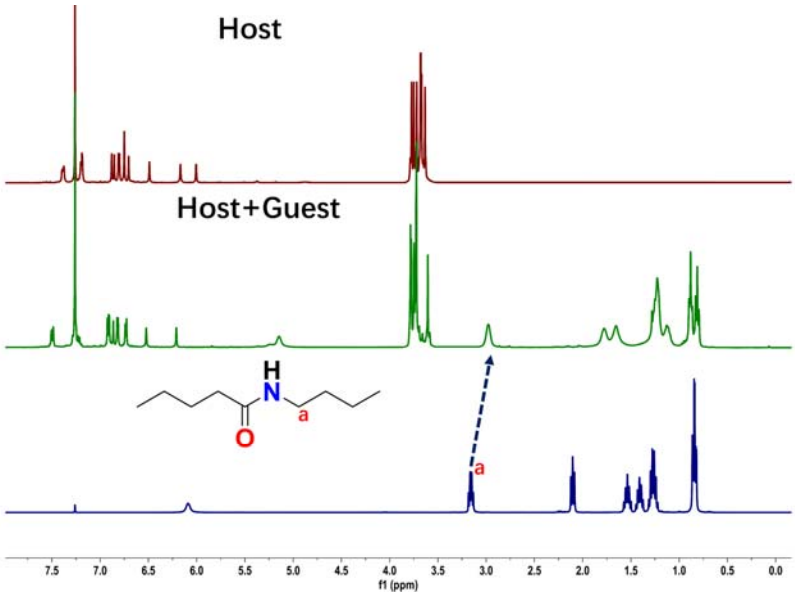

Figure 31. ^{1}H NMR spectra (400 MHz, $CDCl_3$, 298 K) of *N*-butylpentanamide (**25**), **[P4-(OH)BPO]** (10.0 mM), and an equimolar mixture of **25** and **[P4-(OH)BPO]**.

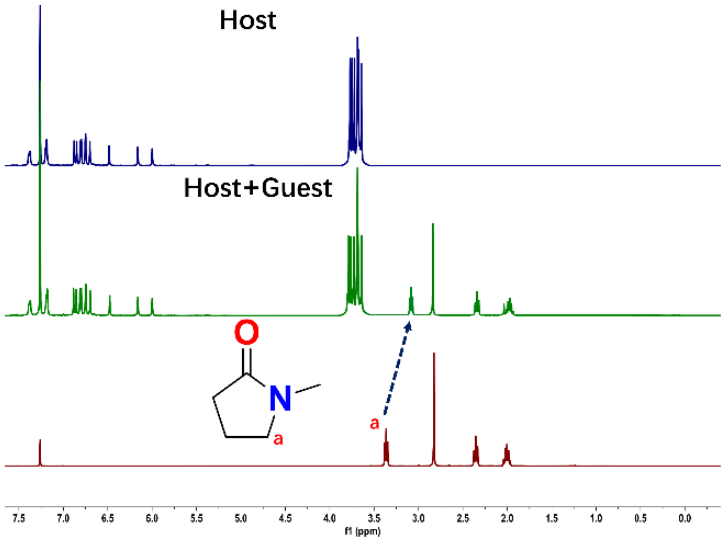

Figure S32. ^{1}H NMR spectra (400 MHz, $CDCl_3$, 298 K) of *N*-methyl pyrrolidone (**26**), **[P4-(OH)BPO]** (10.0 mM), and an equimolar mixture of **26** and **[P4-(OH)BPO]**.

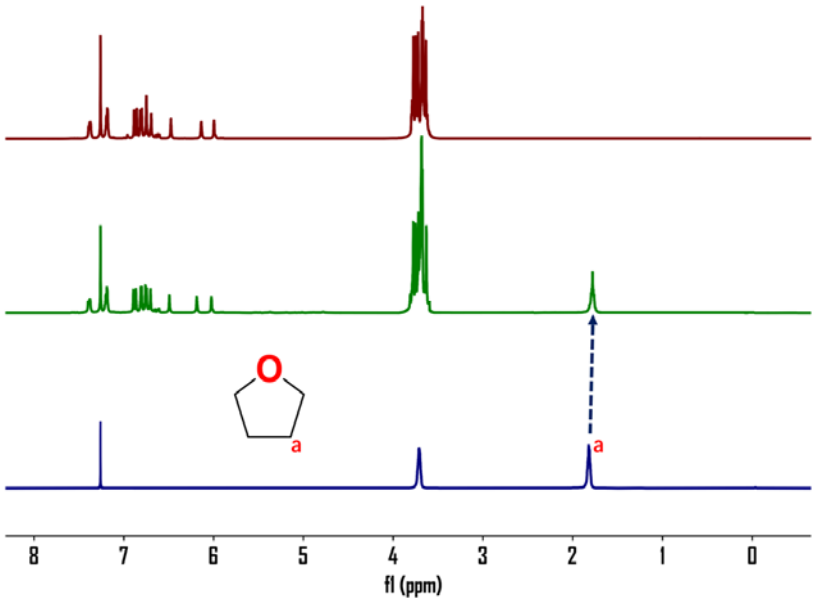

Figure S33. ^{1}H NMR spectra (400 MHz, $CDCl_3$, 298 K) of tetrahydrofuran (**27**), **[P4-(OH)BPO]** (10.0 mM), and an equimolar mixture of **27** and **[P4-(OH)BPO]**.

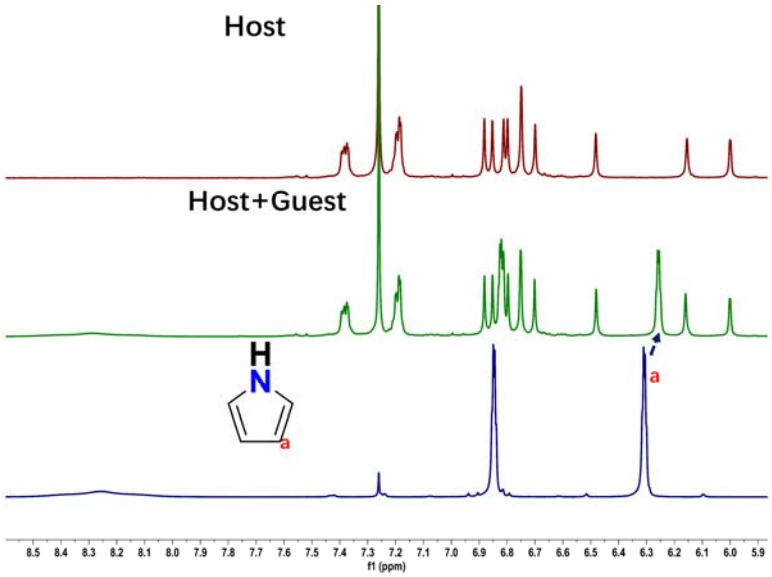

Figure S34. ^{1}H NMR spectra (400 MHz, $CDCl_3$, 298 K) of pyrole (**28**), **[P4-(OH)BPO]** (10.0 mM), and an equimolar mixture of **28** and **[P4-(OH)BPO]**.

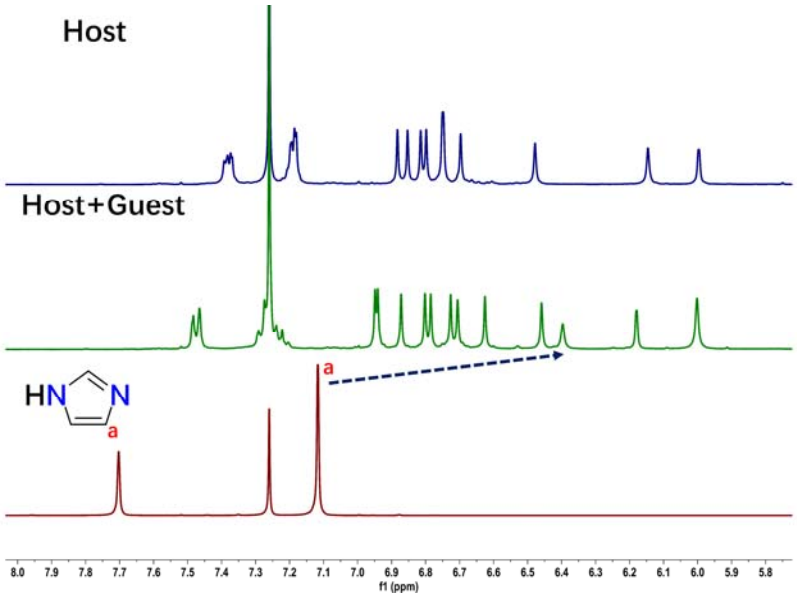

Figure S35. ^{1}H NMR spectra (400 MHz, $CDCl_3$, 298 K) of imidazole (**29**), **[P4-(OH)BPO]** (10.0 mM), and an equimolar mixture of **29** and **[P4-(OH)BPO]**.

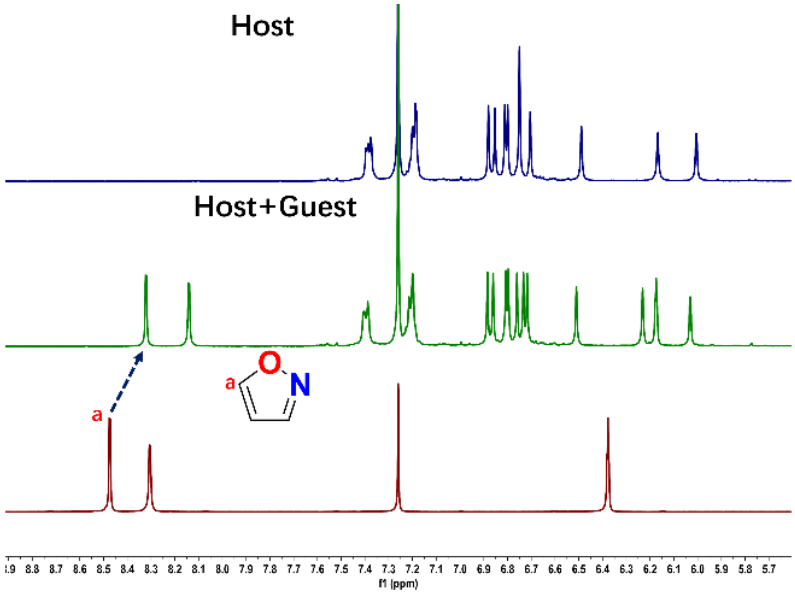

Figure S36. ^{1}H NMR spectra (400 MHz, $CDCl_3$, 298 K) of oxazole (**30**), **[P4-(OH)BPO]** (10.0 mM), and an equimolar mixture of **30** and **[P4-(OH)BPO]**.

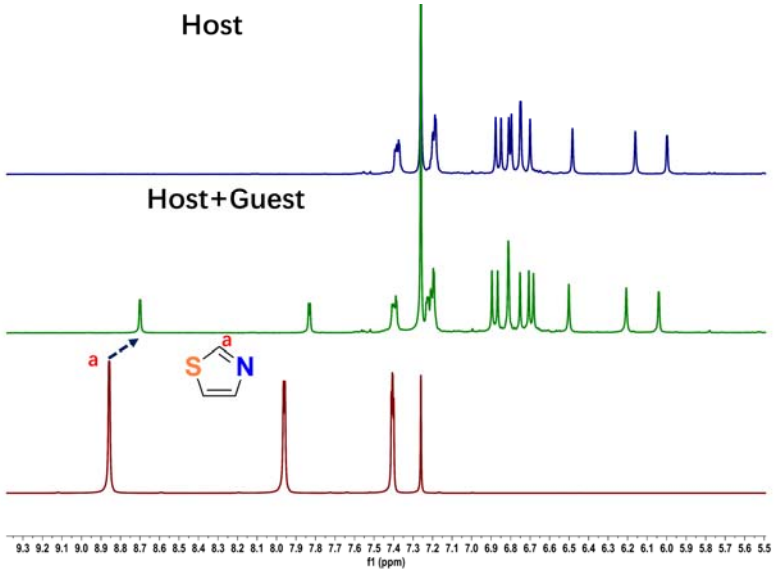

Figure S37. ^{1}H NMR spectra (400 MHz, $CDCl_3$, 298 K) of thiazole (**31**), **[P4-(OH)BPO]** (10.0 mM), and an equimolar mixture of **31** and **[P4-(OH)BPO]**.

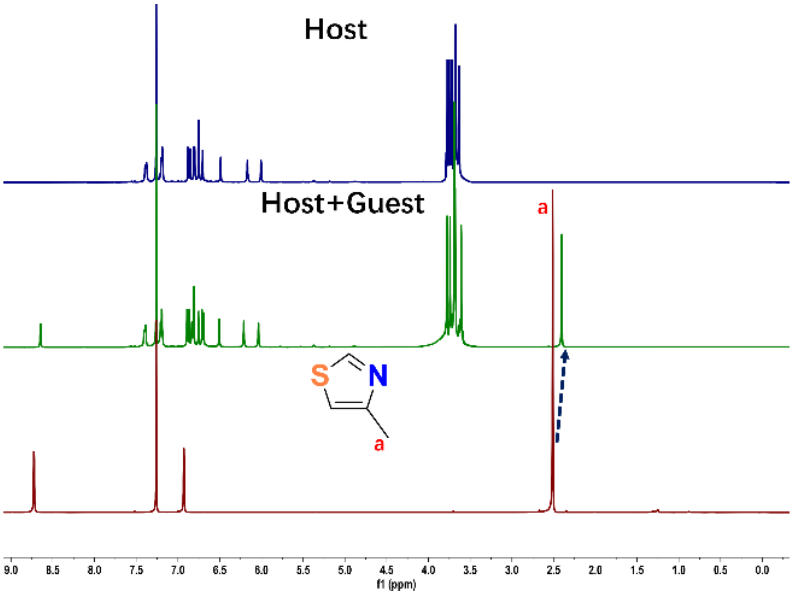

Figure S38. ^{1}H NMR spectra (400 MHz, $CDCl_3$, 298 K) of 4-methylthiazole (**32**), **[P4-(OH)BPO]** (10.0 mM), and an equimolar mixture of **32** and **[P4-(OH)BPO]**.

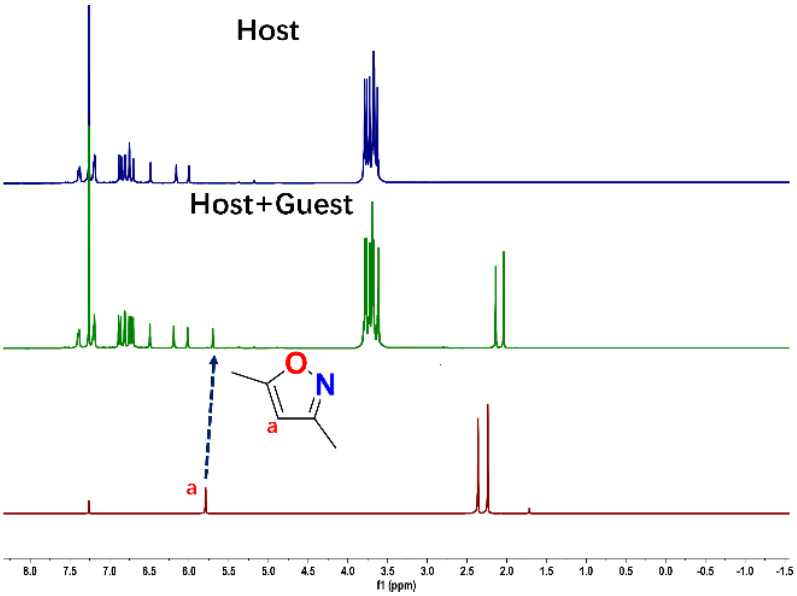

Figure S39. ^{1}H NMR spectra (400 MHz, $CDCl_3$, 298 K) of 3,5-dimethylisoxazole (**33**), **[P4-(OH)BPO]** (10.0 mM), and an equimolar mixture of **33** and **[P4-(OH)BPO]**.

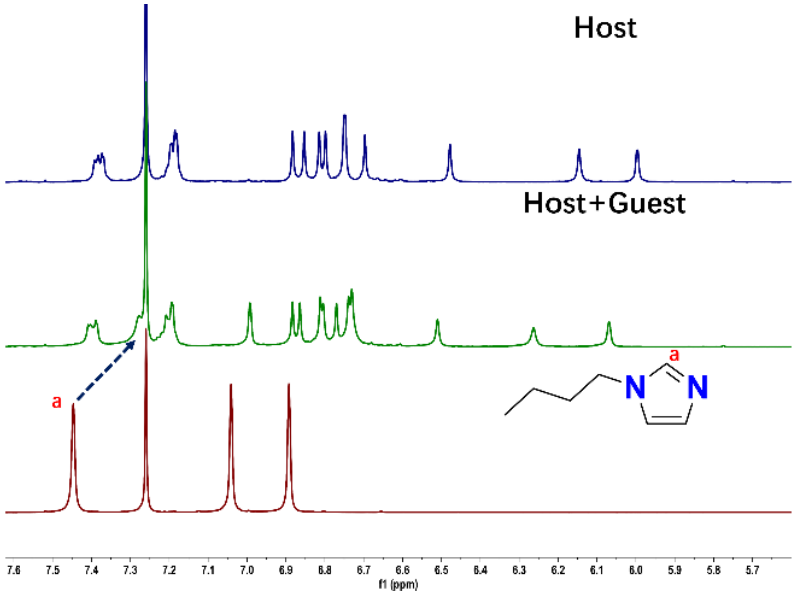

Figure S40. ^{1}H NMR spectra (400 MHz, $CDCl_3$, 298 K) of 1-butylimidazole (**34**), **[P4-(OH)BPO]** (10.0 mM), and an equimolar mixture of **34** and **[P4-(OH)BPO]**.

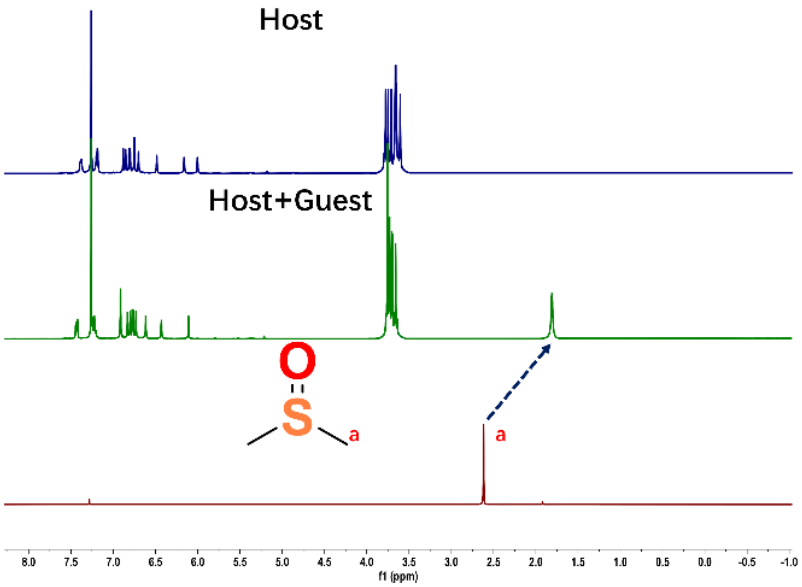

Figure S41. ^{1}H NMR spectra (400 MHz, $CDCl_3$, 298 K) of dimethylsulfoxide (**35**), **[P4-(OH)BPO]** (10.0 mM), and an equimolar mixture of **35** and **[P4-(OH)BPO]**.

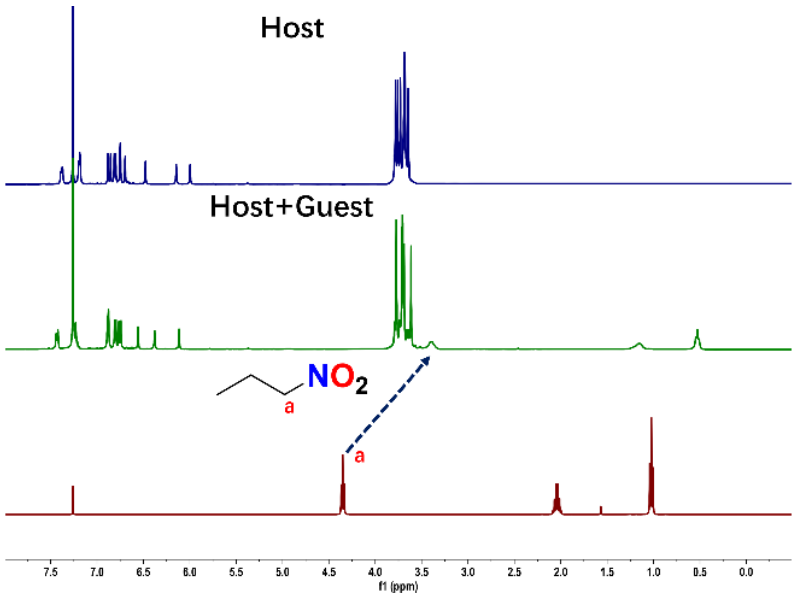

Figure S42. ^{1}H NMR spectra (400 MHz, $CDCl_3$, 298 K) of 1-nitropropane (**36**), **[P4-(OH)BPO]** (10.0 mM), and an equimolar mixture of **36** and **[P4-(OH)BPO]**.

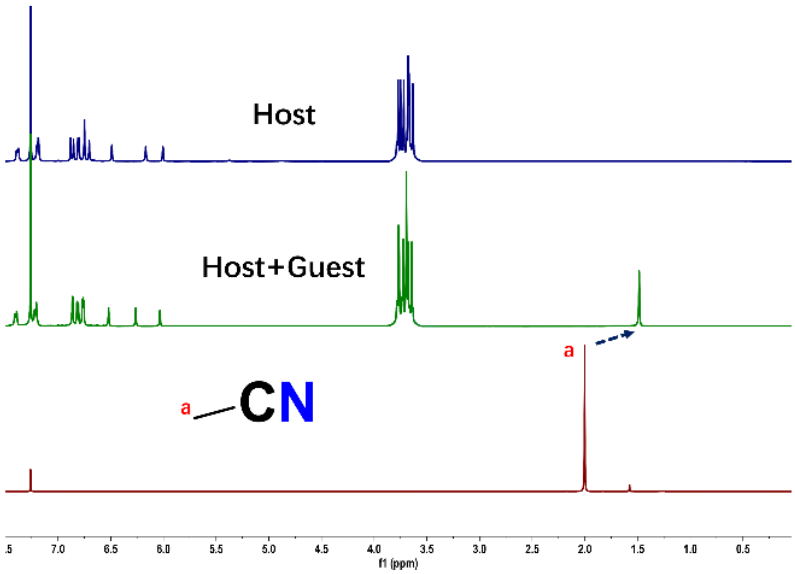

Figure S43. ^{1}H NMR spectra (400 MHz, $CDCl_3$, 298 K) of acetonitrile (**37**), **[P4-(OH)BPO]** (10.0 mM), and an equimolar mixture of **37** and **[P4-(OH)BPO]**.

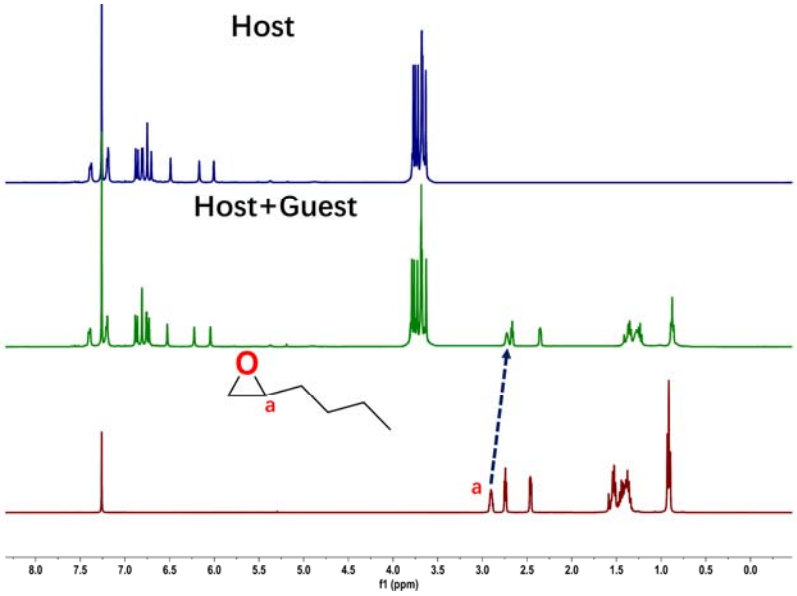

Figure S44. ^{1}H NMR spectra (400 MHz, $CDCl_3$, 298 K) of 2-butyloxirane (**38**), **[P4-(OH)BPO]** (10.0 mM), and an equimolar mixture of **38** and **[P4-(OH)BPO]**.

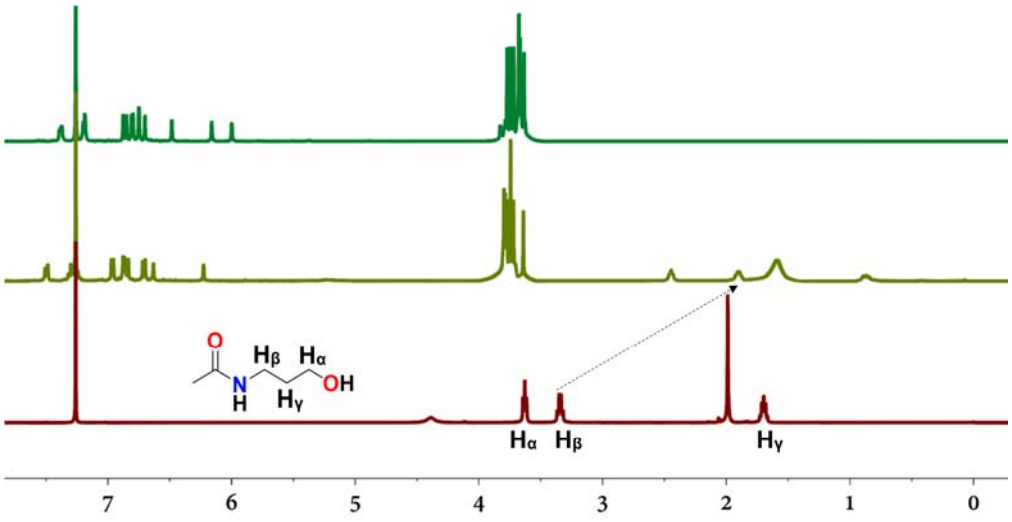

Figure S45. ^{1}H NMR spectra (400 MHz, $CDCl_3$, 298 K) of *N*-(3-hydroxypropyl)acetamide (**39**), **[P4-(OH)BPO]** (10.0 mM), and an equimolar mixture of **39** and **[P4-(OH)BPO]**..

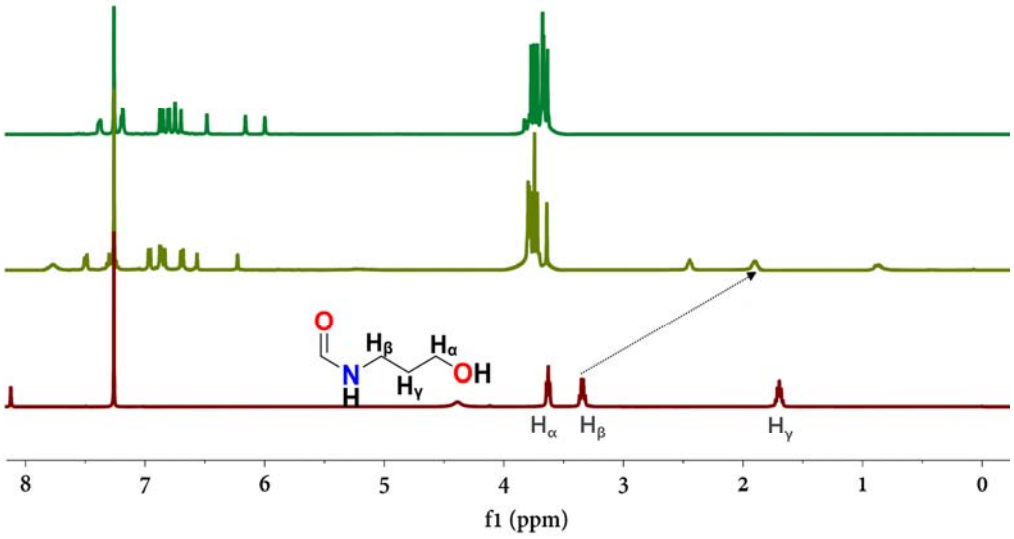

Figure S46. ^{1}H NMR spectra (400 MHz, $CDCl_3$, 298 K) of *N*-(3-hydroxypropyl)formamide (**40**), **[P4-(OH)BPO]** (10.0 mM), and an equimolar mixture of **40** and **[P4-(OH)BPO]**.

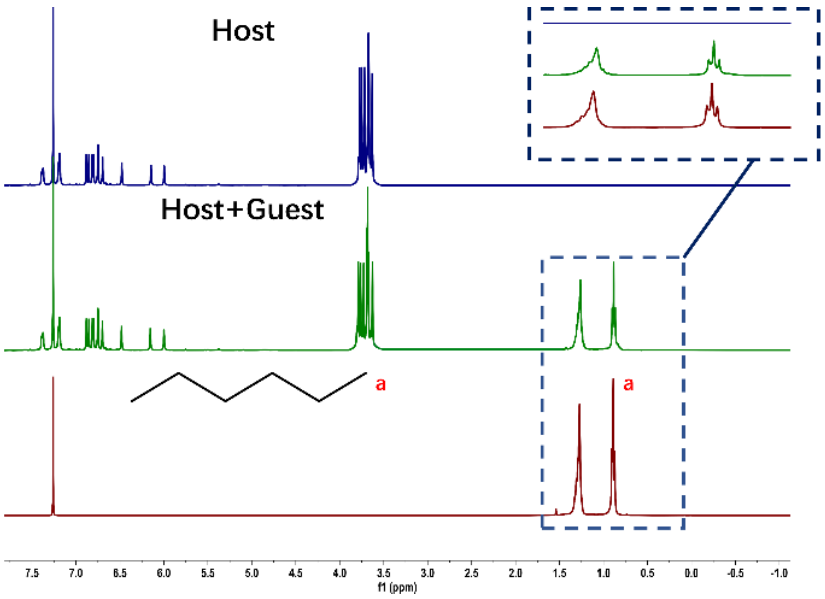

Figure S47. ^{1}H NMR spectra (400 MHz, $CDCl_3$ 298 K) of hexane, **[P4-(OH)BPO]** (10.0 mM), and an equimolar mixture of hexane and **[P4-(OH)BPO]**.

.

Job Plots Deriving from a 1:1 Complexation of *endo*-[P4-BPO(1-OH)] and Guests

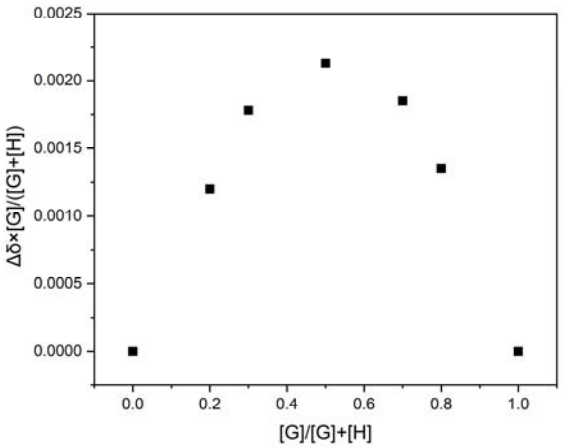

Figure S48. Job plot showing a 1:1 binding stoichiometry between ***endo*-[P4-BPO(1-OH)]** and *n*-butylamine (**1**).

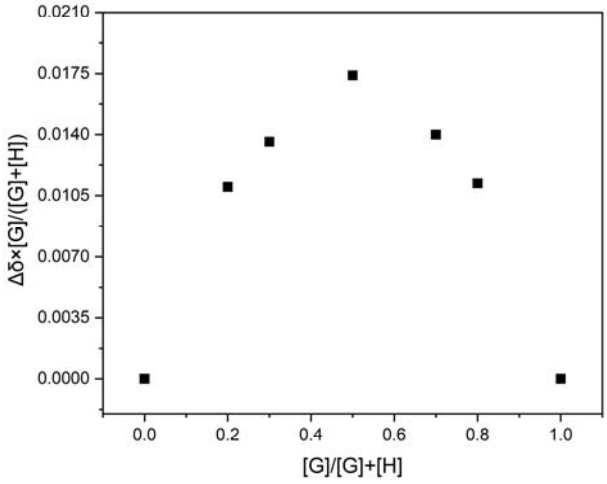

Figure S49. Job plot showing a 1:1 binding stoichiometry between ***endo*-[P4-BPO(1-OH)]** and *n*-hexylamine (**2**).

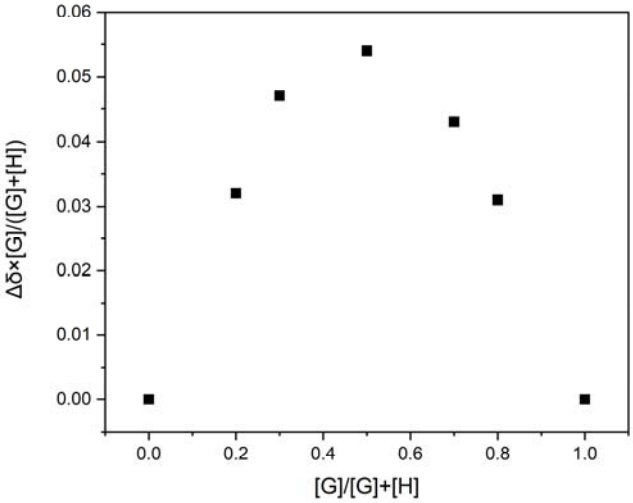

Figure S50. Job plot showing a 1:1 binding stoichiometry between ***endo*-[P4-BPO(1-OH)]** and *n*-octylamine (**3**).

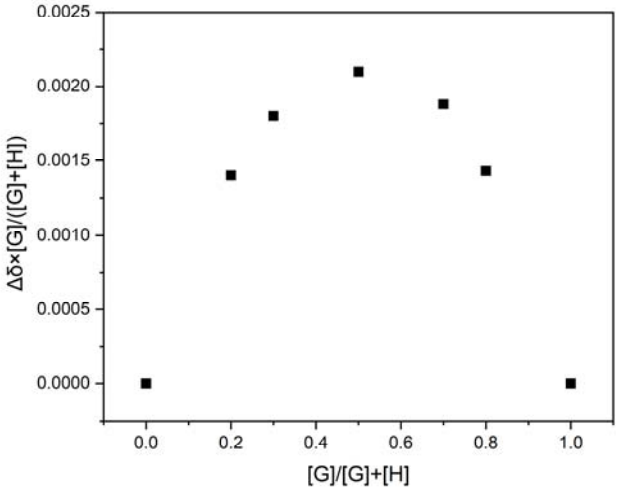

Figure S51. Job plot showing a 1:1 binding stoichiometry between ***endo*-[P4-BPO(1-OH)]** and *n*-butanol (**4**).

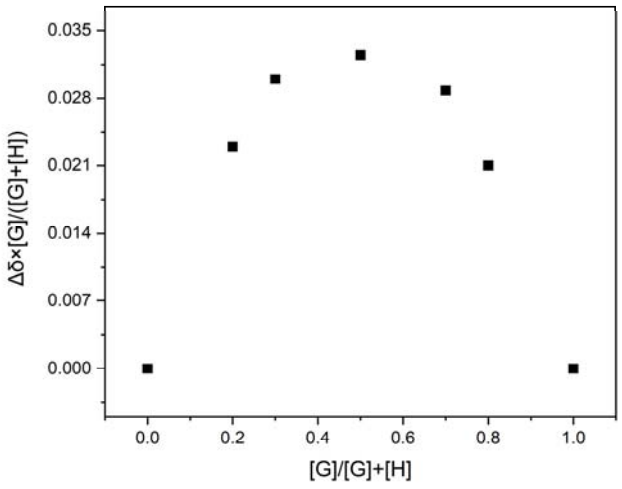

Figure S52. Job plot showing a 1:1 binding stoichiometry between ***endo*-[P4-BPO(1-OH)]** and *n*-hexanol (**5**).

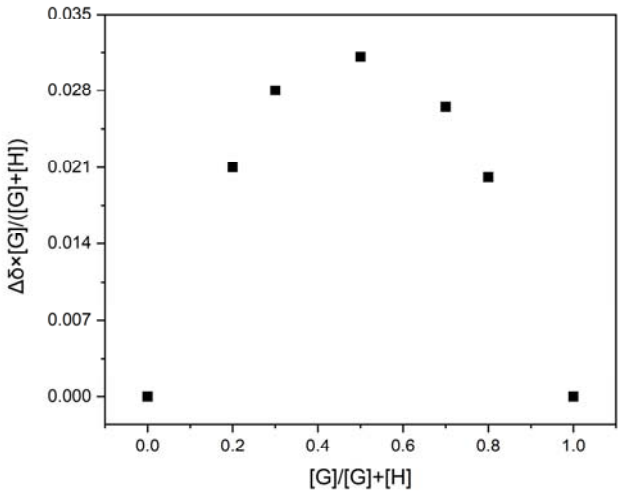

Figure S53. Job plot showing a 1:1 binding stoichiometry between ***endo*-[P4-BPO(1-OH)]** and *n*-octanol (**6**).

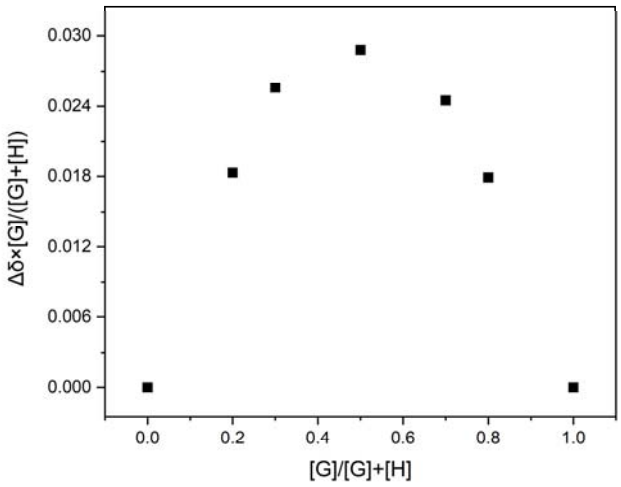

Figure S54. Job plot showing a 1:1 binding stoichiometry between ***endo*-[P4-BPO(1-OH)]** and *n*-butyraldehyde (**7**).

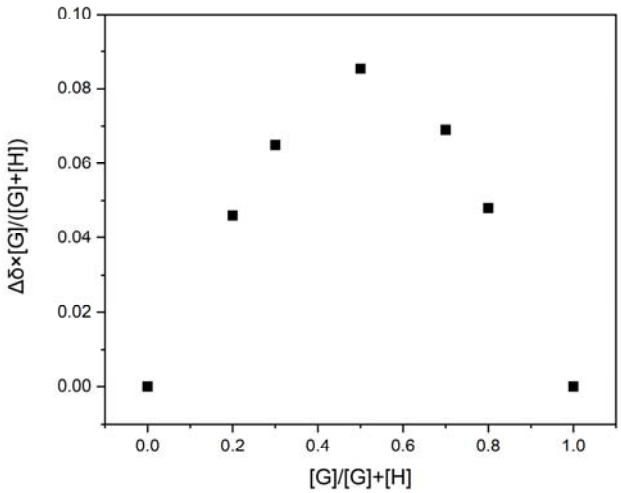

Figure S55. Job plot showing a 1:1 binding stoichiometry between ***endo*-[P4-BPO(1-OH)]** and *n*-hexanaldehyde (**8**).

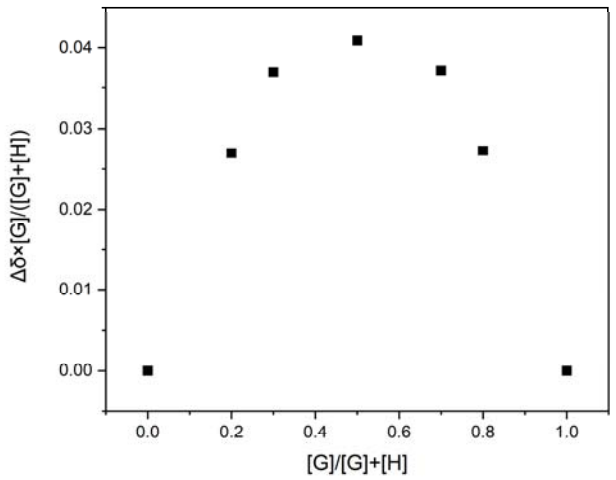

Figure S56. Job plot showing a 1:1 binding stoichiometry between ***endo*-[P4-BPO(1-OH)]** and *n*-octanaldehyde (**9**).

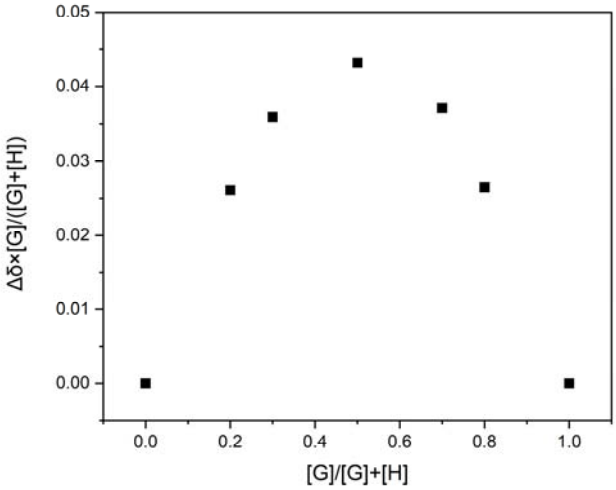

Figure S57. Job plot showing a 1:1 binding stoichiometry between ***endo*-[P4-BPO(1-OH)]** and methyl butyrate (**10**).

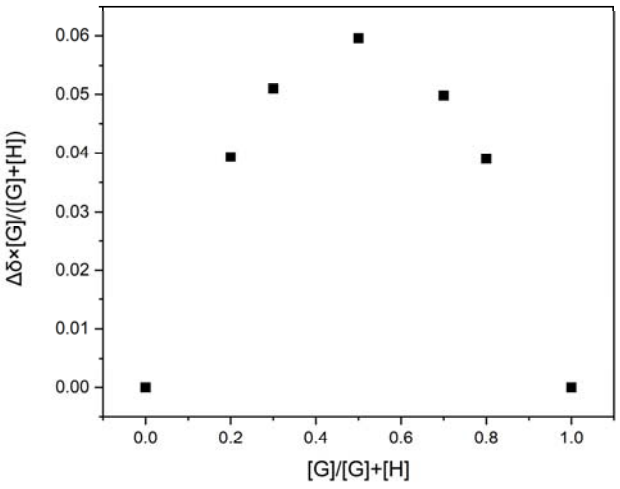

Figure S58. Job plot showing a 1:1 binding stoichiometry between ***endo*-[P4-BPO(1-OH)]** and methyl hexanoate (**11**).

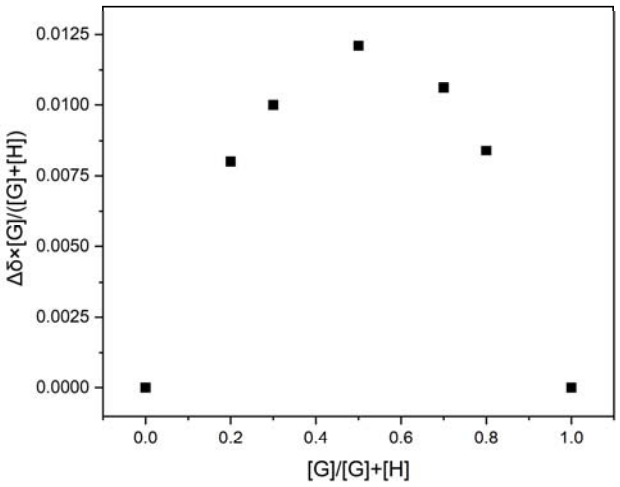

Figure S59. Job plot showing a 1:1 binding stoichiometry between ***endo*-[P4-BPO(1-OH)]** and methyl octanoate (**12**).

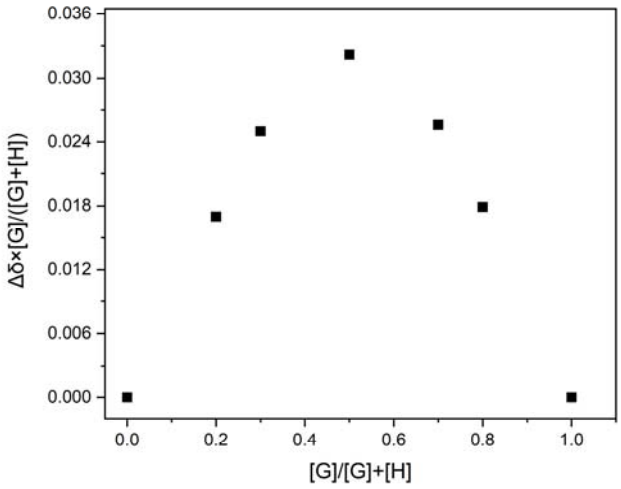

Figure S60. Job plot showing a 1:1 binding stoichiometry between ***endo*-[P4-BPO(1-OH)]** and *n*-butanoic acid (**13**).

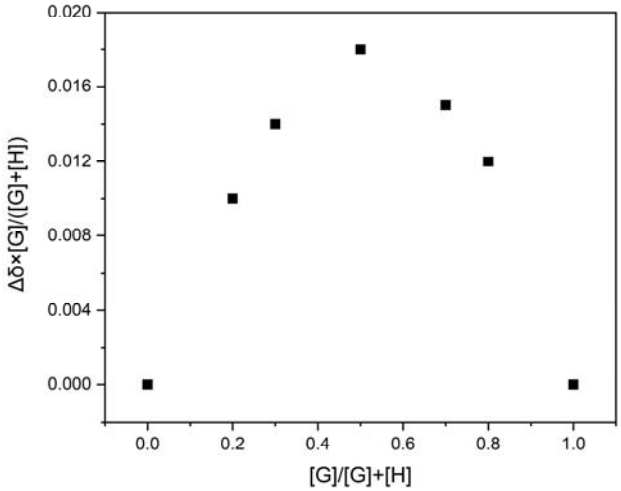

Figure S61. Job plot showing a 1:1 binding stoichiometry between ***endo*-[P4-BPO(1-OH)]** and *n*-hexanoic acid (**14**).

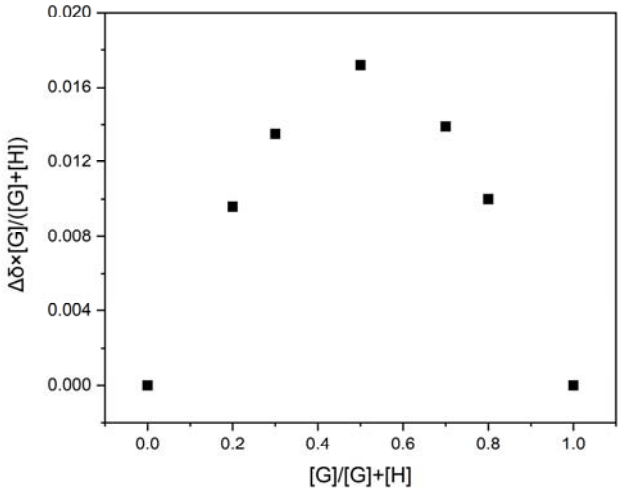

Figure S62. Job plot showing a 1:1 binding stoichiometry between ***endo*-[P4-BPO(1-OH)]** and *n*-butanoic acid (**15**).

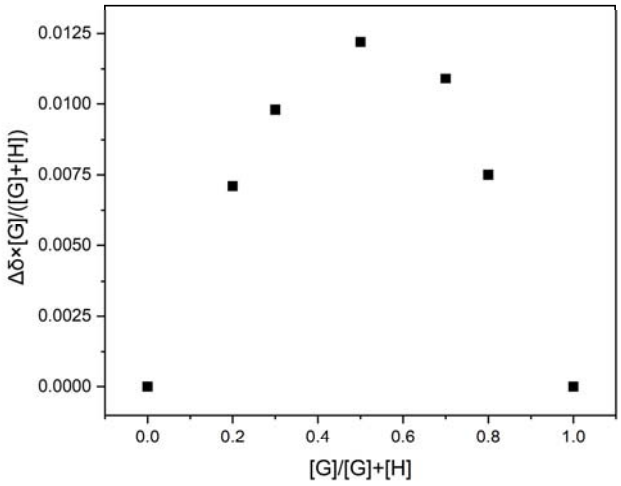

Figure S63. Job plot showing a 1:1 binding stoichiometry between ***endo*-[P4-BPO(1-OH)]** and *N*-methylformamide (**16**).

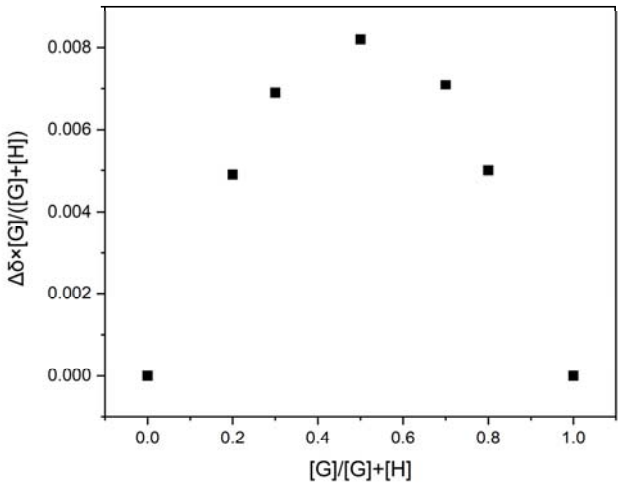

Figure S64. Job plot showing a 1:1 binding stoichiometry between ***endo*-[P4-BPO(1-OH)]** and *N*,*N*-dimethylformamide (**17**).

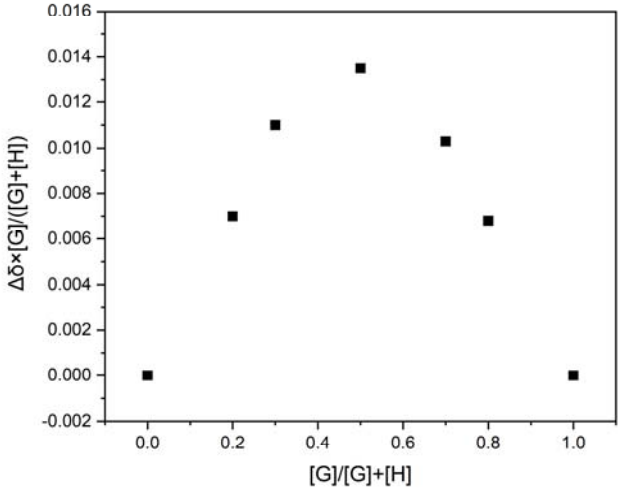

Figure S65. Job plot showing a 1:1 binding stoichiometry between ***endo*-[P4-BPO(1-OH)]** and *N*-ethylformamide (**18**).

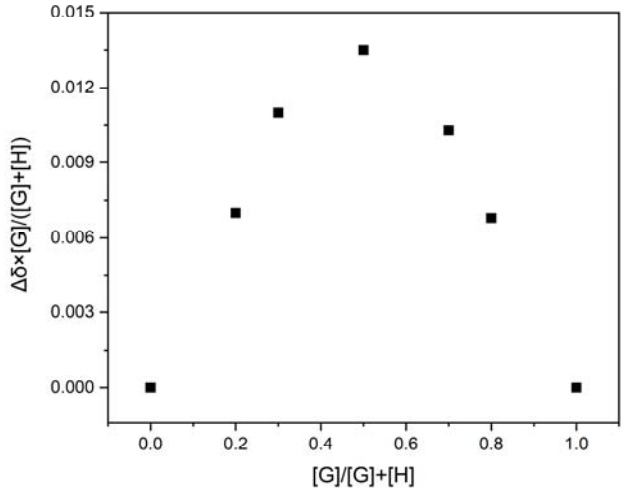

Figure S66. Job plot showing a 1:1 binding stoichiometry between ***endo*-[P4-BPO(1-OH)]** and *N*-octylformamide (**19**).

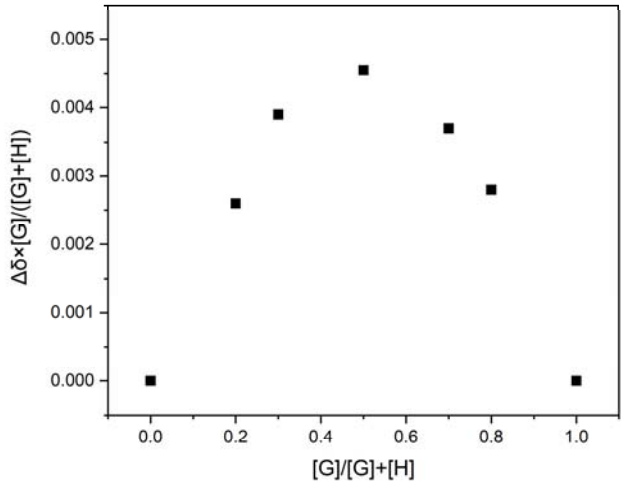

Figure S67. Job plot showing a 1:1 binding stoichiometry between ***endo*-[P4-BPO(1-OH)]** and *N*-methylacetamide (**20**).

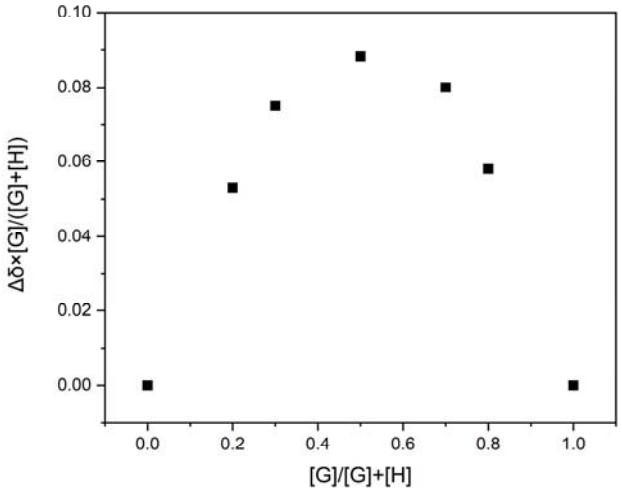

Figure S68. Job plot showing a 1:1 binding stoichiometry between ***endo*-[P4-BPO(1-OH)]** and *N*-ethylacetamide (**21**).

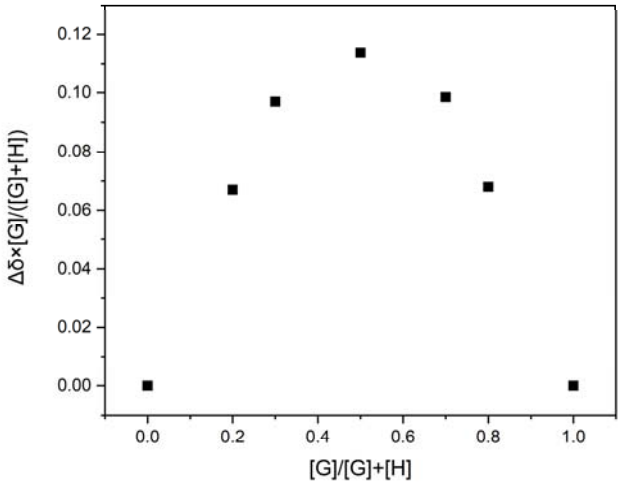

Figure S69. Job plot showing a 1:1 binding stoichiometry between ***endo*-[P4-BPO(1-OH)]** and *N*-propylacetamide (**22**).

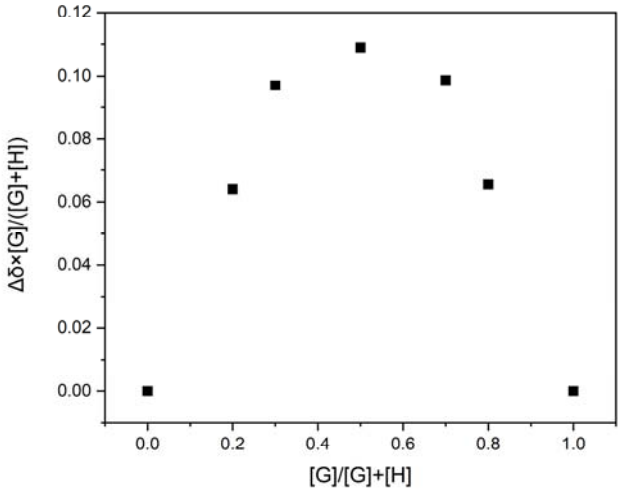

Figure S70. Job plot showing a 1:1 binding stoichiometry between ***endo*-[P4-BPO(1-OH)]** and *N*-butylacetamide (**23**).

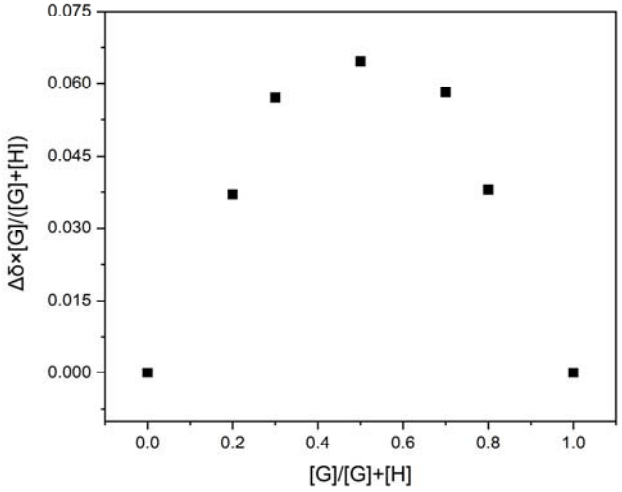

Figure S71. Job plot showing a 1:1 binding stoichiometry between ***endo*-[P4-BPO(1-OH)]** and *N*-methylpropionamide (**24**).

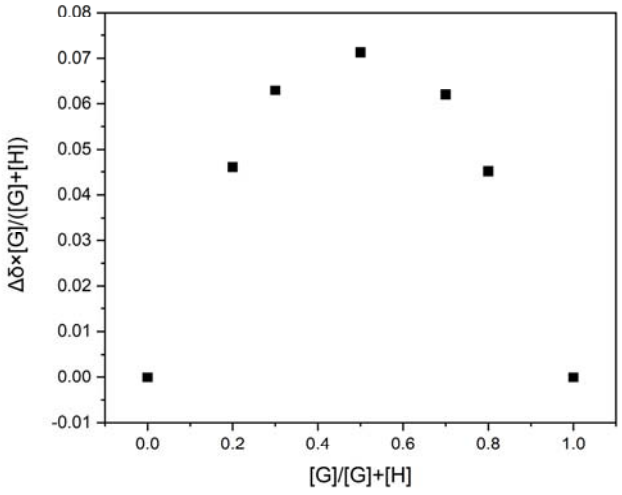

Figure S72. Job plot showing a 1:1 binding stoichiometry between ***endo*-[P4-BPO(1-OH)]** and *N*-butylpentanamide (**25**).

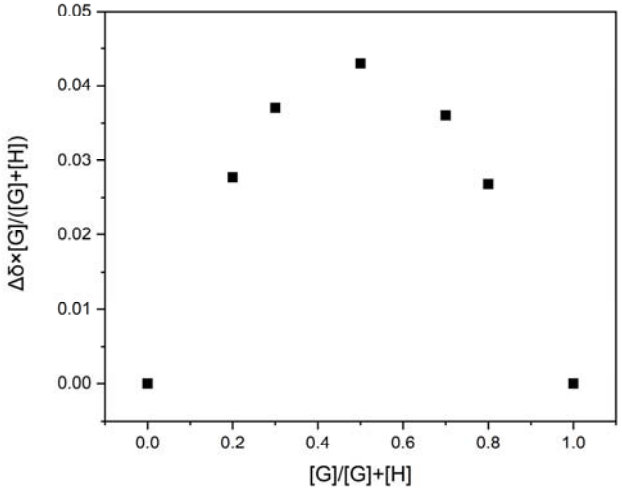

Figure S73 Job plot showing a 1:1 binding stoichiometry between ***endo*-[P4-BPO(1-OH)]** and *N*-methyl pyrrolidone (**26**).

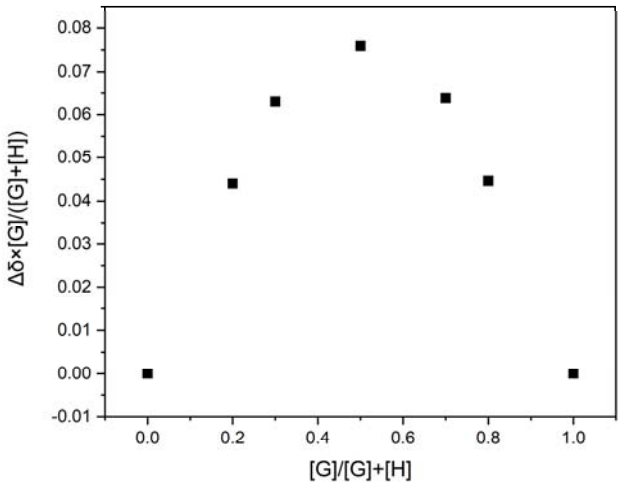

Figure S74. Job plot showing a 1:1 binding stoichiometry between ***endo*-[P4-BPO(1-OH)]** and tetrahydrofuran (**27**).

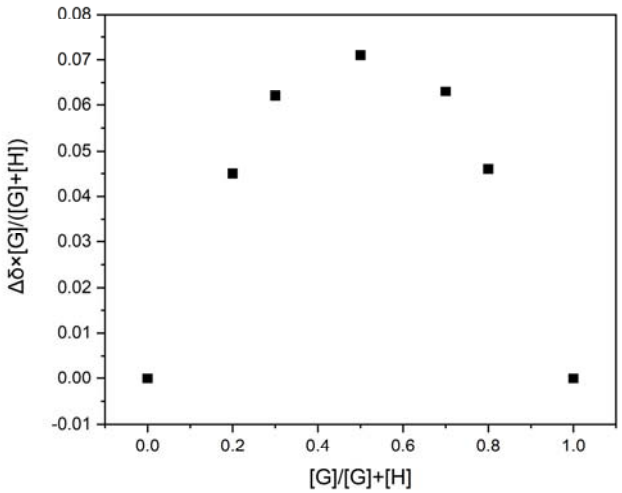

Figure S75. Job plot showing a 1:1 binding stoichiometry between ***endo*-[P4-BPO(1-OH)]** and pyrole (**28**).

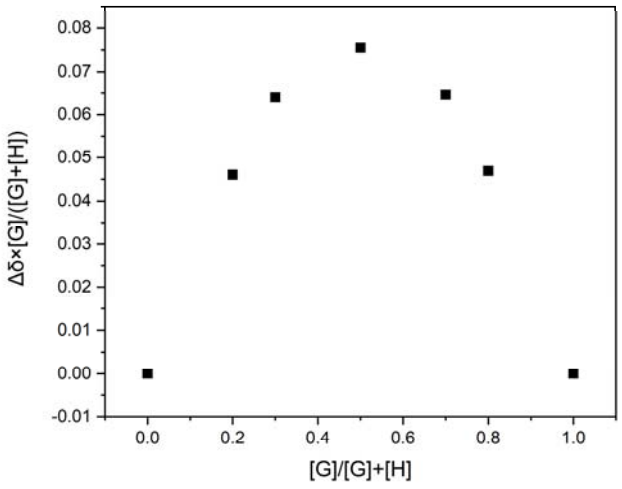

Figure S76. Job plot showing a 1:1 binding stoichiometry between ***endo*-[P4-BPO(1-OH)]** and imidazole (**29**).

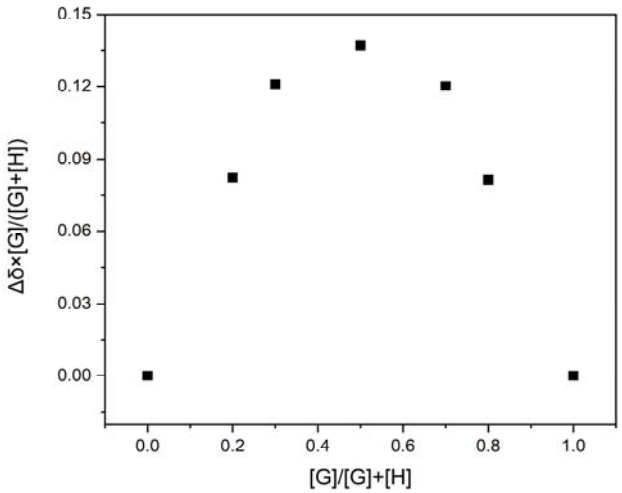

Figure S77. Job plot showing a 1:1 binding stoichiometry between ***endo*-[P4-BPO(1-OH)]** and oxazole (**30**).

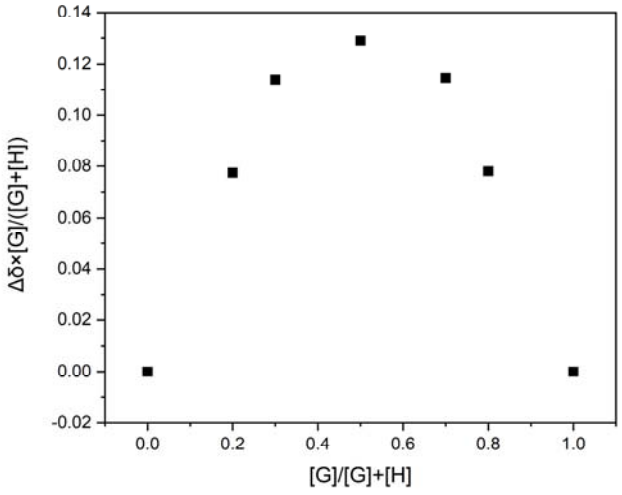

Figure S78. Job plot showing a 1:1 binding stoichiometry between ***endo*-[P4-BPO(1-OH)]** and thiazole (**31**).

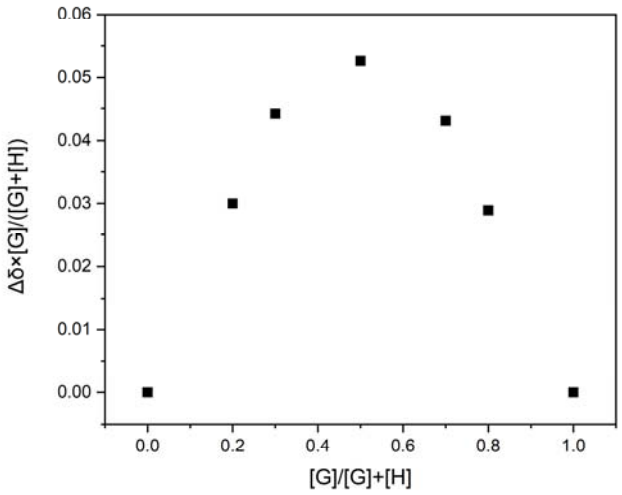

Figure S79. Job plot showing a 1:1 binding stoichiometry between ***endo*-[P4-BPO(1-OH)]** and 4-methylthiazole (**32**).

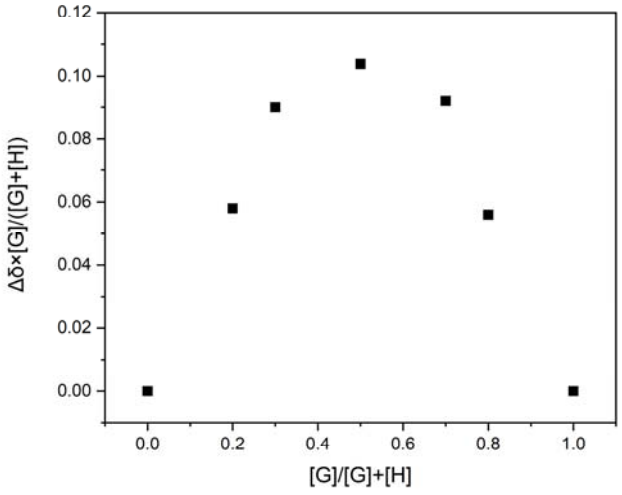

Figure S80. Job plot showing a 1:1 binding stoichiometry between ***endo*-[P4-BPO(1-OH)]** and 3,5-dimethylisoxazole (**33**).

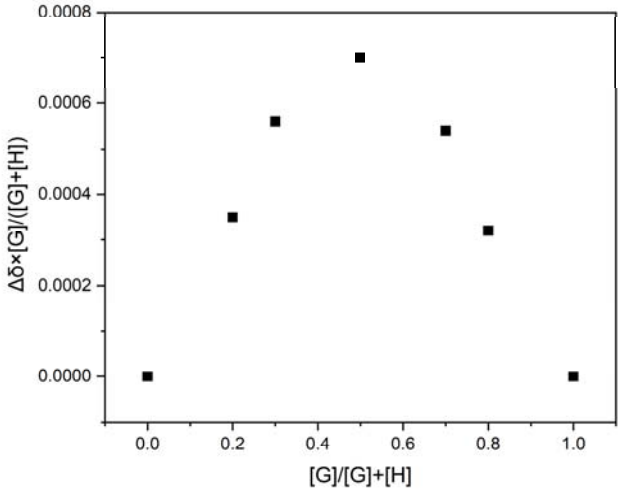

Figure S81. Job plot showing a 1:1 binding stoichiometry between ***endo*-[P4-BPO(1-OH)]** and 1-butylimidazole (**34**).

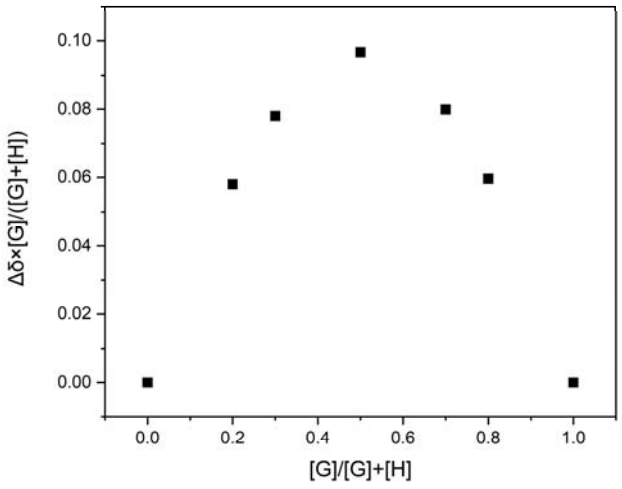

Figure S82. Job plot showing a 1:1 binding stoichiometry between ***endo*-[P4-BPO(1-OH)]** and dimethylsulfoxide (**35**).

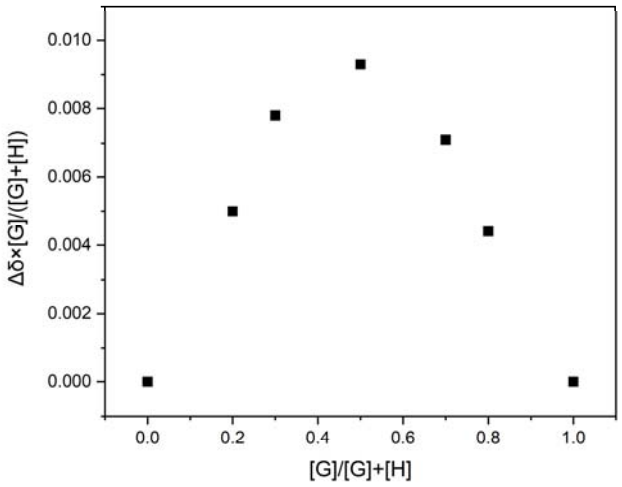

Figure S83. Job plot showing a 1:1 binding stoichiometry between ***endo*-[P4-BPO(1-OH)]** and 1-nitropropane (**36**).

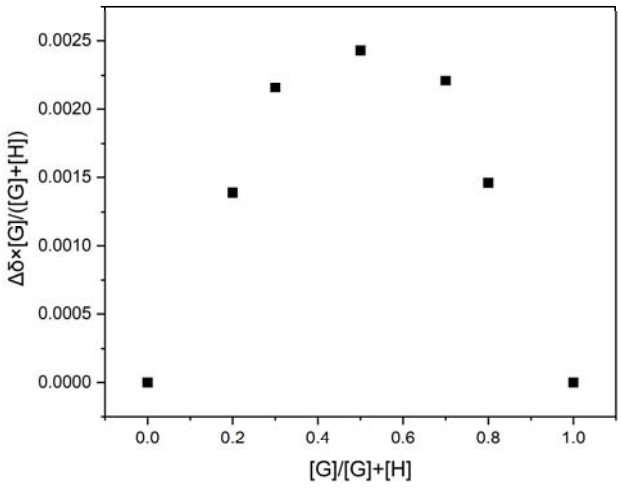

Figure S84. Job plot showing a 1:1 binding stoichiometry between ***endo*-[P4-BPO(1-OH)]** and acetonitrile (**37**).

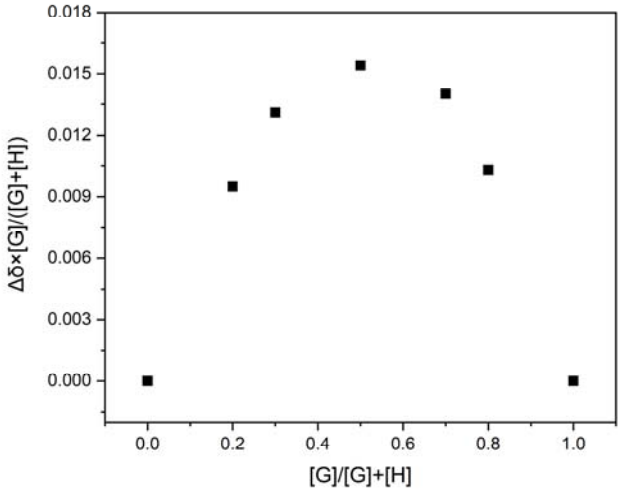

Figure S85. Job plot showing a 1:1 binding stoichiometry between ***endo*-[P4-BPO(1-OH)]** and 2-butyloxirane (**38**).

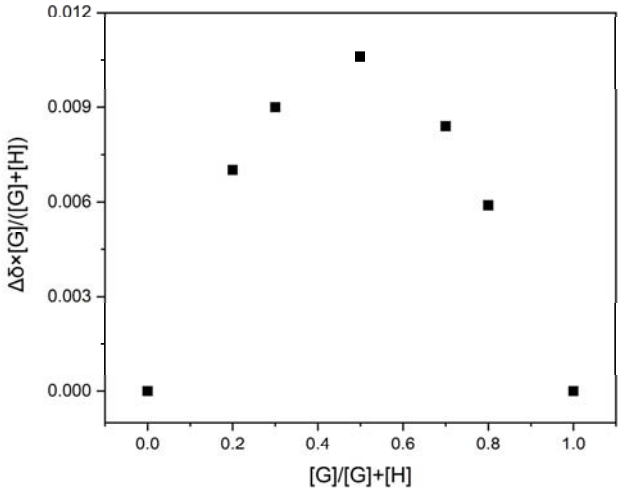

Figure S86. Job plot showing a 1:1 binding stoichiometry between ***endo*-[P4-BPO(1-OH)]** and *N*-(3-hydroxypropyl)acetamide (**39**).

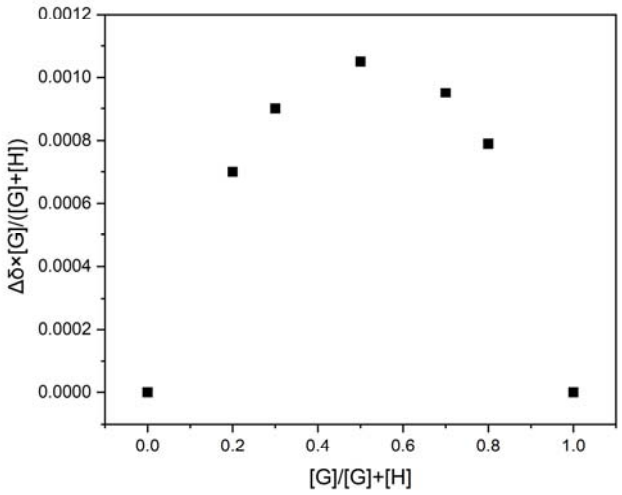

Figure S87. Job plot showing a 1:1 binding stoichiometry between ***endo*-[P4-BPO(1-OH)]** and *N*-(3-hydroxypropyl)formamide (**40**).

Nonlinear Curve Fitting of NMR Titrations

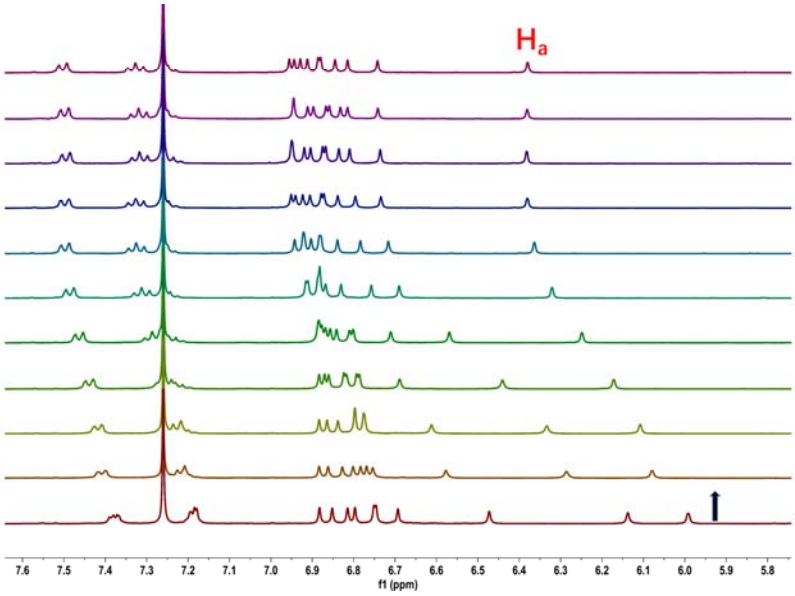

Figure S88. Partial ^{1}H NMR spectra (400 MHz, $CDCl_3$, 298 K) of a mixture of **[P4-(OH)BPO]** (10.0 mM) and *n*-butylamine (**1**) at the concentrations of 0, 2.0, 6.0, 10.0, 20.0, 40.0, 80.0, 120.0, 160.0, 320.0, and 640.0 mM (from bottom to top).

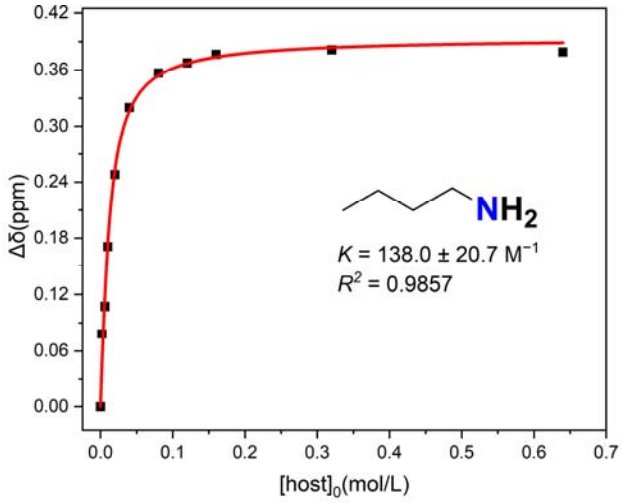

Figure S89. The nonlinear curve fitting of NMR titration (Δδ of H_α) for the complexation of **[P4-(OH)BPO]** (10.0 mM) with *n*-butylamine (**1**) in $CDCl_3$ at 298 K.

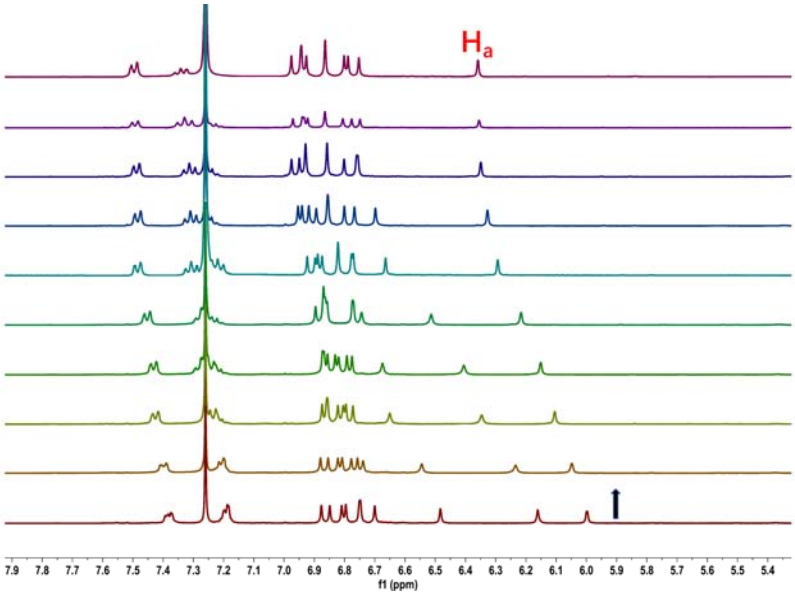

Figure S90. Partial ^{1}H NMR spectra (400 MHz, $CDCl_3$, 298 K) of a mixture of **[P4-(OH)BPO]** (10.0 mM) and *n*-hexylamine (**2**) at the concentrations of 0, 2.0, 6.0, 10.0, 20.0, 40.0, 80.0, 120.0, 160.0, 320.0, and 640.0 mM (from bottom to top).

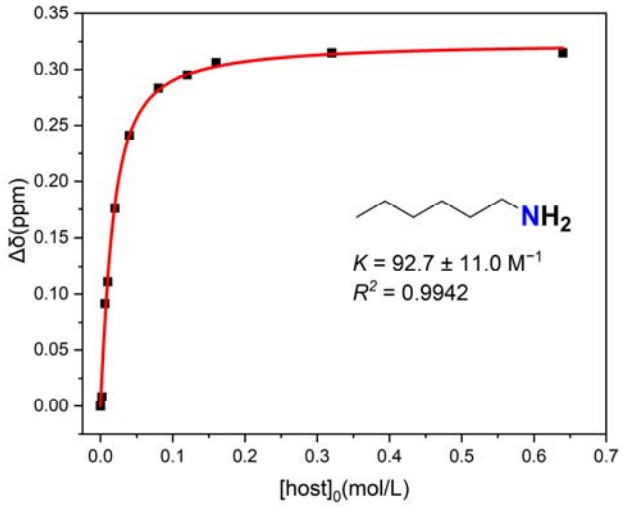

Figure S91. The nonlinear curve fitting of NMR titration (Δδ of H_α) for the complexation of **[P4-(OH)BPO]** (10.0 mM) with *n*-hexylamine (**2**) in $CDCl_3$ at 298 K.

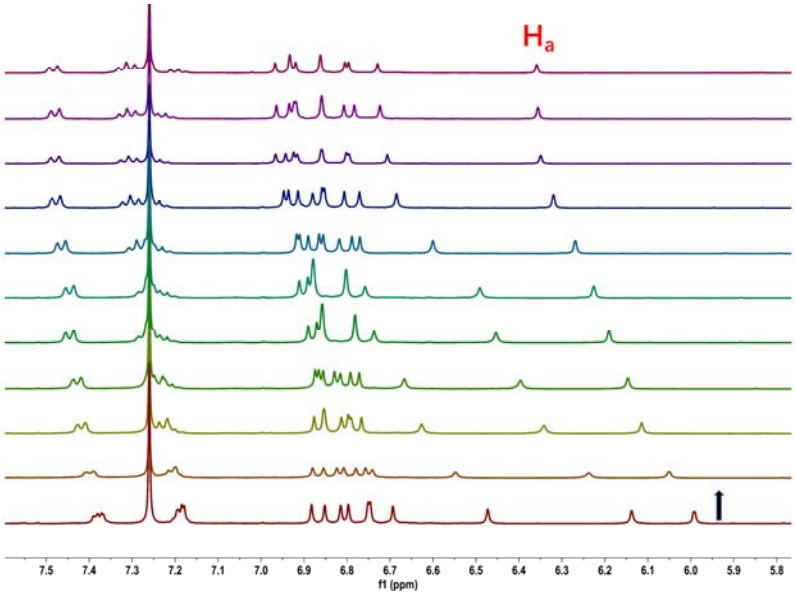

Figure S92. Partial ^{1}H NMR spectra (400 MHz, $CDCl_3$, 298 K) of a mixture of **[P4-(OH)BPO]** (10.0 mM) and *n*-octylamine (**3**) at the concentrations of 0, 2.0, 6.0, 10.0, 20.0, 40.0, 80.0, 120.0, 160.0, 320.0, and 640.0 mM (from bottom to top).

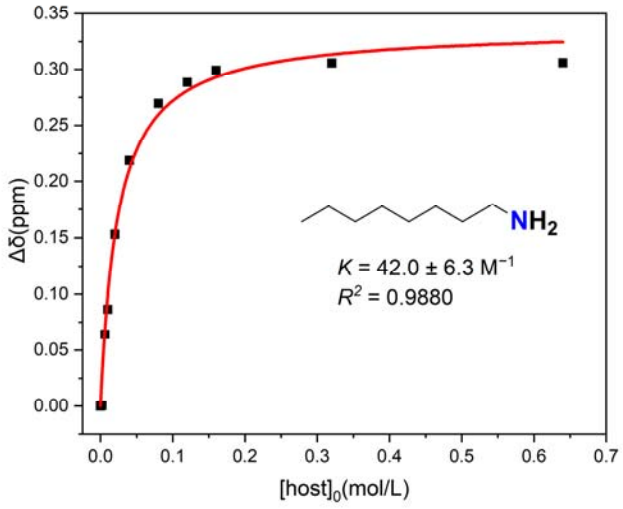

Figure S93. The nonlinear curve fitting of NMR titration (Δδ of H_α) for the complexation of **[P4-(OH)BPO]** (10.0 mM) with *n*-octylamine (**3**) in $CDCl_3$ at 298 K.

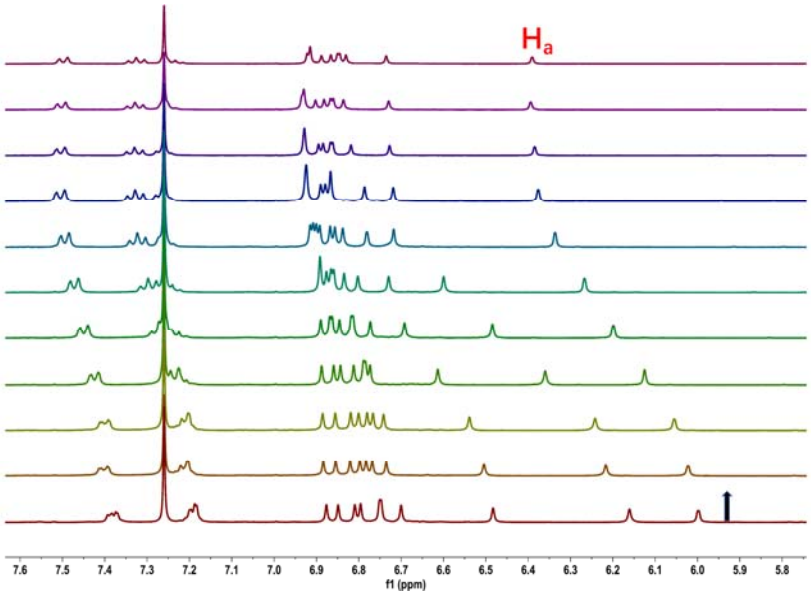

Figure S94. Partial ^{1}H NMR spectra (400 MHz, $CDCl_3$, 298 K) of a mixture of **[P4-(OH)BPO]** (10.0 mM) and *n*-butanol (**4**) at the concentrations of 0, 2.0, 6.0, 10.0, 20.0, 40.0, 80.0, 120.0, 160.0, 320.0, and 640.0 mM (from bottom to top).

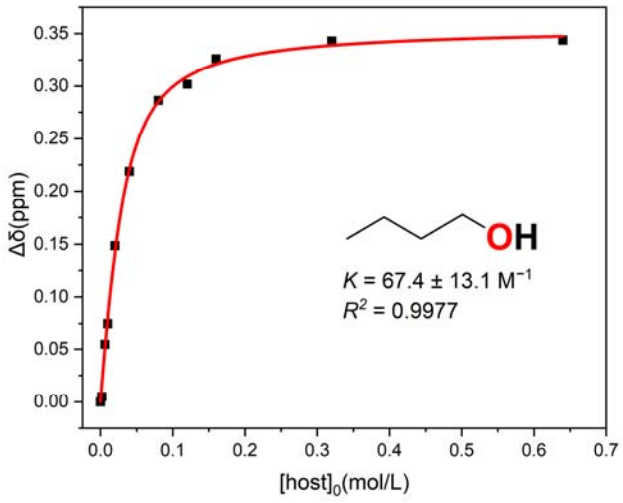

Figure S95. The nonlinear curve fitting of NMR titration ($\Delta\delta$ of H_α) for the complexation of **[P4-(OH)BPO]** (10.0 mM) with *n*-butanol (**4**) in $CDCl_3$ at 298 K.

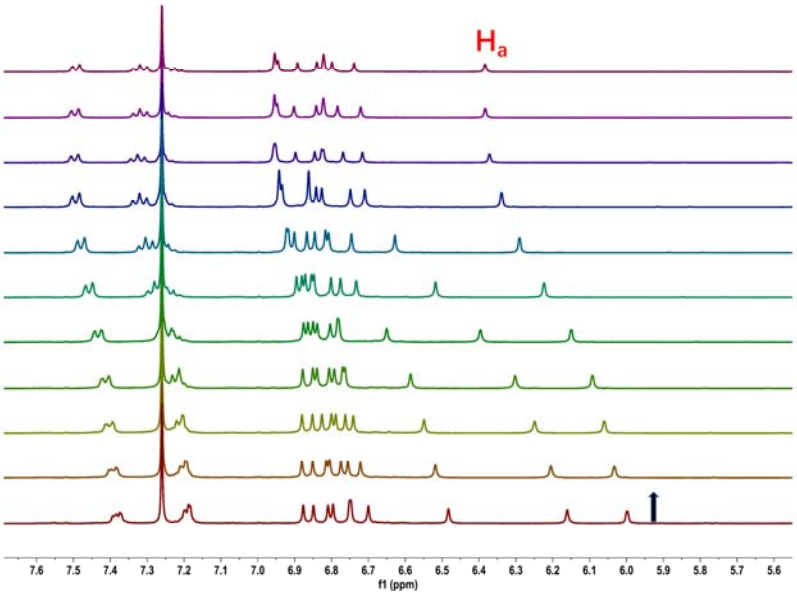

Figure S96. Partial ^{1}H NMR spectra (400 MHz, $CDCl_3$, 298 K) of a mixture of **[P4-(OH)BPO]** (10.0 mM) and *n*-hexanol (**5**) at the concentrations of 0, 2.0, 6.0, 10.0, 20.0, 40.0, 80.0, 120.0, 160.0, 320.0, and 640.0 mM (from bottom to top).

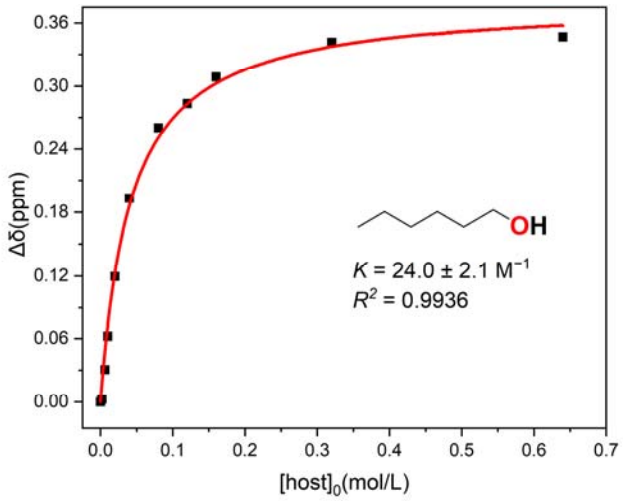

Figure S97. The nonlinear curve fitting of NMR titration (Δδ of H_α) for the complexation of **[P4-(OH)BPO]** (10.0 mM) with *n*-hexanol (**5**) in $CDCl_3$ at 298 K.

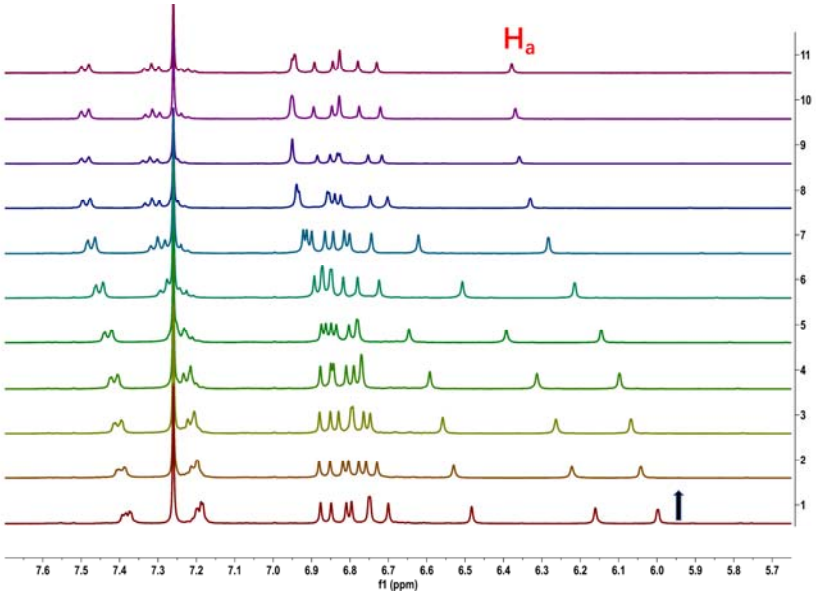

Figure S98. Partial ^{1}H NMR spectra (400 MHz, $CDCl_3$, 298 K) of a mixture of **[P4-(OH)BPO]** (10.0 mM) and *n*-octanol (**6**) at the concentrations of 0, 2.0, 6.0, 10.0, 20.0, 40.0, 80.0, 120.0, 160.0, 320.0, and 640.0 mM (from bottom to top).

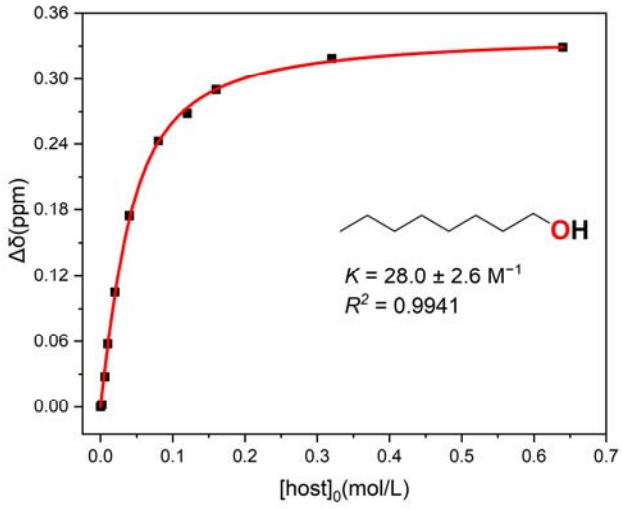

Figure S99. The nonlinear curve fitting of NMR titration ($\Delta\delta$ of H_α) for the complexation of **[P4-(OH)BPO]** (10.0 mM) with *n*-octanol (**6**) in $CDCl_3$ at 298 K.

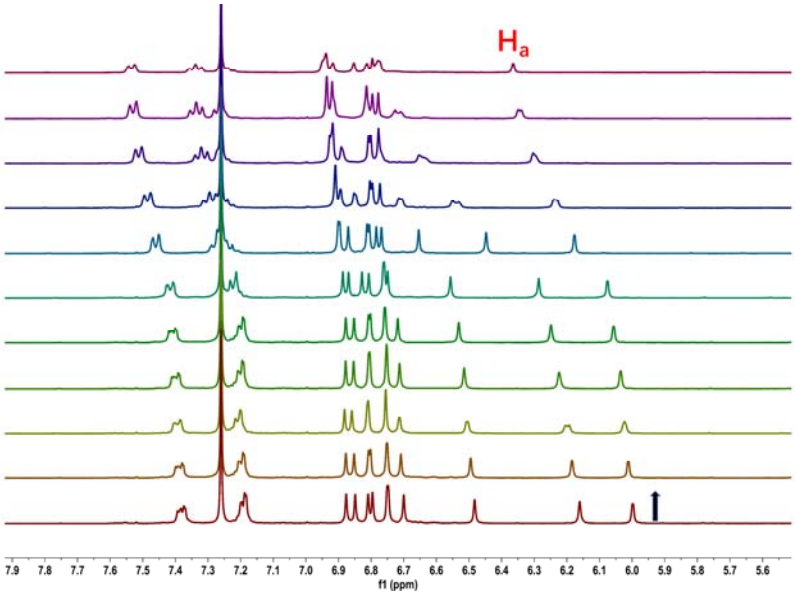

Figure S100. Partial ^{1}H NMR spectra (400 MHz, $CDCl_3$, 298 K) of a mixture of **[P4-(OH)BPO]** (10.0 mM) and *n*-butyraldehyde (**7**) at the concentrations of 0, 2.0, 6.0, 10.0, 20.0, 40.0, 80.0, 120.0, 160.0, 320.0, and 640.0 mM (from bottom to top).

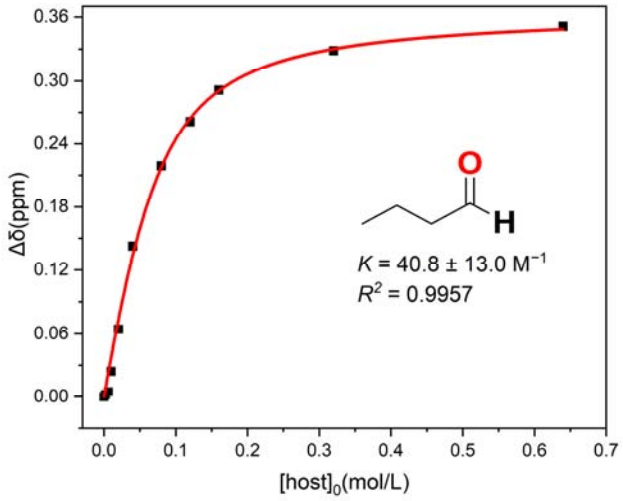

Figure S101. The nonlinear curve fitting of NMR titration (Δδ of H_α) for the complexation of **[P4-(OH)BPO]** (10.0 mM) with *n*-butyraldehyde (**7**) in $CDCl_3$ at 298 K.

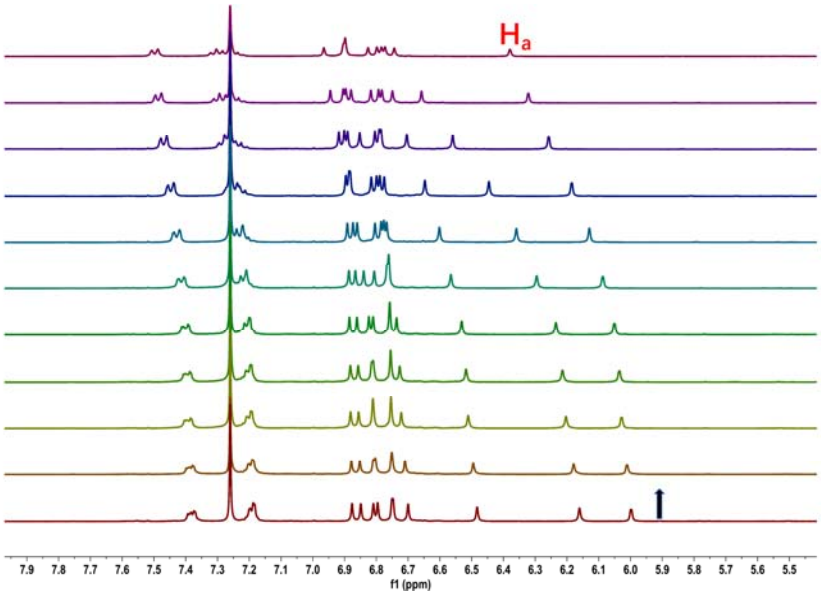

Figure S102. Partial ^{1}H NMR spectra (400 MHz, $CDCl_3$, 298 K) of a mixture of **[P4-(OH)BPO]** (10.0 mM) and *n*-hexanaldehyde (**8**) at the concentrations of 0, 2.0, 6.0, 10.0, 20.0, 40.0, 80.0, 120.0, 160.0, 320.0, and 640.0 mM (from bottom to top).

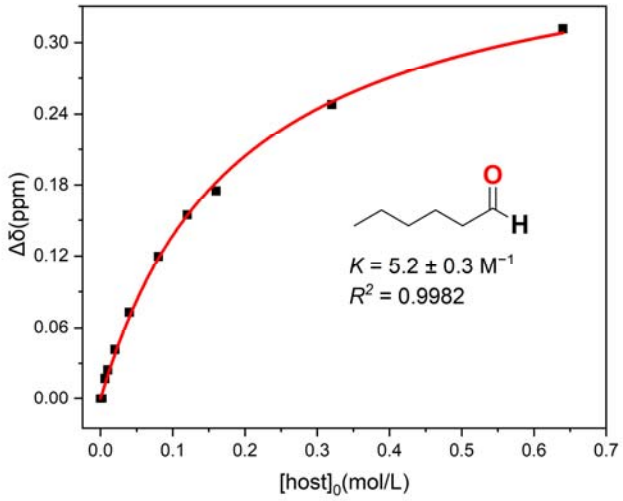

Figure S103. The nonlinear curve fitting of NMR titration ($\Delta\delta$ of H_α) for the complexation of **[P4-(OH)BPO]** (10.0 mM) with *n*-hexanaldehyde (**8**) in $CDCl_3$ at 298 K.

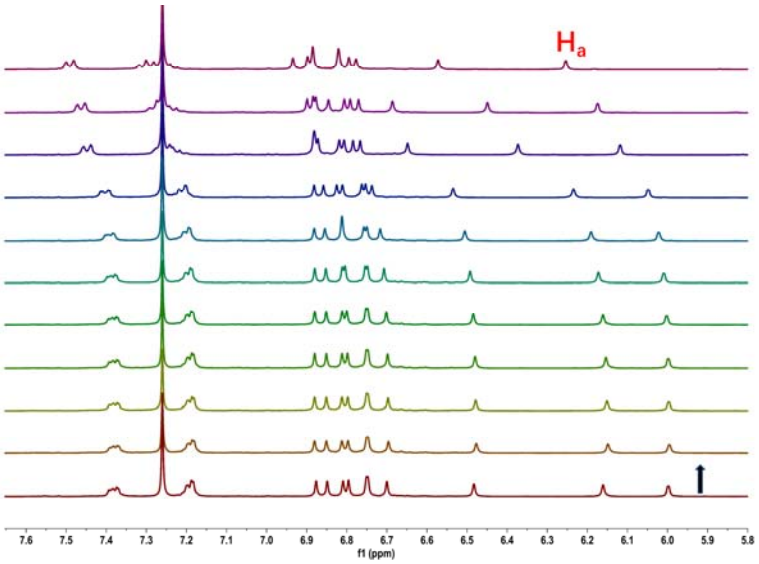

Figure S104. Partial ^{1}H NMR spectra (400 MHz, $CDCl_3$, 298 K) of a mixture of **[P4-(OH)BPO]** (10.0 mM) and *n*-octanaldehyde (**9**) at the concentrations of 0, 2.0, 6.0, 10.0, 20.0, 40.0, 80.0, 120.0, 160.0, 320.0, and 640.0 mM (from bottom to top).

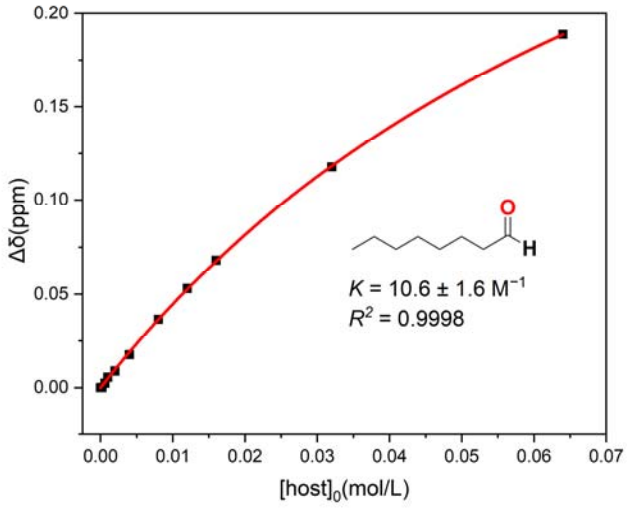

Figure S105. The nonlinear curve fitting of NMR titration ($\Delta\delta$ of H_α) for the complexation of **[P4-(OH)BPO]** (10.0 mM) with *n*-octanaldehyde (**9**) in $CDCl_3$ at 298 K.

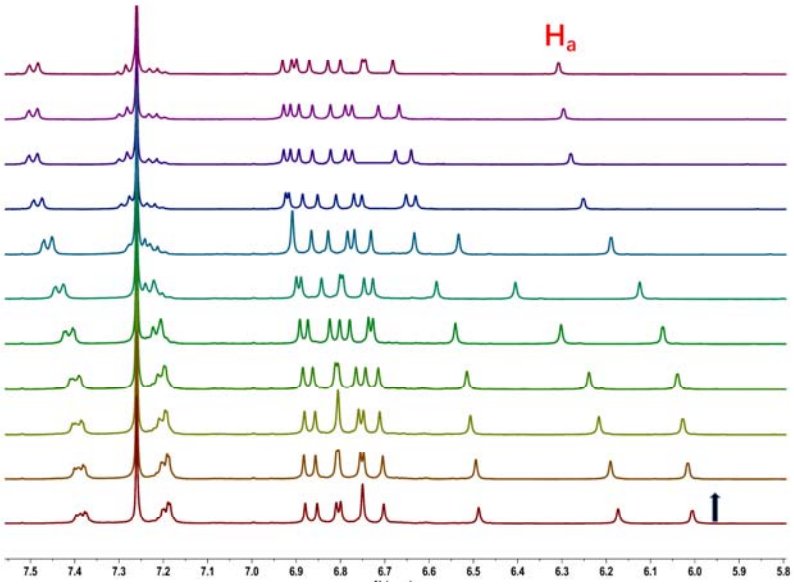

Figure S106. Partial ^{1}H NMR spectra (400 MHz, $CDCl_3$, 298 K) of a mixture of **[P4-(OH)BPO]** (10.0 mM) and methyl butyrate (**10**) at the concentrations of 0, 2.0, 6.0, 10.0, 20.0, 40.0, 80.0, 120.0, 160.0, 320.0, and 640.0 mM (from bottom to top).

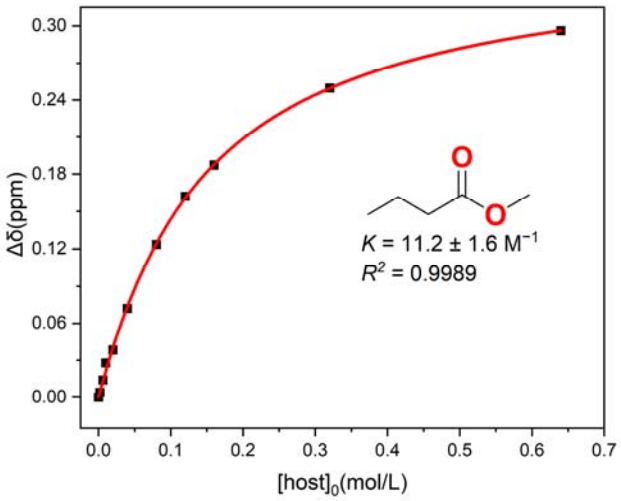

Figure S107. The nonlinear curve fitting of NMR titration ($\Delta\delta$ of H_α) for the complexation of **[P4-(OH)BPO]** (10.0 mM) with methyl butyrate (**10**) in $CDCl_3$ at 298 K.

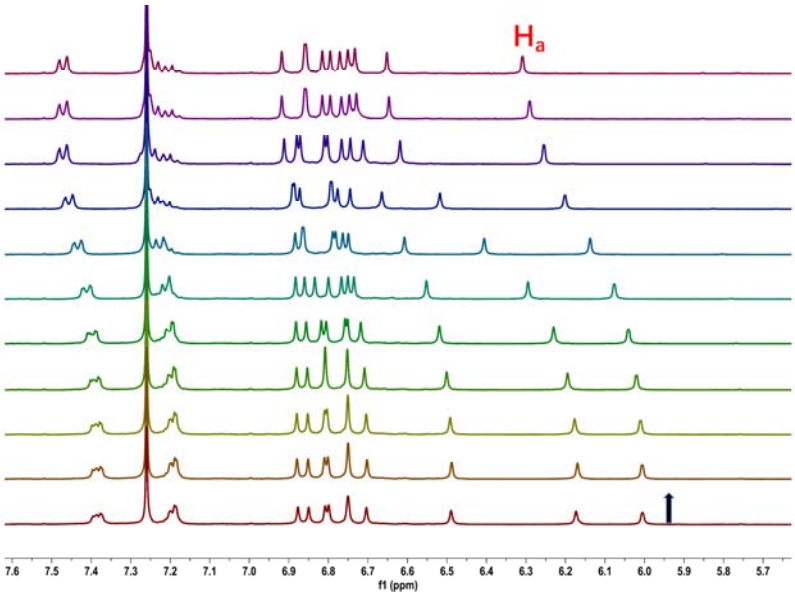

Figure S108. Partial ^{1}H NMR spectra (400 MHz, $CDCl_3$, 298 K) of a mixture of **[P4-(OH)BPO]** (10.0 mM) and methyl hexanoate (**11**) at the concentrations of 0, 2.0, 6.0, 10.0, 20.0, 40.0, 80.0, 120.0, 160.0, 320.0, and 640.0 mM (from bottom to top).

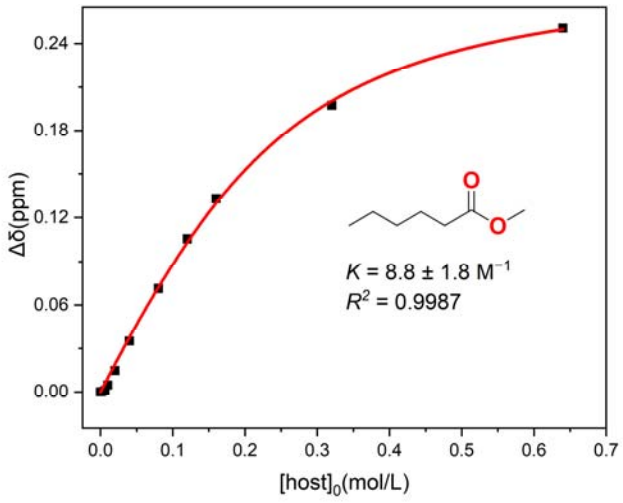

Figure S109. The nonlinear curve fitting of NMR titration (Δδ of H_α) for the complexation of **[P4-(OH)BPO]** (10.0 mM) with methyl hexanoate (**11**) in $CDCl_3$ at 298 K.

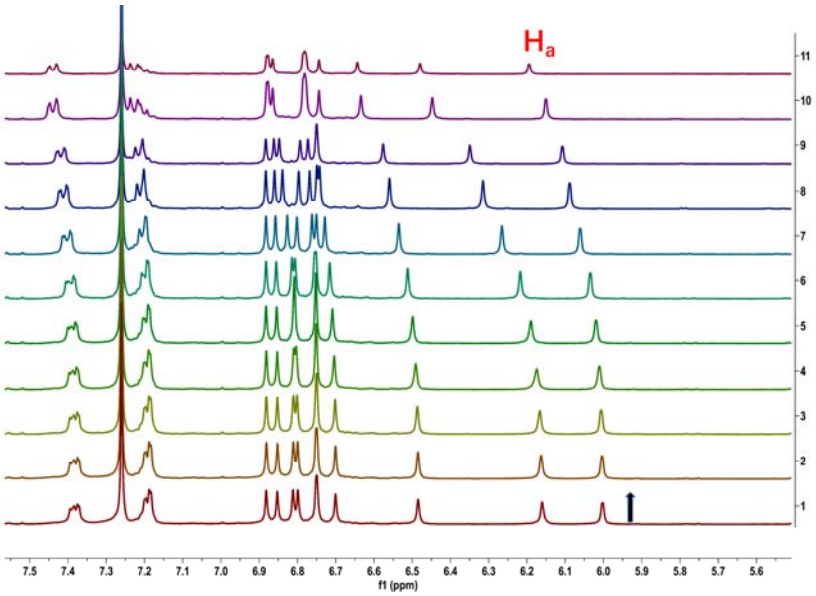

Figure S110. Partial ^{1}H NMR spectra (400 MHz, $CDCl_3$, 298 K) of a mixture of **[P4-(OH)BPO]** (10.0 mM) and methyl octanoate (**12**) at the concentrations of 0, 2.0, 6.0, 10.0, 20.0, 40.0, 80.0, 120.0, 160.0, 320.0, and 640.0 mM (from bottom to top).

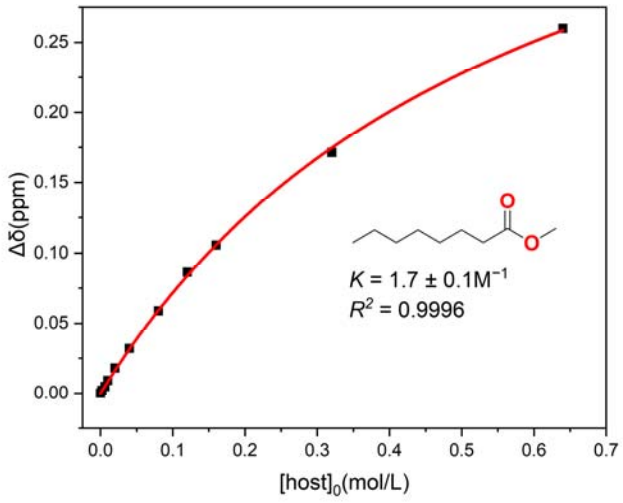

Figure S111. The nonlinear curve fitting of NMR titration ($\Delta\delta$ of H_α) for the complexation of **[P4-(OH)BPO]** (10.0 mM) with methyl octanoate (**12**) in $CDCl_3$ at 298 K.

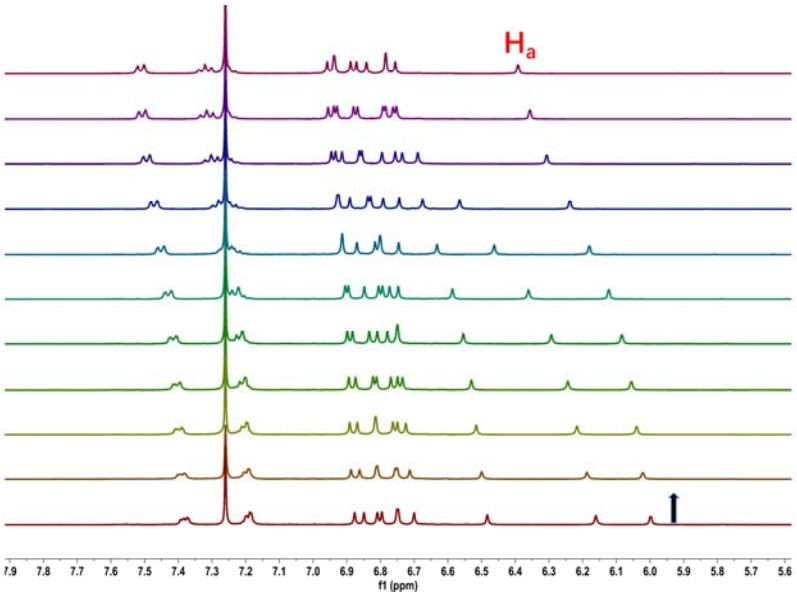

Figure S112. Partial ^{1}H NMR spectra (400 MHz, $CDCl_3$, 298 K) of a mixture of **[P4-(OH)BPO]** (10.0 mM) and *n*-butanoic acid (**13**) at the concentrations of 0, 2.0, 6.0, 10.0, 20.0, 40.0, 80.0, 120.0, 160.0, 320.0, and 640.0 mM (from bottom to top).

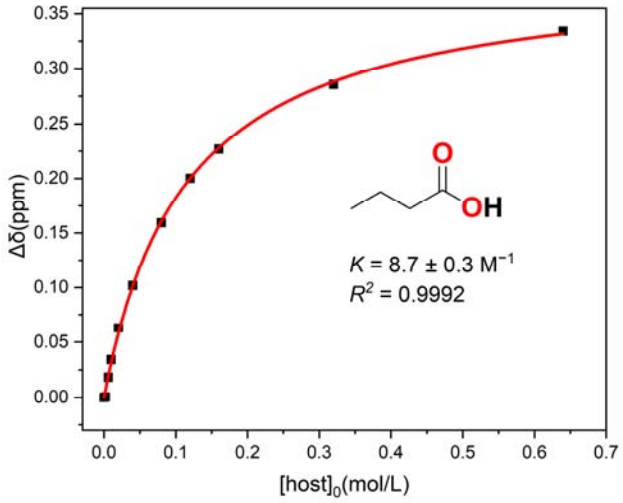

Figure S113. The nonlinear curve fitting of NMR titration (Δδ of H_α) for the complexation of **[P4-(OH)BPO]** (10.0 mM) with *n*-butanoic acid (**13**) in $CDCl_3$ at 298 K.

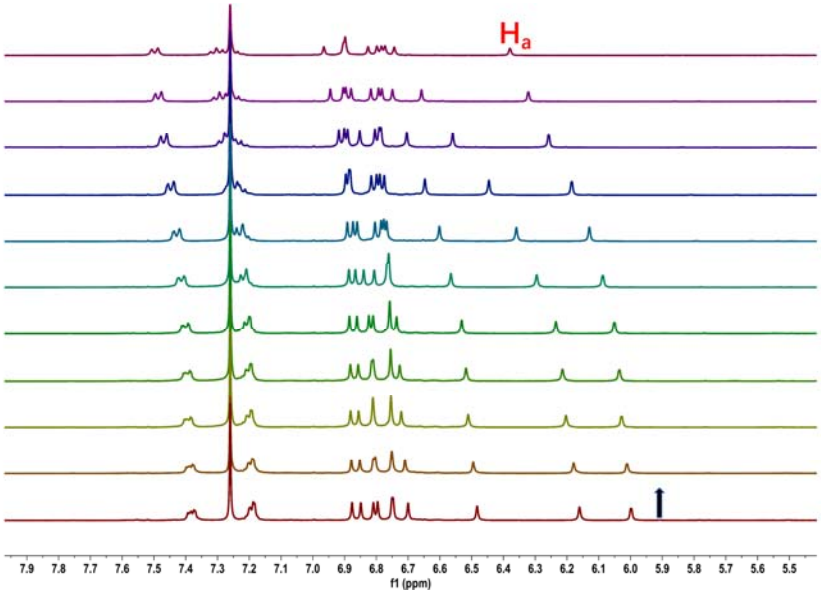

Figure S114. Partial ^{1}H NMR spectra (400 MHz, $CDCl_3$, 298 K) of a mixture of **[P4-(OH)BPO]** (10.0 mM) and *n*-hexanoic acid (**14**) at the concentrations of 0, 2.0, 6.0, 10.0, 20.0, 40.0, 80.0, 120.0, 160.0, 320.0, and 640.0 mM (from bottom to top).

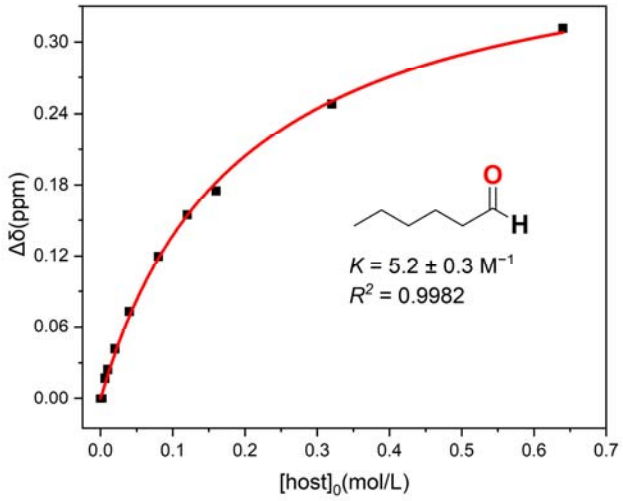

Figure S115. The nonlinear curve fitting of NMR titration ($\Delta\delta$ of H_α) for the complexation of **[P4-(OH)BPO]** (10.0 mM) with *n*-hexanoic acid (**14**) in $CDCl_3$ at 298 K.

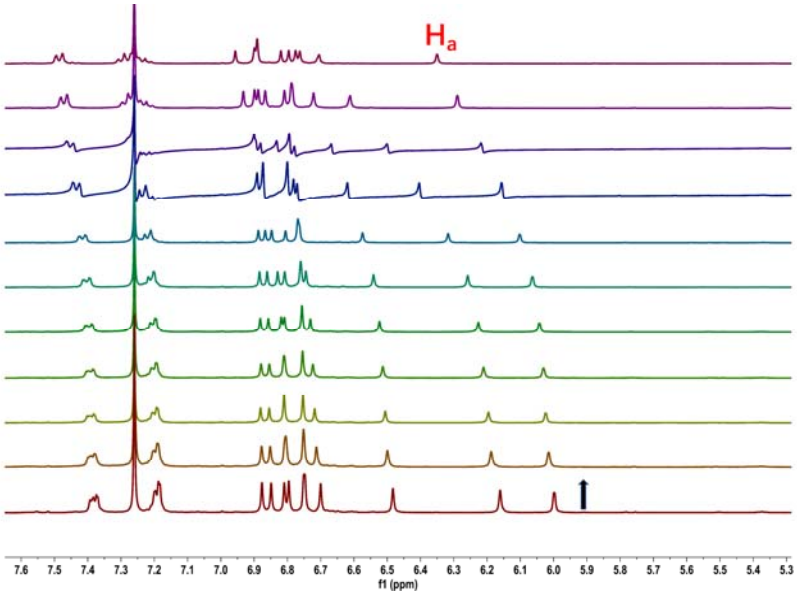

Figure S116. Partial ^{1}H NMR spectra (400 MHz, $CDCl_3$, 298 K) of a mixture of **[P4-(OH)BPO]** (10.0 mM) and *n*-octanoic acid (**15**) at the concentrations of 0, 2.0, 6.0, 10.0, 20.0, 40.0, 80.0, 120.0, 160.0, 320.0, and 640.0 mM (from bottom to top).

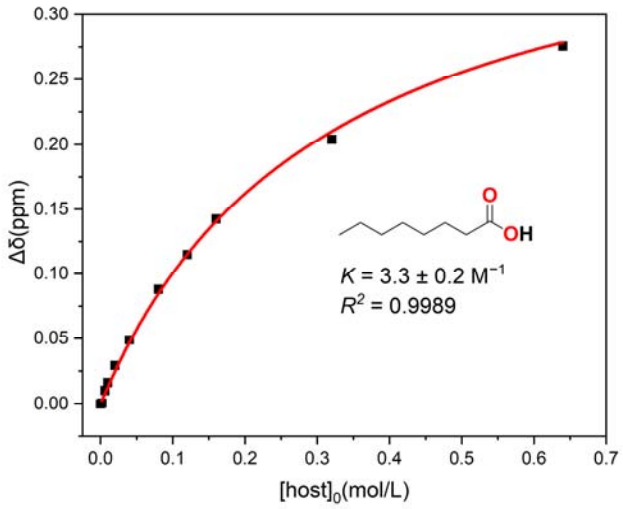

Figure S117. The nonlinear curve fitting of NMR titration (Δδ of H_α) for the complexation of **[P4-(OH)BPO]** (10.0 mM) with *n*-octanoic acid (**15**) in $CDCl_3$ at 298 K.

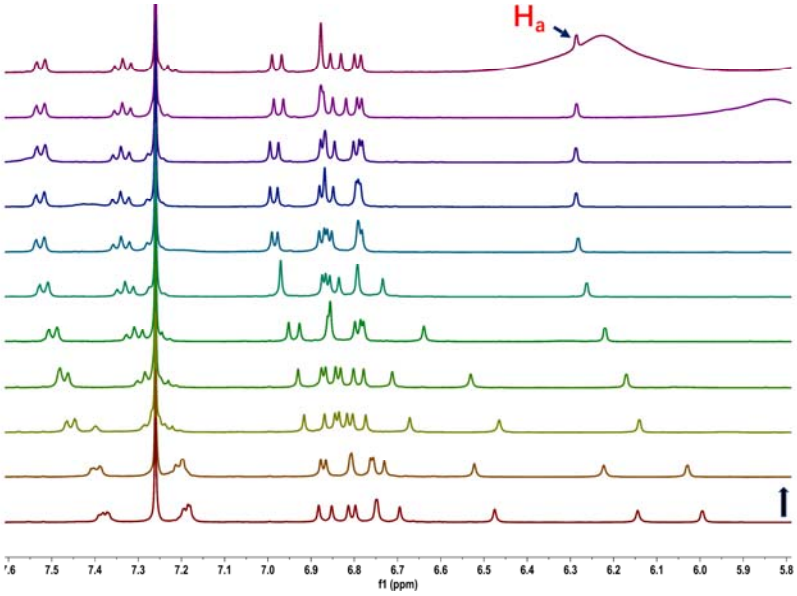

Figure S118. Partial ^{1}H NMR spectra (400 MHz, $CDCl_3$, 298 K) of a mixture of **[P4-(OH)BPO]** (10.0 mM) and *N*-methylformamide (**16**) at the concentrations of 0, 2.0, 6.0, 10.0, 20.0, 40.0, 80.0, 120.0, 160.0, 320.0, and 640.0 mM (from bottom to top).

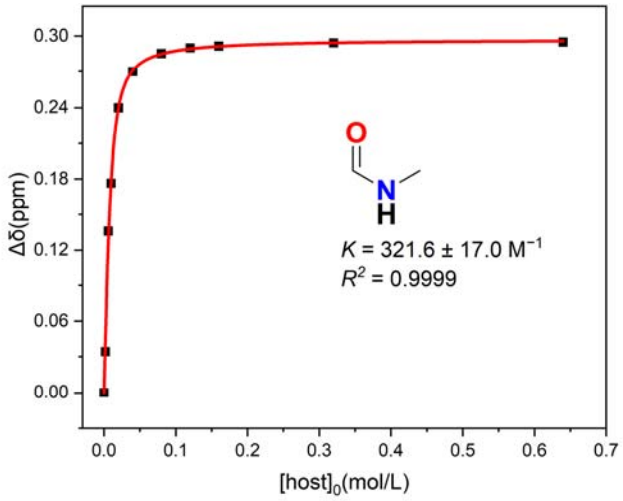

Figure S119. The nonlinear curve fitting of NMR titration (Δδ of H_α) for the complexation of **[P4-(OH)BPO]** (10.0 mM) with *N*-methylformamide (**16**) in $CDCl_3$ at 298 K.

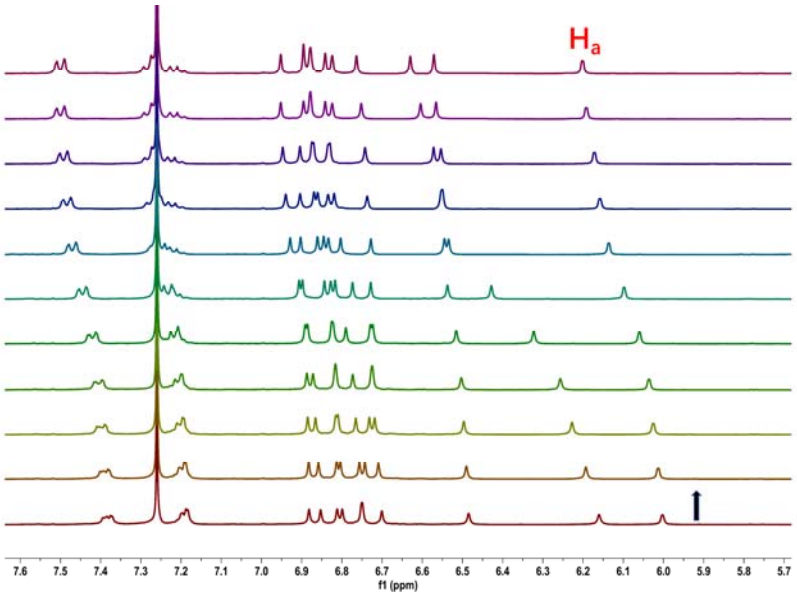

Figure S120. Partial ^{1}H NMR spectra (400 MHz, $CDCl_3$, 298 K) of a mixture of **[P4-(OH)BPO]** (10.0 mM) and *N*,*N*-dimethylformamide (**17**) at the concentrations of 0, 2.0, 6.0, 10.0, 20.0, 40.0, 80.0, 120.0, 160.0, 320.0, and 640.0 mM (from bottom to top).

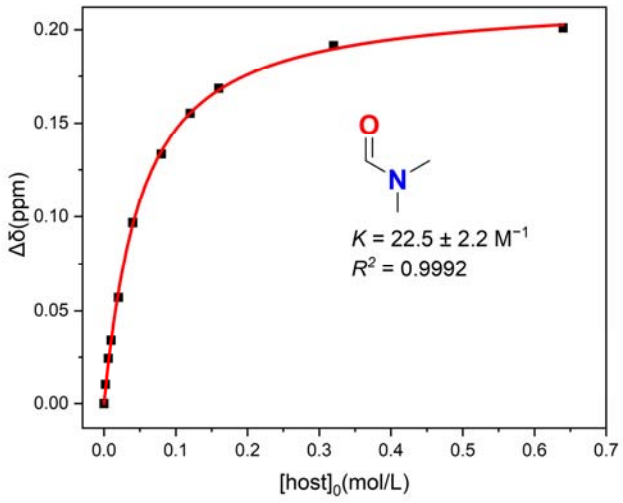

Figure S121. The nonlinear curve fitting of NMR titration ($\Delta\delta$ of H_α) for the complexation of **[P4-(OH)BPO]** (10.0 mM) with *N*,*N*-dimethylformamide (**17**) in $CDCl_3$ at 298 K.

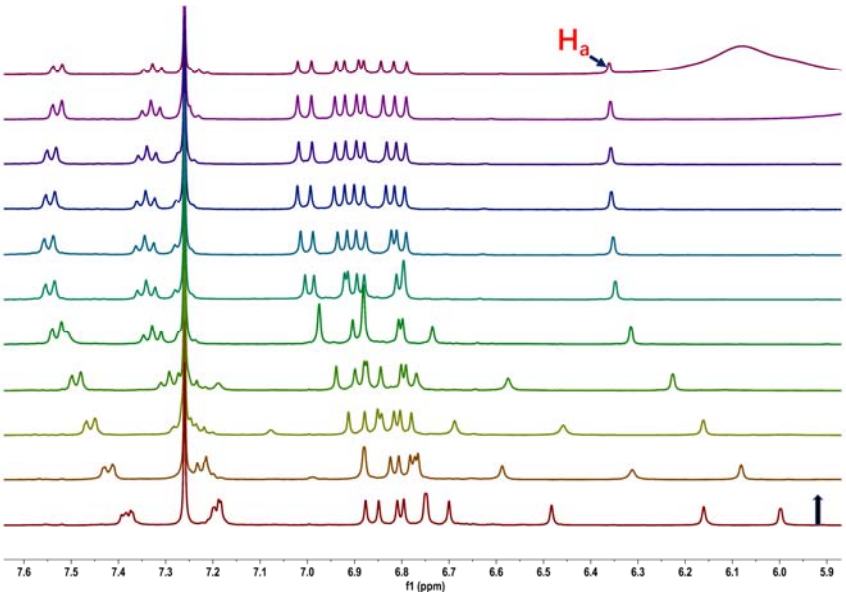

Figure S122. Partial ^{1}H NMR spectra (400 MHz, $CDCl_3$, 298 K) of a mixture of **[P4-(OH)BPO]** (10.0 mM) and *N*-ethylformamide (**18**) at the concentrations of 0, 2.0, 6.0, 10.0, 20.0, 40.0, 80.0, 120.0, 160.0, 320.0, and 640.0 mM (from bottom to top).

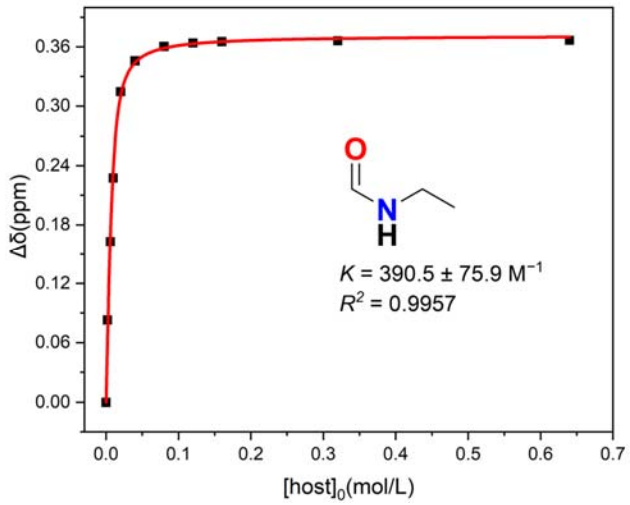

Figure S123. The nonlinear curve fitting of NMR titration (Δδ of H_α) for the complexation of **[P4-(OH)BPO]** (10.0 mM) with *N*-ethylformamide (**18**) in $CDCl_3$ at 298 K.

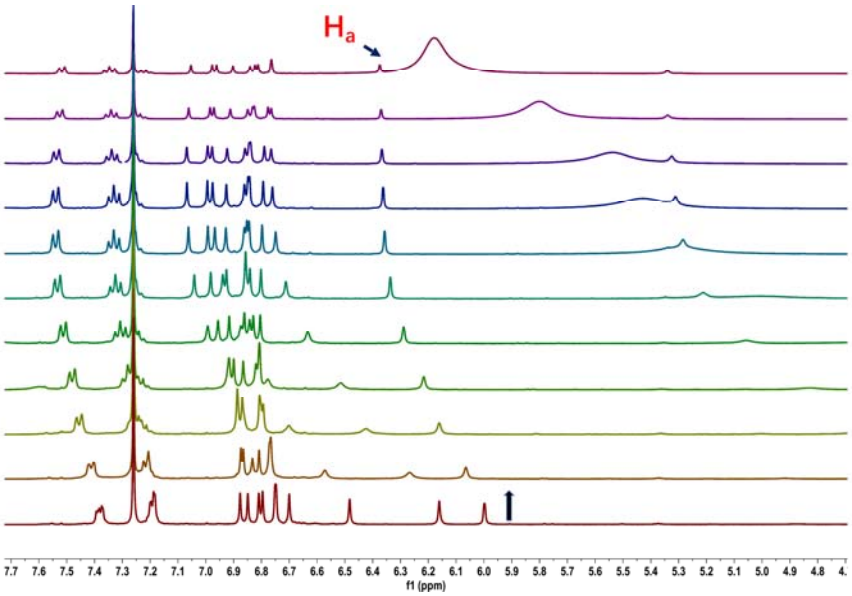

Figure S124. Partial ^{1}H NMR spectra (400 MHz, $CDCl_3$, 298 K) of a mixture of **[P4-(OH)BPO]** (10.0 mM) and *N*-octylformamide (**19**) at the concentrations of 0, 2.0, 6.0, 10.0, 20.0, 40.0, 80.0, 120.0, 160.0, 320.0, and 640.0 mM (from bottom to top).

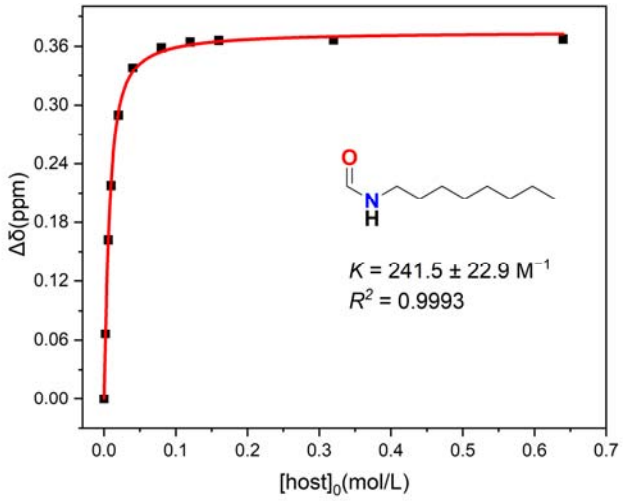

Figure S125. The nonlinear curve fitting of NMR titration ($\Delta\delta$ of H_α) for the complexation of **[P4-(OH)BPO]** (10.0 mM) with *N*-octylformamide (**19**) in $CDCl_3$ at 298 K.

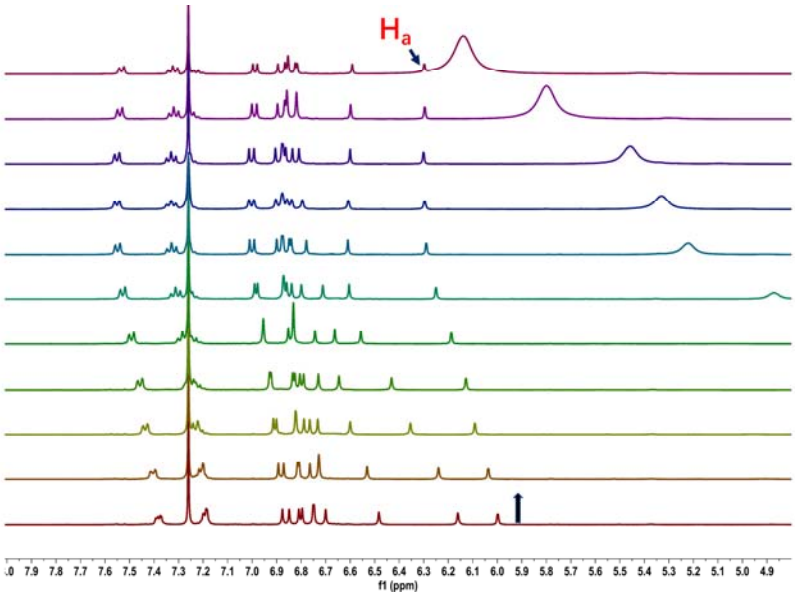

Figure S126. Partial ^{1}H NMR spectra (400 MHz, $CDCl_3$, 298 K) of a mixture of **[P4-(OH)BPO]** (10.0 mM) and *N*-methylacetamide (**20**) at the concentrations of 0, 2.0, 6.0, 10.0, 20.0, 40.0, 80.0, 120.0, 160.0, 320.0, and 640.0 mM (from bottom to top).

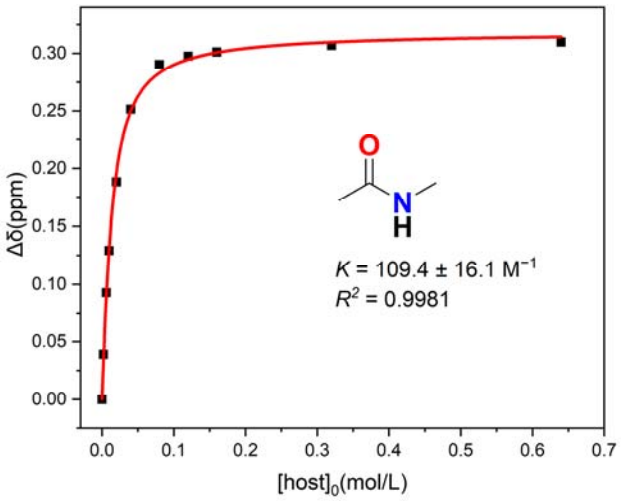

Figure S127. The nonlinear curve fitting of NMR titration ($\Delta\delta$ of H_α) for the complexation of **[P4-(OH)BPO]** (10.0 mM) with *N*-methylacetamide (**20**) in $CDCl_3$ at 298 K.

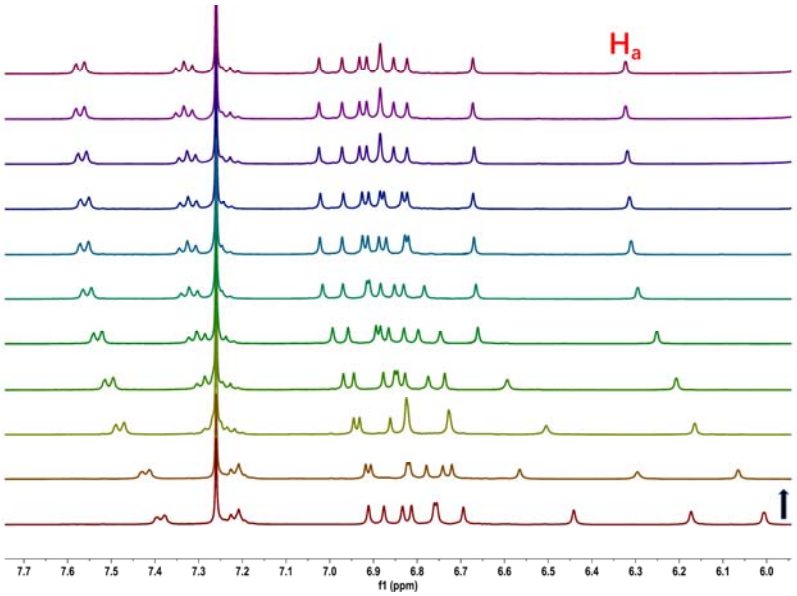

Figure S128. Partial ^{1}H NMR spectra (400 MHz, $CDCl_3$, 298 K) of a mixture of **[P4-(OH)BPO]** (10.0 mM) and *N*-ethylacetamide (**21**) at the concentrations of 0, 2.0, 6.0, 10.0, 20.0, 40.0, 80.0, 120.0, 160.0, 320.0, and 640.0 mM (from bottom to top).

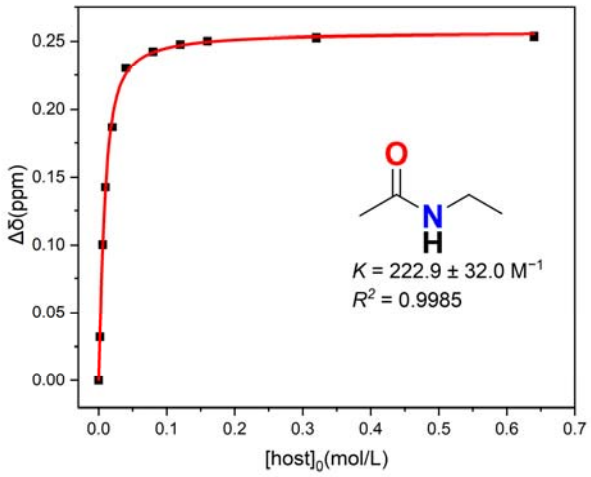

Figure S129. The nonlinear curve fitting of NMR titration ($\Delta\delta$ of H_α) for the complexation of **[P4-(OH)BPO]** (10.0 mM) with *N*-ethylacetamide (**21**) in $CDCl_3$ at 298 K.

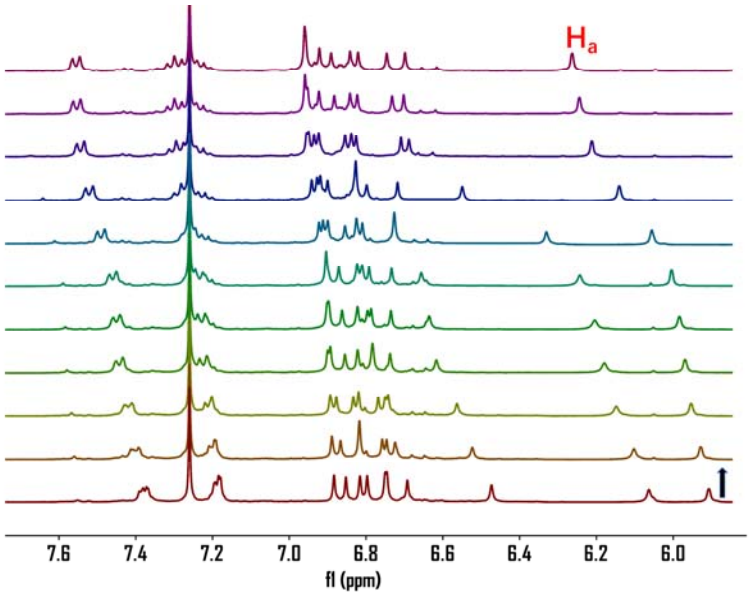

Figure S130. Partial ^{1}H NMR spectra (400 MHz, $CDCl_3$, 298 K) of a mixture of **[P4-(OH)BPO]** (10.0 mM) and *N*-propylacetamide (**22**) at the concentrations of 0, 2.0, 6.0, 10.0, 20.0, 40.0, 80.0, 120.0, 160.0, 320.0, and 640.0 mM (from bottom to top).

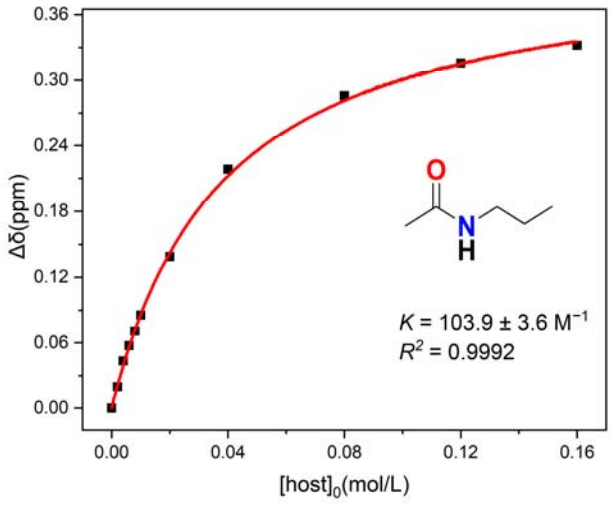

Figure S131. The nonlinear curve fitting of NMR titration ($\Delta\delta$ of H_α) for the complexation of **[P4-(OH)BPO]** (10.0 mM) with *N*-propylacetamide (**22**) in $CDCl_3$ at 298 K.

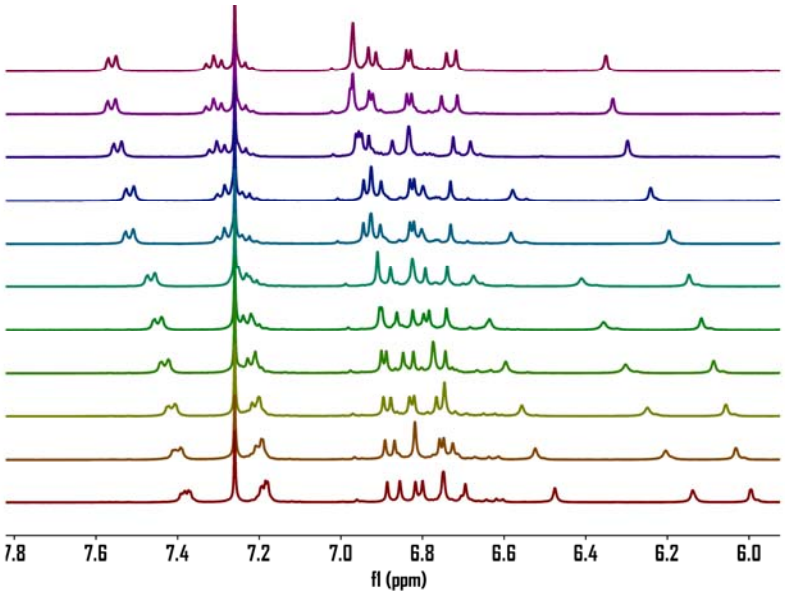

Figure S132. Partial ^{1}H NMR spectra (400 MHz, $CDCl_3$, 298 K) of a mixture of **[P4-(OH)BPO]** (10.0 mM) and *N*-butylacetamide (**23**) at the concentrations of 0, 2.0, 6.0, 10.0, 20.0, 40.0, 80.0, 120.0, 160.0, 320.0, and 640.0 mM (from bottom to top).

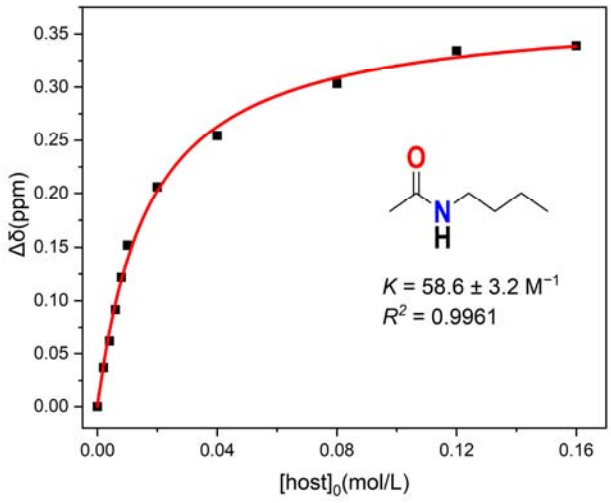

Figure S133. The nonlinear curve fitting of NMR titration ($\Delta\delta$ of H_α) for the complexation of **[P4-(OH)BPO]** (10.0 mM) with *N*-methylpropionamide (**24**) in $CDCl_3$ at 298 K.

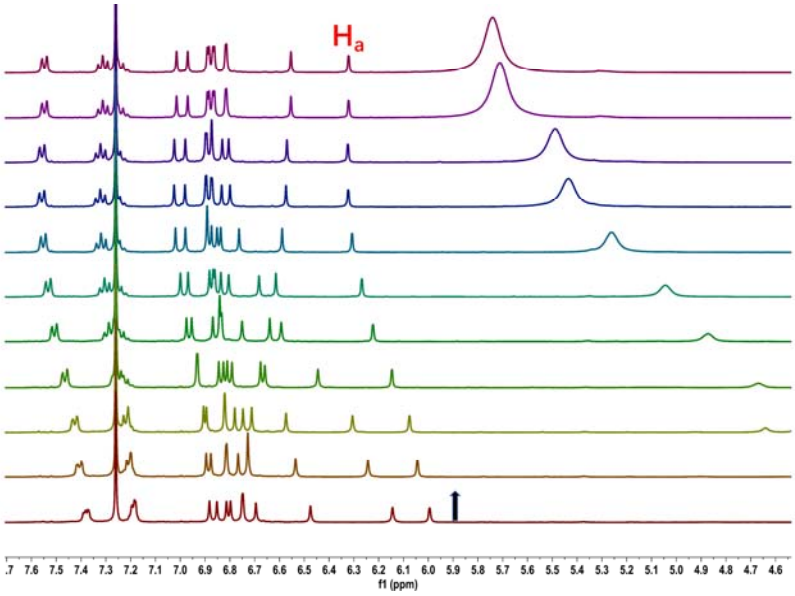

Figure S134. Partial ^{1}H NMR spectra (400 MHz, $CDCl_3$, 298 K) of a mixture of **[P4-(OH)BPO]** (10.0 mM) and *N*-methylpropionamide (**24**) at the concentrations of 0, 2.0, 6.0, 10.0, 20.0, 40.0, 80.0, 120.0, 160.0, 320.0, and 640.0 mM (from bottom to top).

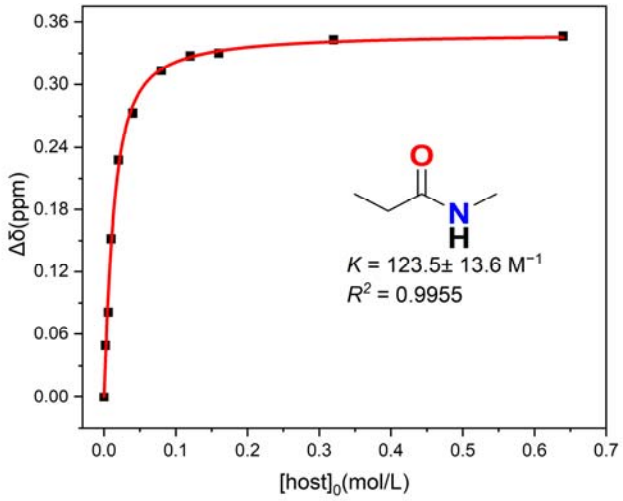

Figure S135. The nonlinear curve fitting of NMR titration ($\Delta\delta$ of H_α) for the complexation of **[P4-(OH)BPO]** (10.0 mM) with *N*-methylpropionamide (**24**) in $CDCl_3$ at 298 K.

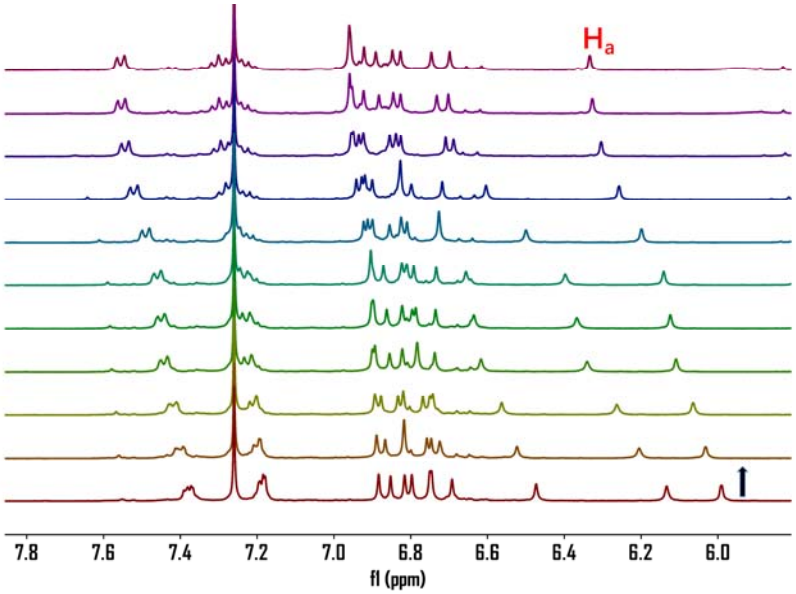

Figure S136. Partial ^{1}H NMR spectra (400 MHz, $CDCl_3$, 298 K) of a mixture of **[P4-(OH)BPO]** (10.0 mM) and *N*-butylpentanamide (**25**) at the concentrations of 0, 2.0, 6.0, 10.0, 20.0, 40.0, 80.0, 120.0, 160.0, 320.0, and 640.0 mM (from bottom to top).

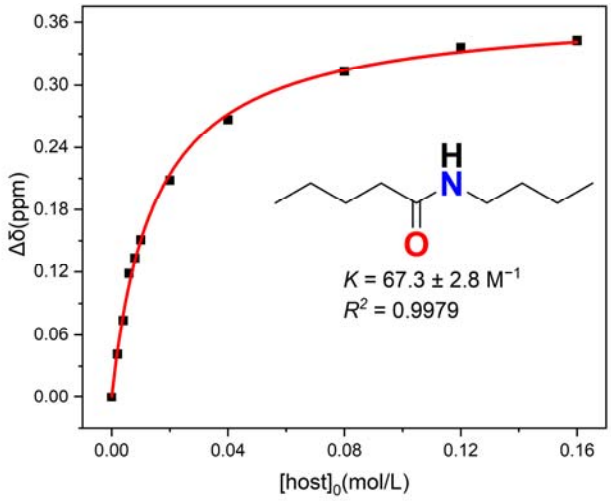

Figure S137. The nonlinear curve fitting of NMR titration ($\Delta\delta$ of H_α) for the complexation of **[P4-(OH)BPO]** (10.0 mM) with *N*-butylpentanamide (**25**) in $CDCl_3$ at 298 K.

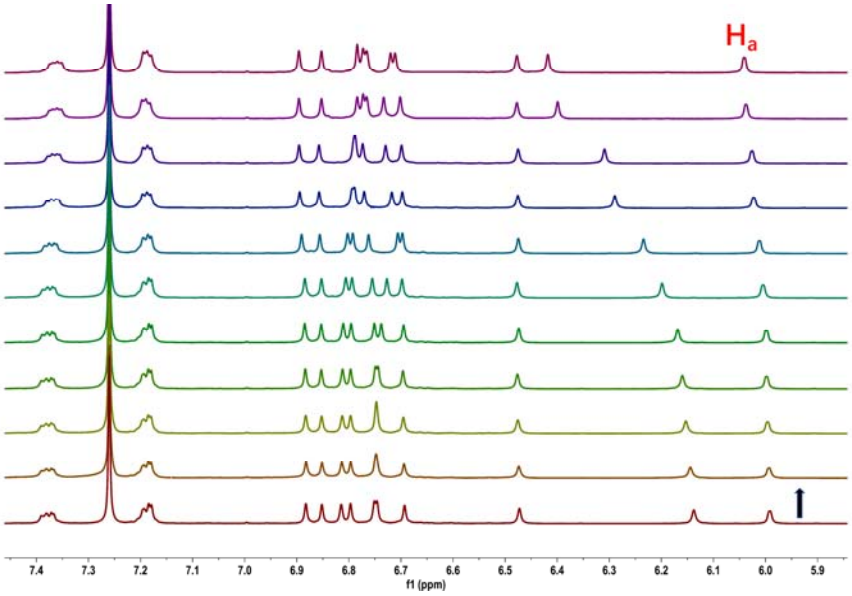

Figure S138. Partial ^{1}H NMR spectra (400 MHz, $CDCl_3$, 298 K) of a mixture of **[P4-(OH)BPO]** (10.0 mM) and *N*-methyl pyrrolidone (**26**) at the concentrations of 0, 2.0, 6.0, 10.0, 20.0, 40.0, 80.0, 120.0, 160.0, 320.0, and 640.0 mM (from bottom to top).

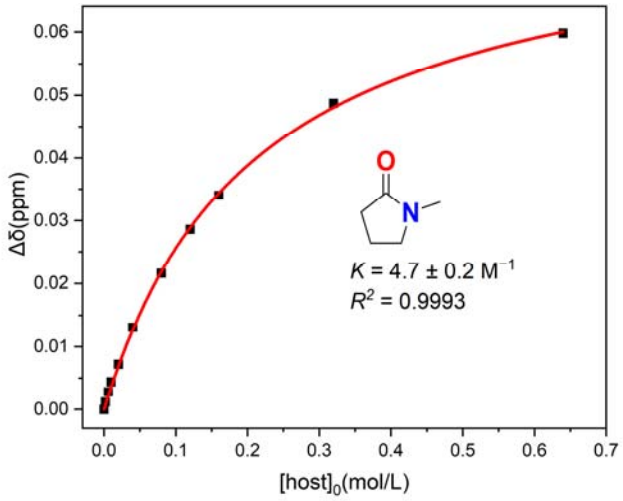

Figure S139. The nonlinear curve fitting of NMR titration (Δδ of H_α) for the complexation of**[P4-(OH)BPO]** (10.0 mM) with *N*-methyl pyrrolidone (**26**) in $CDCl_3$ at 298 K.

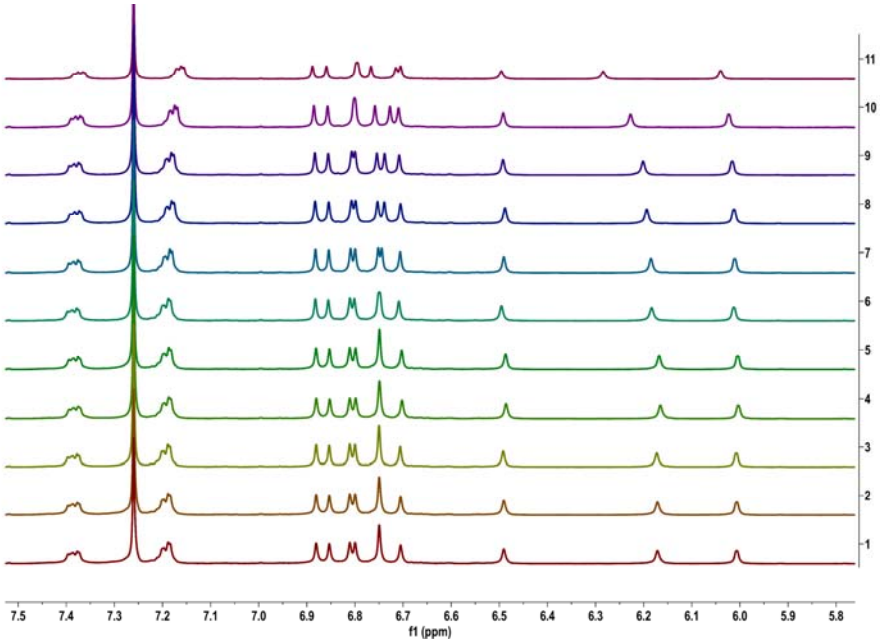

Figure S140. Partial ^{1}H NMR spectra (400 MHz, $CDCl_3$, 298 K) of a mixture of **[P4-(OH)BPO]** (10.0 mM) and THF (**27**) at the concentrations of 0, 2.0, 6.0, 10.0, 20.0, 40.0, 80.0, 120.0, 160.0, 320.0, and 640.0 mM (from bottom to top).

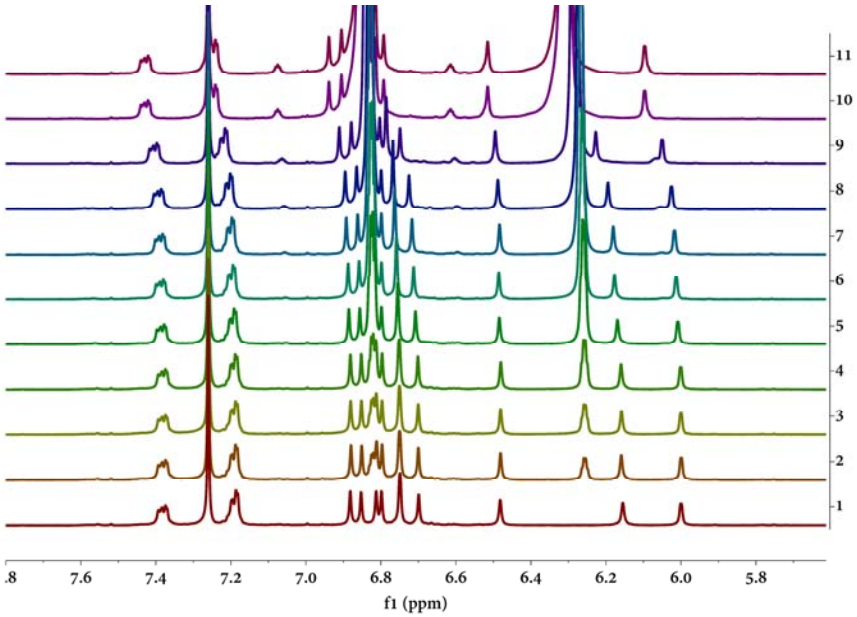

Figure S141. Partial ^{1}H NMR spectra (400 MHz, $CDCl_3$, 298 K) of a mixture of **[P4-(OH)BPO]** (10.0 mM) and pyrole (**28**) at the concentrations of 0, 2.0, 6.0, 10.0, 20.0, 40.0, 80.0, 120.0, 160.0, 320.0, and 640.0 mM (from bottom to top).

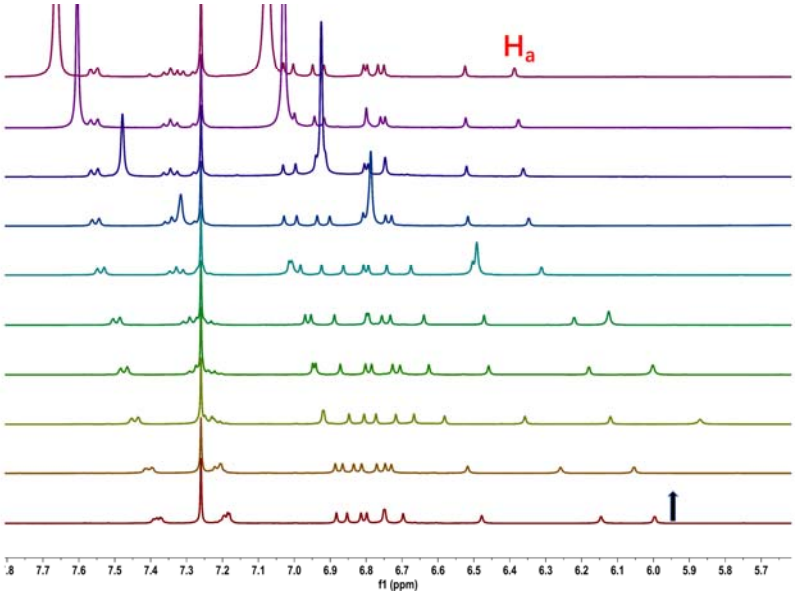

Figure S142. Partial ^{1}H NMR spectra (400 MHz, $CDCl_3$, 298 K) of a mixture of **[P4-(OH)BPO]** (10.0 mM) and imidazole (**29**) at the concentrations of 0, 2.0, 6.0, 10.0, 20.0, 40.0, 80.0, 120.0, 160.0, 320.0, and 640.0 mM (from bottom to top).

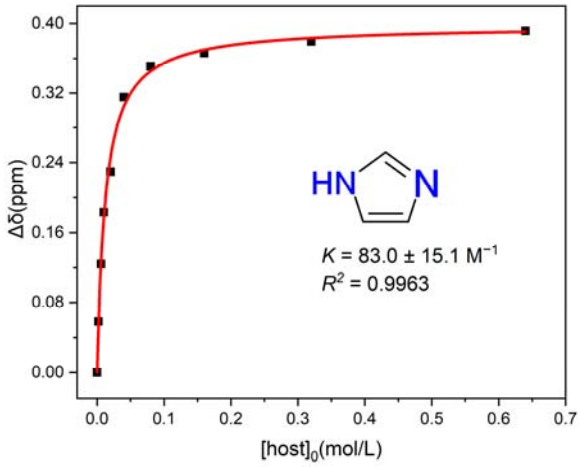

Figure S143. The nonlinear curve fitting of NMR titration ($\Delta\delta$ of H_α) for the complexation of **[P4-(OH)BPO]** (10.0 mM) with imidazole (**29**) in $CDCl_3$ at 298 K.

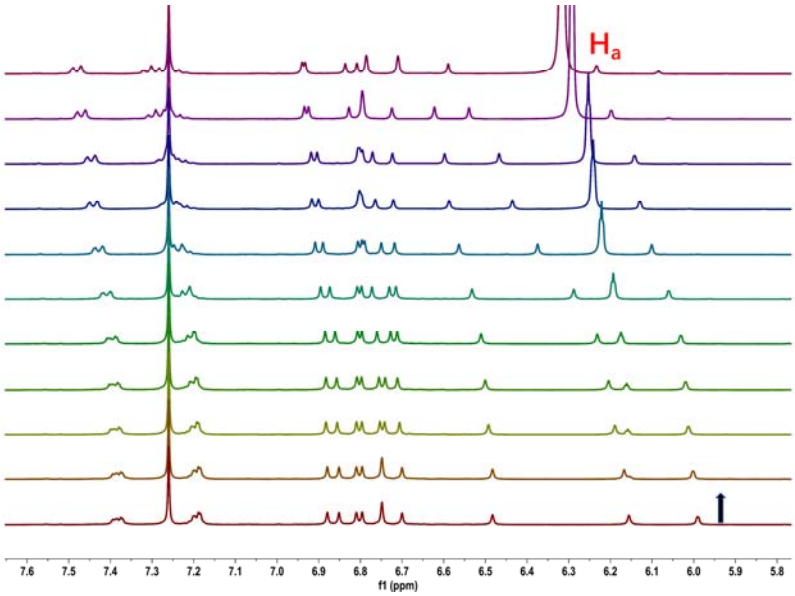

Figure S144. Partial ^{1}H NMR spectra (400 MHz, $CDCl_3$, 298 K) of a mixture of **[P4-(OH)BPO]** (10.0 mM) and oxazole (**30**) at the concentrations of 0, 2.0, 6.0, 10.0, 20.0, 40.0, 80.0, 120.0, 160.0, 320.0, and 640.0 mM (from bottom to top).

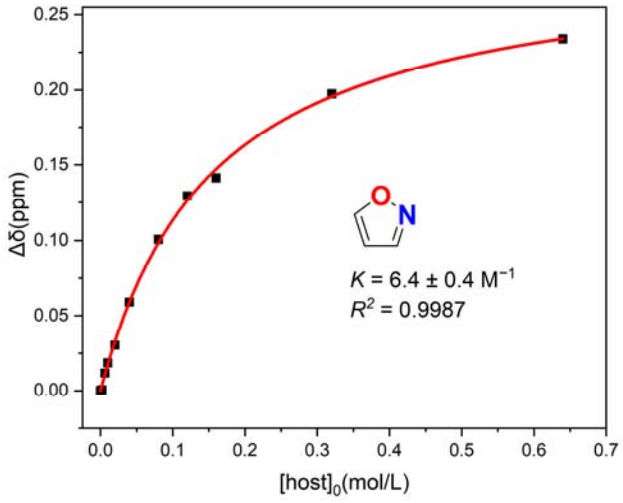

Figure S145. The nonlinear curve fitting of NMR titration ($\Delta\delta$ of H_α) for the complexation of **[P4-(OH)BPO]** (10.0 mM) with oxazole (**30**) in $CDCl_3$ at 298 K.

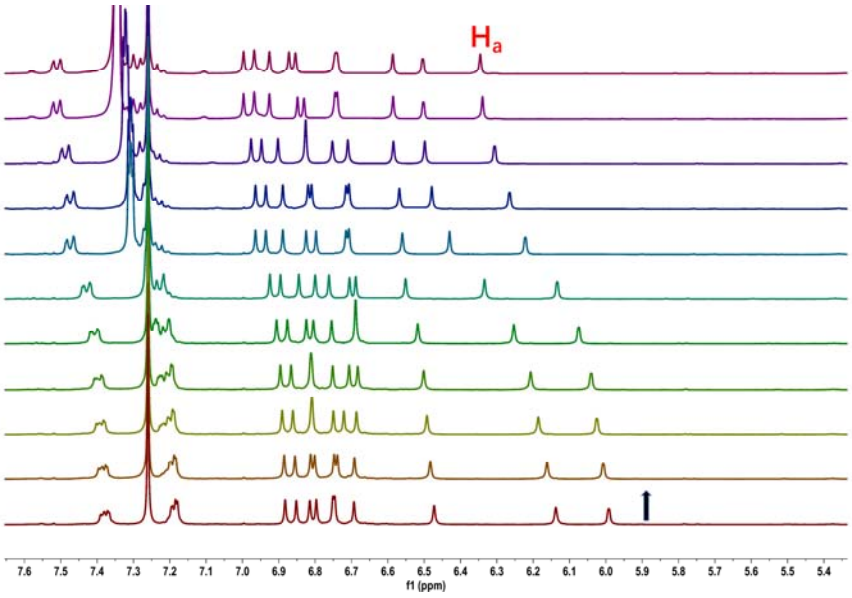

Figure S146. Partial ^{1}H NMR spectra (400 MHz, $CDCl_3$, 298 K) of a mixture of **[P4-(OH)BPO]** (10.0 mM) and thiazole (**31**) at the concentrations of 0, 2.0, 6.0, 10.0, 20.0, 40.0, 80.0, 120.0, 160.0, 320.0, and 640.0 mM (from bottom to top).

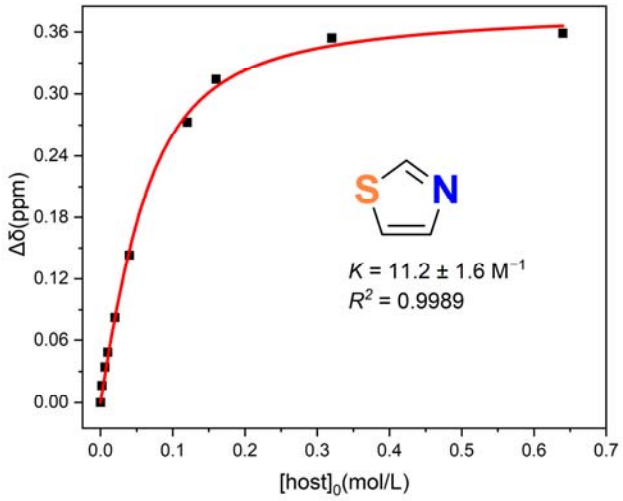

Figure S147. The nonlinear curve fitting of NMR titration ($\Delta\delta$ of H_α) for the complexation of **[P4-(OH)BPO]** (10.0 mM) with thiazole (**31**) in $CDCl_3$ at 298 K.

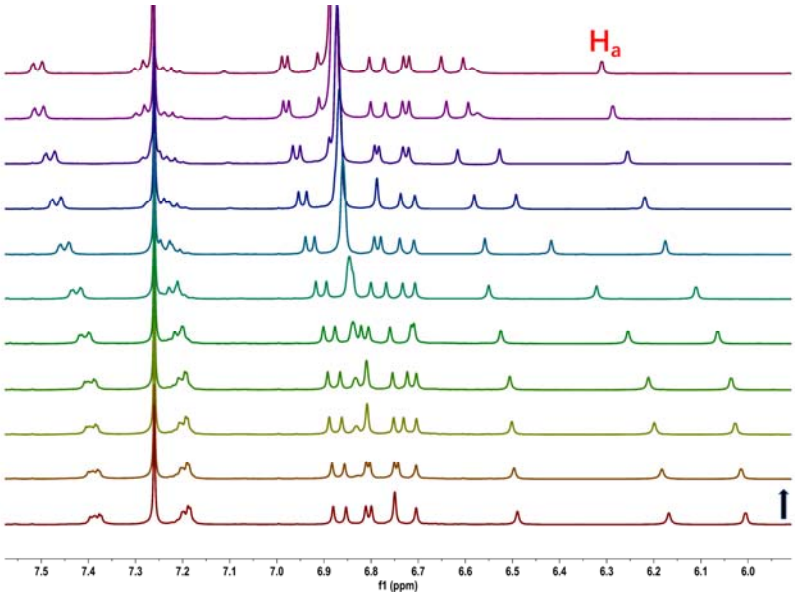

Figure S148. Partial ^{1}H NMR spectra (400 MHz, $CDCl_3$, 298 K) of a mixture of **[P4-(OH)BPO]** (10.0 mM) and 4-methylthiazole (**32**) at the concentrations of 0, 2.0, 6.0, 10.0, 20.0, 40.0, 80.0, 120.0, 160.0, 320.0, and 640.0 mM (from bottom to top).

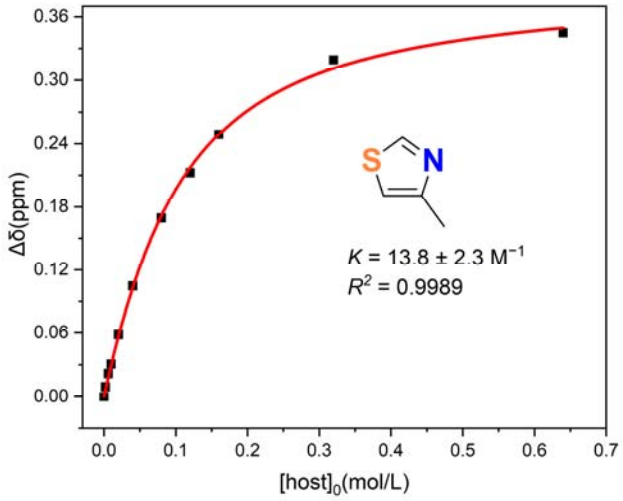

Figure S149. The nonlinear curve fitting of NMR titration ($\Delta\delta$ of H_α) for the complexation of **[P4-(OH)BPO]** (10.0 mM) with 4-methylthiazole (**32**) in $CDCl_3$ at 298 K.

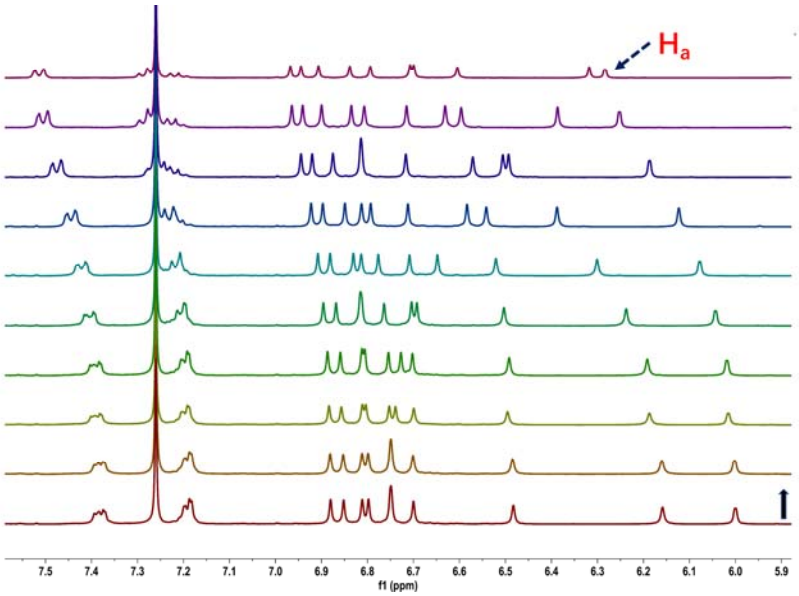

Figure S150. Partial ^{1}H NMR spectra (400 MHz, $CDCl_3$, 298 K) of a mixture of **[P4-(OH)BPO]** (10.0 mM) and 3,5-dimethylisoxazole (**33**) at the concentrations of 0, 2.0, 6.0, 10.0, 20.0, 40.0, 80.0, 120.0, 160.0, 320.0, and 640.0 mM (from bottom to top).

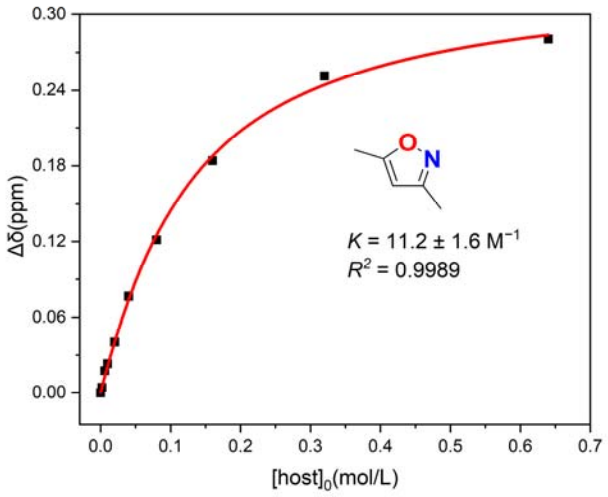

Figure S151. The nonlinear curve fitting of NMR titration (Δδ of H_α) for the complexation of **[P4-(OH)BPO]** (10.0 mM) with 3,5-dimethylisoxazole (**33**) in $CDCl_3$ at 298 K.

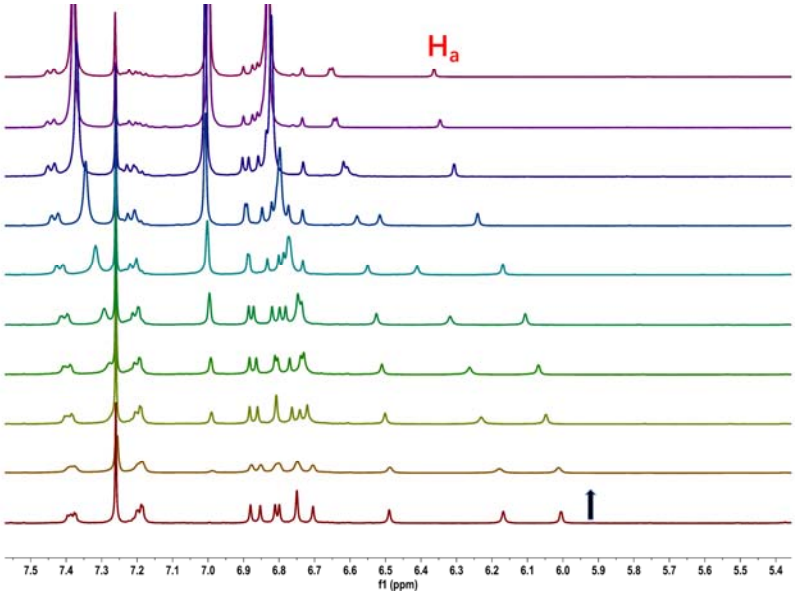

Figure S152. Partial ^{1}H NMR spectra (400 MHz, $CDCl_3$, 298 K) of a mixture of **[P4-(OH)BPO]** (10.0 mM) and 1-butylimidazole (**34**) at the concentrations of 0, 2.0, 6.0, 10.0, 20.0, 40.0, 80.0, 120.0, 160.0, 320.0, and 640.0 mM (from bottom to top).

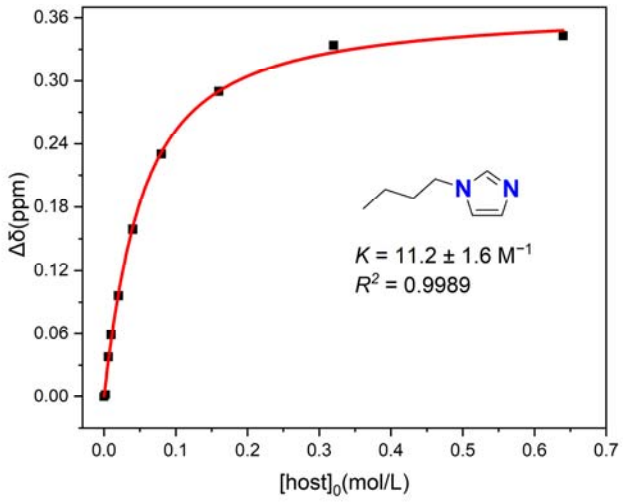

Figure S153. The nonlinear curve fitting of NMR titration ($\Delta\delta$ of H_α) for the complexation of **[P4-(OH)BPO]** (10.0 mM) with 1-butylimidazole (**34**) in $CDCl_3$ at 298 K.

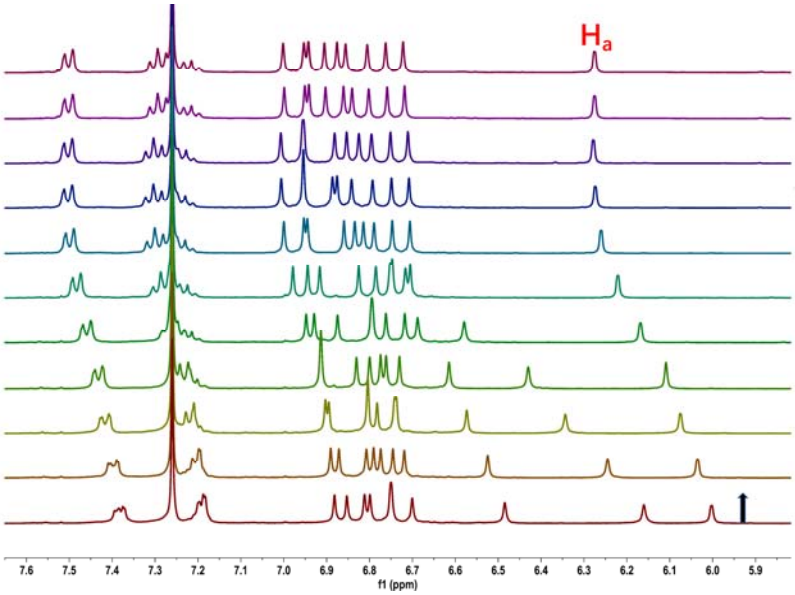

Figure S154. Partial ^{1}H NMR spectra (400 MHz, $CDCl_3$, 298 K) of a mixture of **[P4-(OH)BPO]** (10.0 mM) and dimethylsulfoxide (**35**) at the concentrations of 0, 2.0, 6.0, 10.0, 20.0, 40.0, 80.0, 120.0, 160.0, 320.0, and 640.0 mM (from bottom to top).

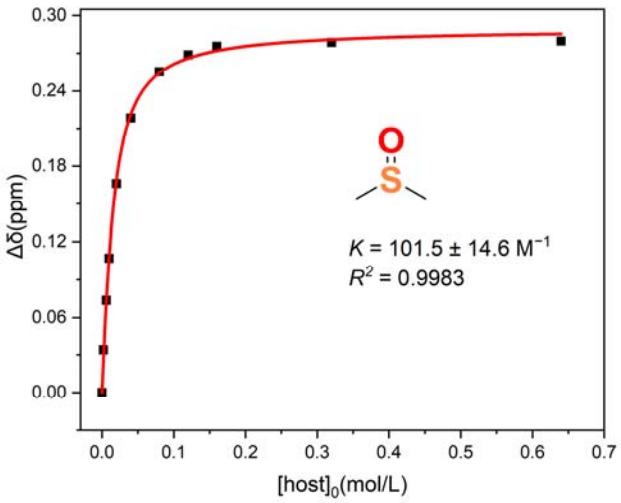

Figure S155. The nonlinear curve fitting of NMR titration (Δδ of H_α) for the complexation of **[P4-(OH)BPO]** (10.0 mM) with dimethylsulfoxide (**35**) in $CDCl_3$ at 298 K.

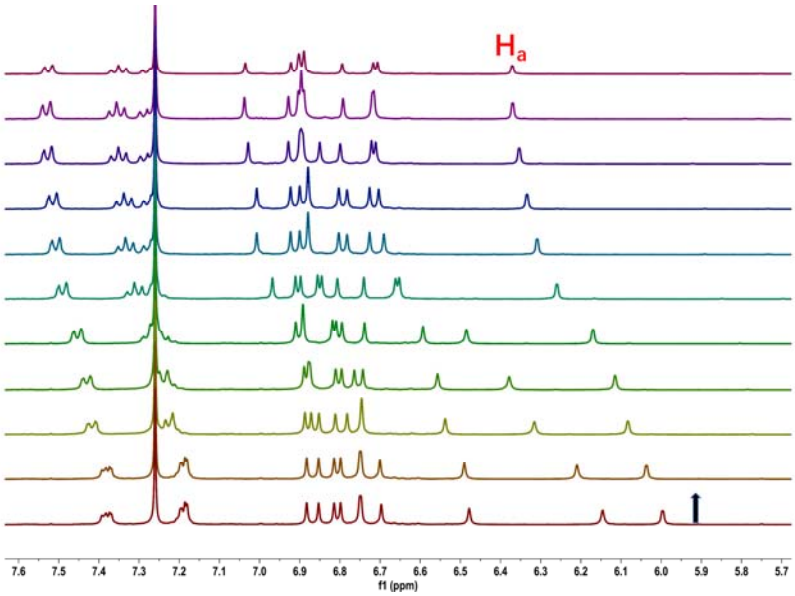

Figure S156. Partial ^{1}H NMR spectra (400 MHz, $CDCl_3$, 298 K) of a mixture of **[P4-(OH)BPO]** (10.0 mM) and 1-nitropropane (**36**) at the concentrations of 0, 2.0, 6.0, 10.0, 20.0, 40.0, 80.0, 120.0, 160.0, 320.0, and 640.0 mM (from bottom to top).

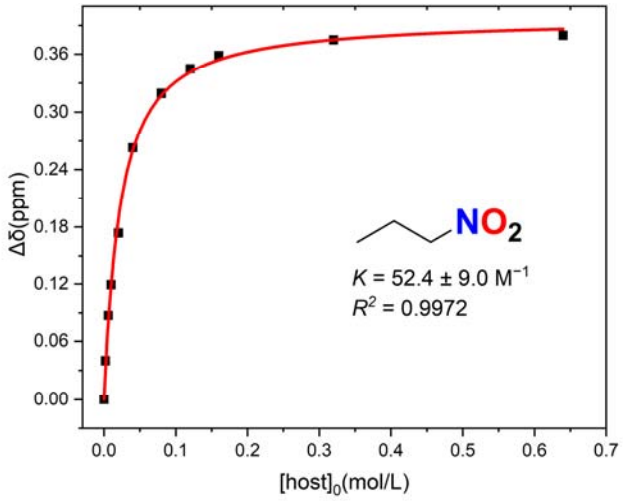

Figure S157. The nonlinear curve fitting of NMR titration (Δδ of H_α) for the complexation of **[P4-(OH)BPO]** (10.0 mM) with 1-nitropropane (**36**) in $CDCl_3$ at 298 K.

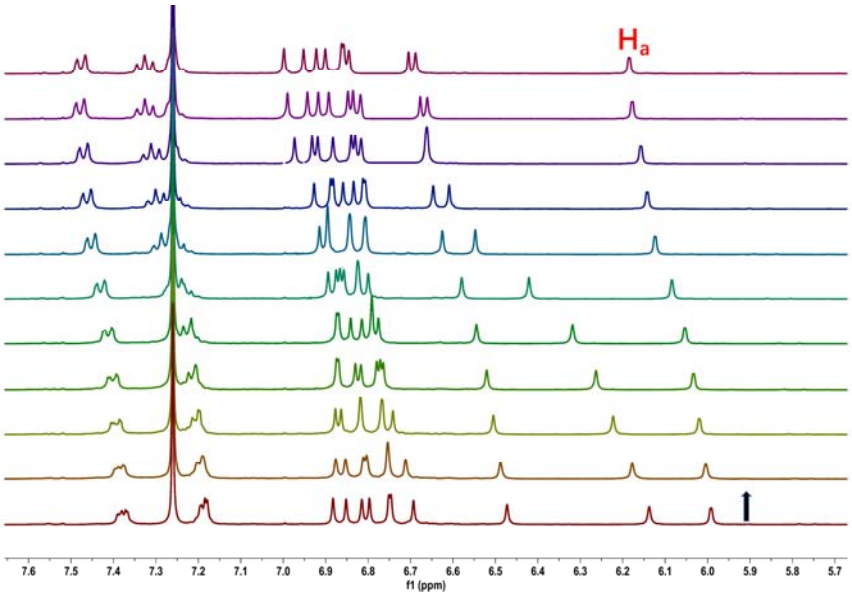

Figure S158. Partial ^{1}H NMR spectra (400 MHz, $CDCl_3$, 298 K) of a mixture of **[P4-(OH)BPO]** (10.0 mM) and acetonitrile (**37**) at the concentrations of 0, 2.0, 6.0, 10.0, 20.0, 40.0, 80.0, 120.0, 160.0, 320.0, and 640.0 mM (from bottom to top).

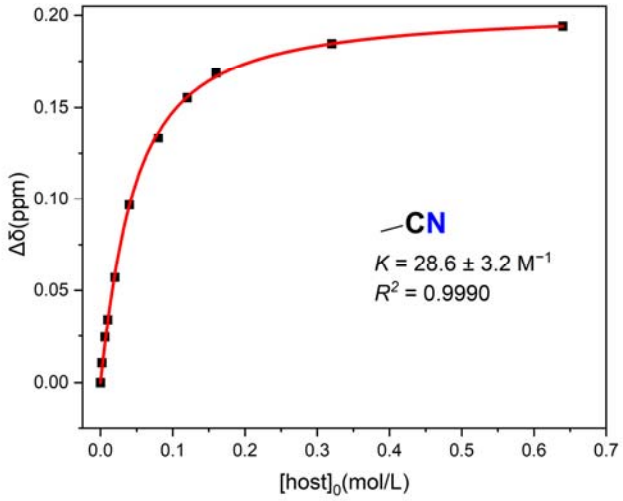

Figure S159. The nonlinear curve fitting of NMR titration ($\Delta\delta$ of H_α) for the complexation of **[P4-(OH)BPO]** (10.0 mM) with acetonitrile (**37**) in $CDCl_3$ at 298 K.

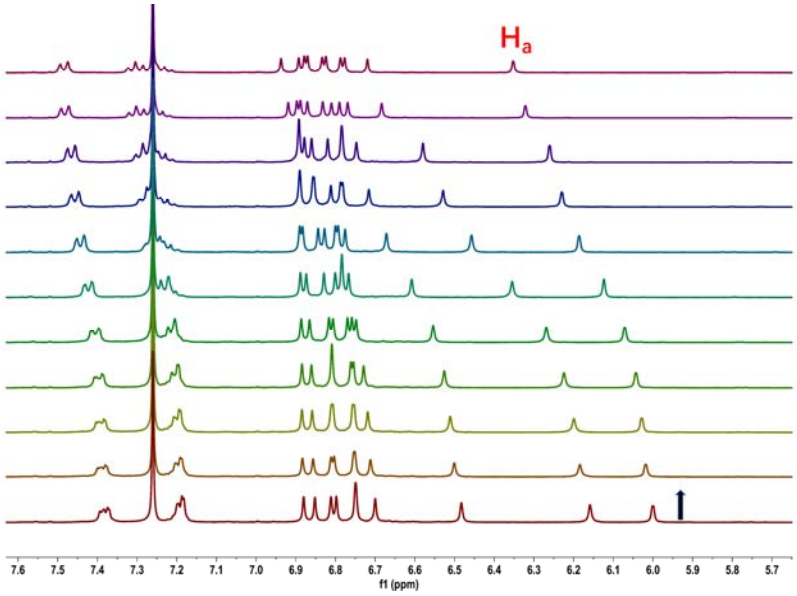

Figure S160. Partial ^{1}H NMR spectra (400 MHz, $CDCl_3$, 298 K) of a mixture of **[P4-(OH)BPO]** (10.0 mM) and of 2-butyloxirane (**38**) at the concentrations of 0, 2.0, 6.0, 10.0, 20.0, 40.0, 80.0, 120.0, 160.0, 320.0, and 640.0 mM (from bottom to top).

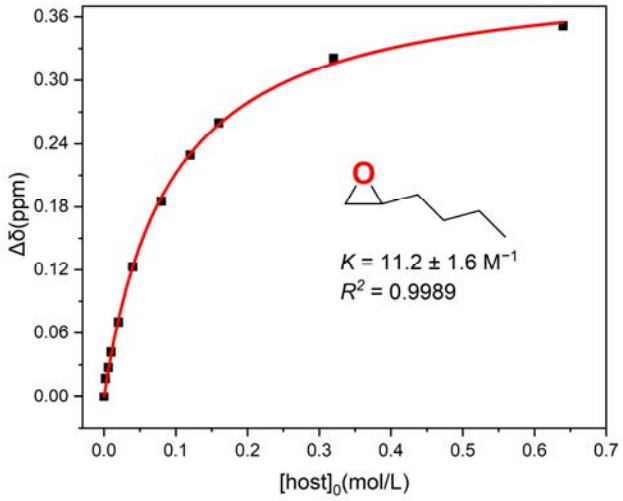

Figure S161. The nonlinear curve fitting of NMR titration ($\Delta\delta$ of H_α) for the complexation of **[P4-(OH)BPO]** (10.0 mM) with 2-butyloxirane (**38**) in $CDCl_3$ at 298 K.

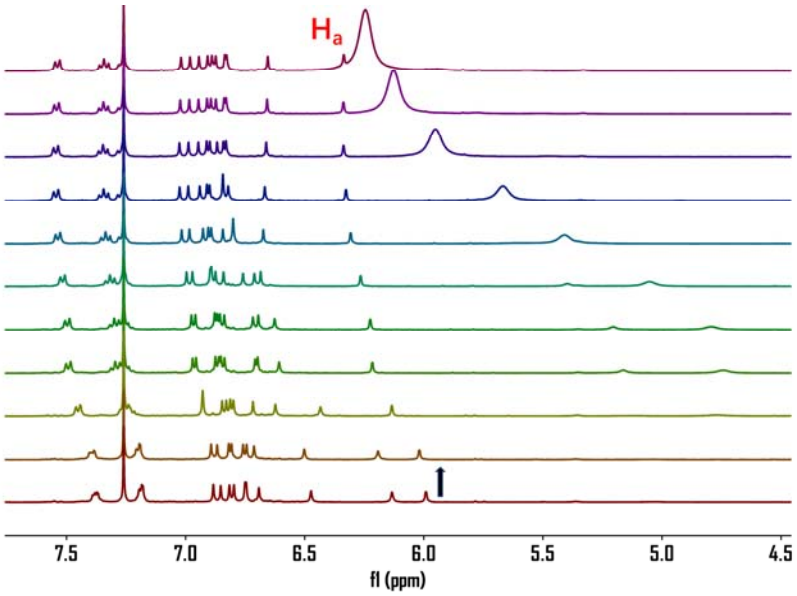

Figure S162. Partial ^{1}H NMR spectra (400 MHz, $CDCl_3$, 298 K) of a mixture of **[P4-(OH)BPO]** (10.0 mM) and *N*-(3-hydroxypropyl)acetamide (**39**) at the concentrations of 0, 2.0, 6.0, 10.0, 20.0, 40.0, 80.0, 120.0, 160.0, 320.0, and 640.0 mM (from bottom to top).

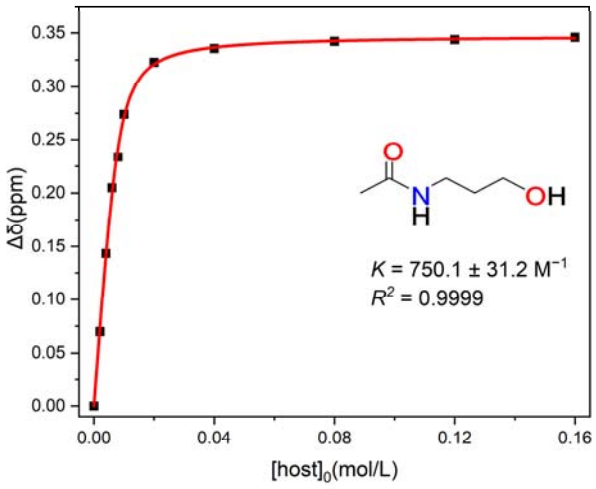

Figure S163. The nonlinear curve fitting of NMR titration (Δδ of H_α) for the complexation of **[P4-(OH)BPO]** (10.0 mM) with *N*-(3-hydroxypropyl)acetamide (**39**) in $CDCl_3$ at 298 K.

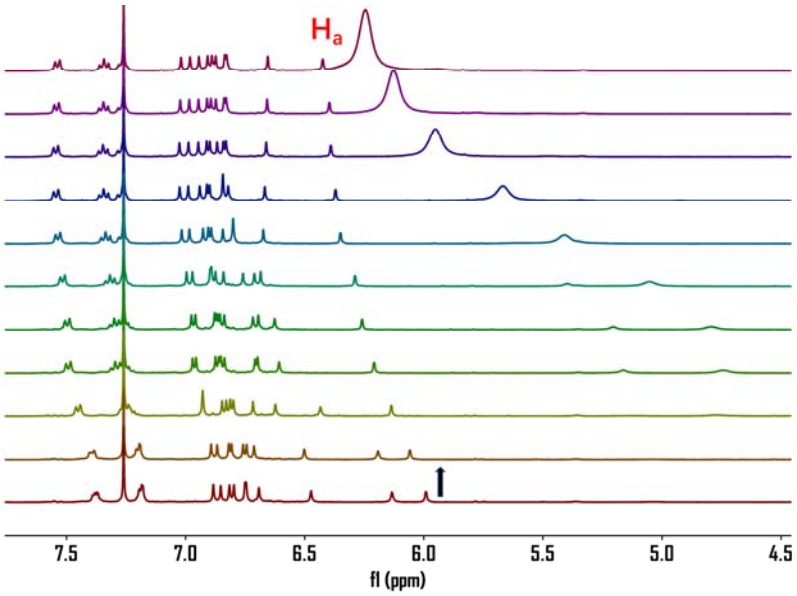

Figure S164. Partial ^{1}H NMR spectra (400 MHz, $CDCl_3$, 298 K) of a mixture of **[P4-(OH)BPO]** (10.0 mM) and *N*-(3-hydroxypropyl)formamide (**40**) at the concentrations of 0, 2.0, 6.0, 10.0, 20.0, 40.0, 80.0, 120.0, 160.0, 320.0, and 640.0 mM (from bottom to top).

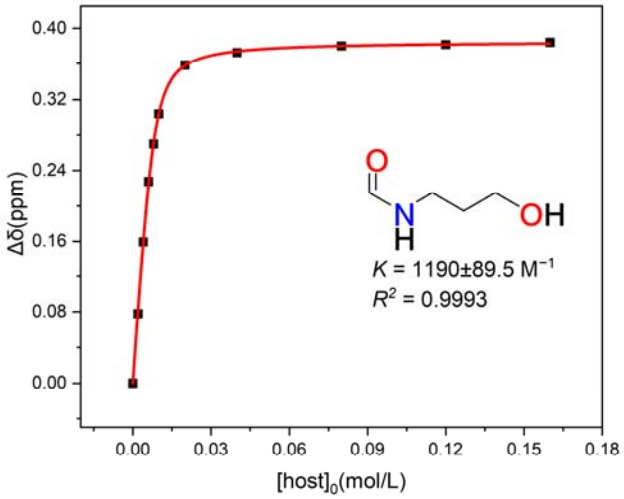

Figure S165. The nonlinear curve fitting of NMR titration (Δδ of H_α) for the complexation of **[P4-(OH)BPO]** (10.0 mM) with *N*-(3-hydroxypropyl)formamide (**40**) in $CDCl_3$ at 298 K.

2D NOESY Spectra

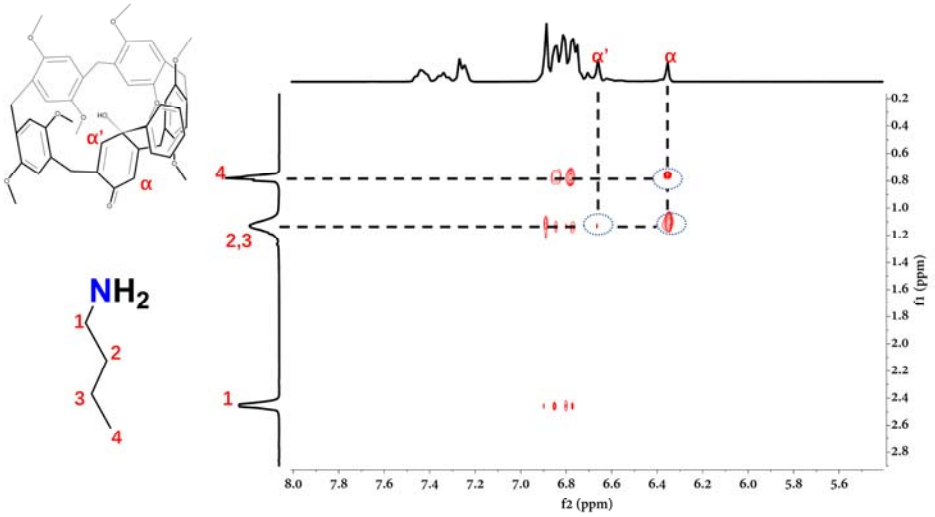

Figure S166. Partial 2D NOESY spectrum (400 MHz, $CDCl_3$, 298 K) of the mixture of **[P4-(OH)BPO]** (40 mM) and *n*-butylamine (**1**) (160 mM).

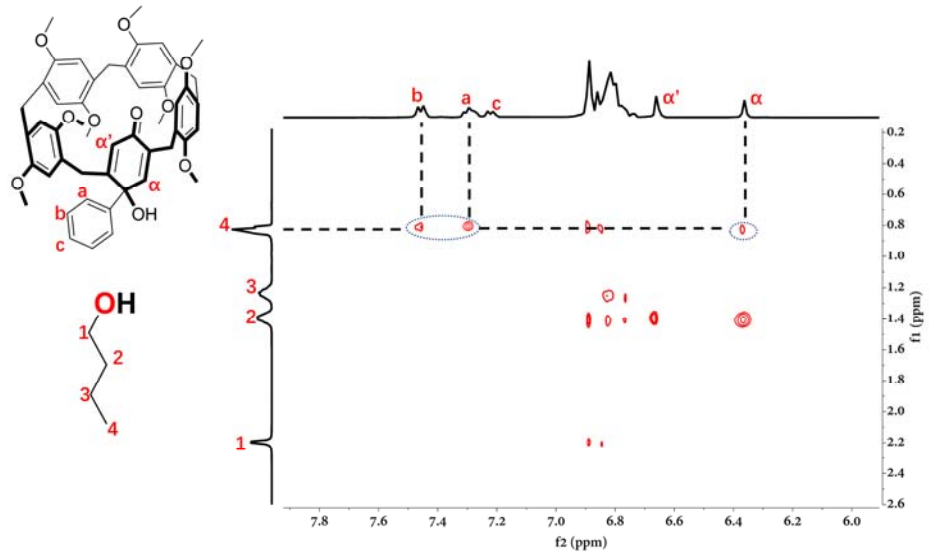

Figure S167. Partial 2D NOESY spectrum (400 MHz, $CDCl_3$, 298 K) of the mixture of **[P4-(OH)BPO]** (40 mM) and *n*-butanol (**4**) (160 mM).

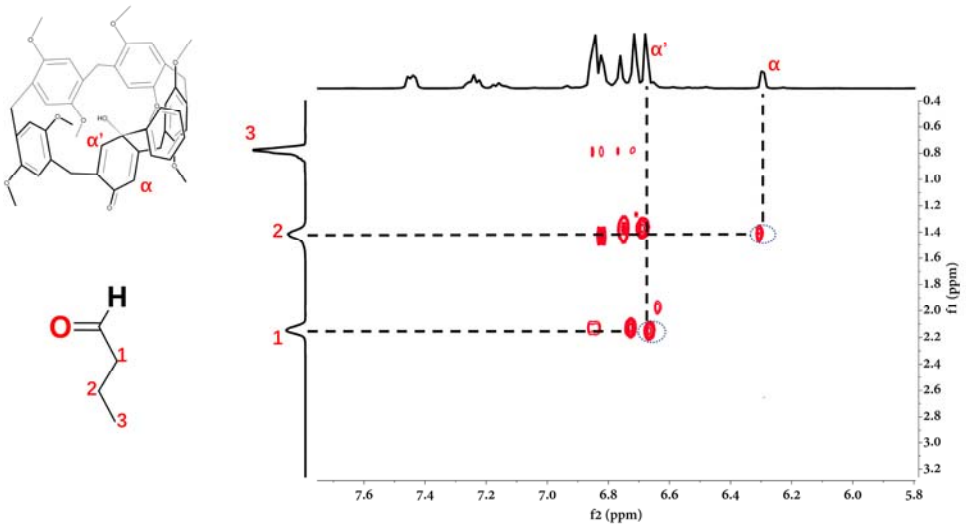

Figure S168. Partial 2D NOESY spectrum (400 MHz, $CDCl_3$, 298 K) of the mixture of **[P4-(OH)BPO]** (40 mM) and *n*-butyraldehyde (**7**) (160 mM).

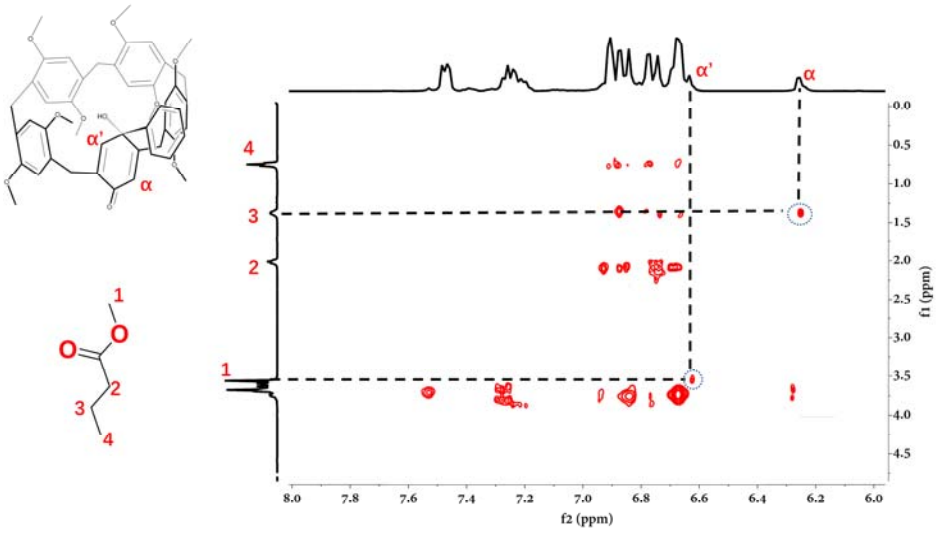

Figure S169. Partial 2D NOESY spectrum (400 MHz, $CDCl_3$, 298 K) of the mixture of **[P4-(OH)BPO]** (40 mM) and methyl butyrate (**10**) (160 mM).

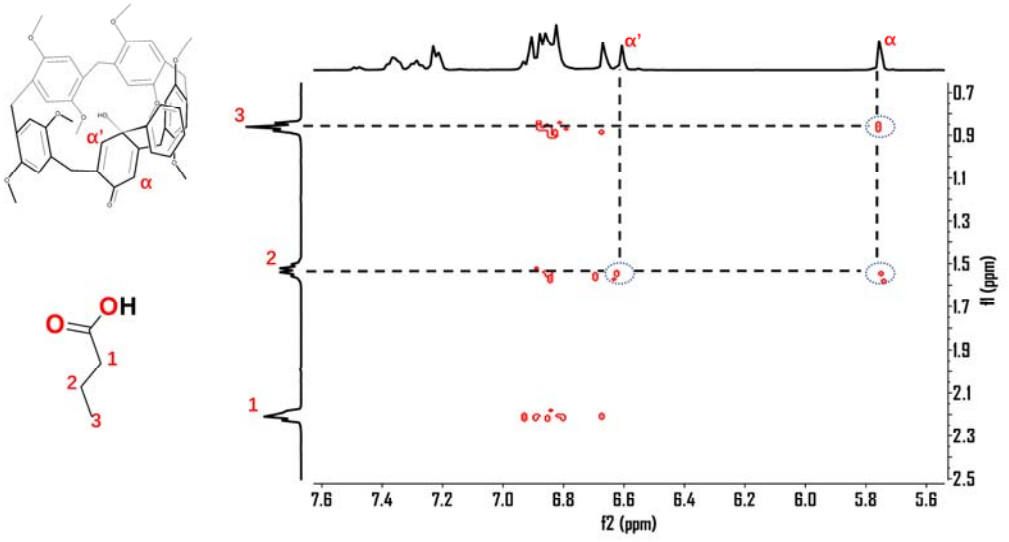

Figure S170. Partial 2D NOESY spectrum (400 MHz, $CDCl_3$, 298 K) of the mixture of **[P4-(OH)BPO]** (40 mM) and *n*-butanoic acid (**13**) (160 mM).

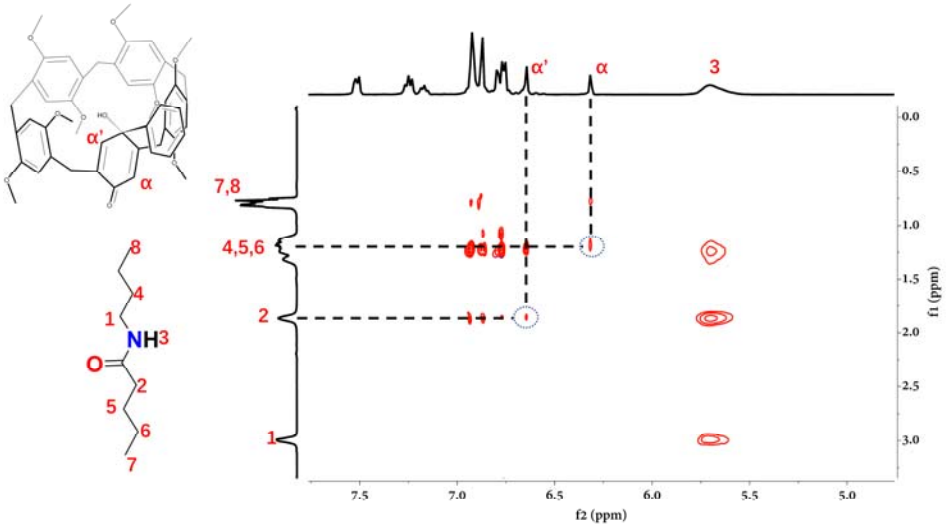

Figure S171. Partial 2D NOESY spectrum (400 MHz, $CDCl_3$, 298 K) of the mixture of **[P4-(OH)BPO]** (40 mM) and *N*-butylpentanamide (**25**) (160 mM).

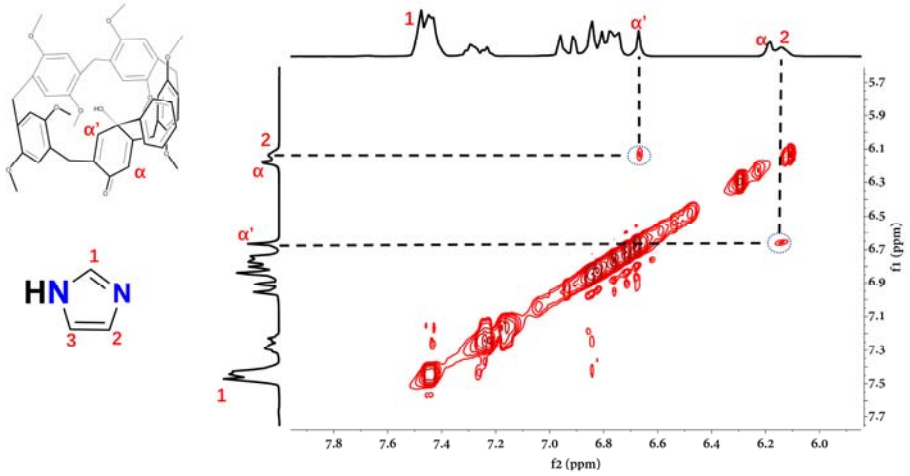

Figure S172. Partial 2D NOESY spectrum (400 MHz, $CDCl_3$, 298 K) of the mixture of **[P4-(OH)BPO]** (40 mM) and imidazole (**29**) (160 mM).

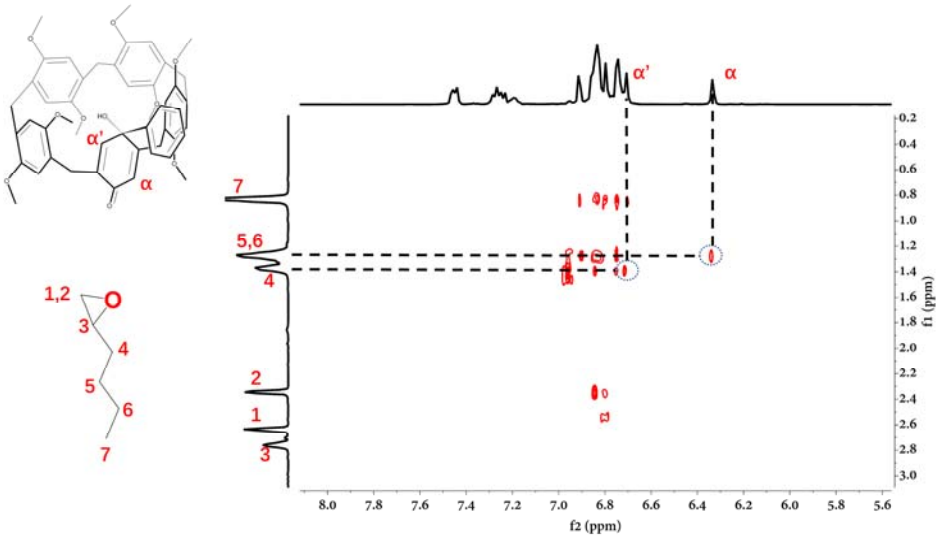

Figure S173. Partial 2D NOESY spectrum (400 MHz, $CDCl_3$, 298 K) of the mixture of **[P4-(OH)BPO]** (40 mM) and 2-butyloxirane (**39**) (160 mM).

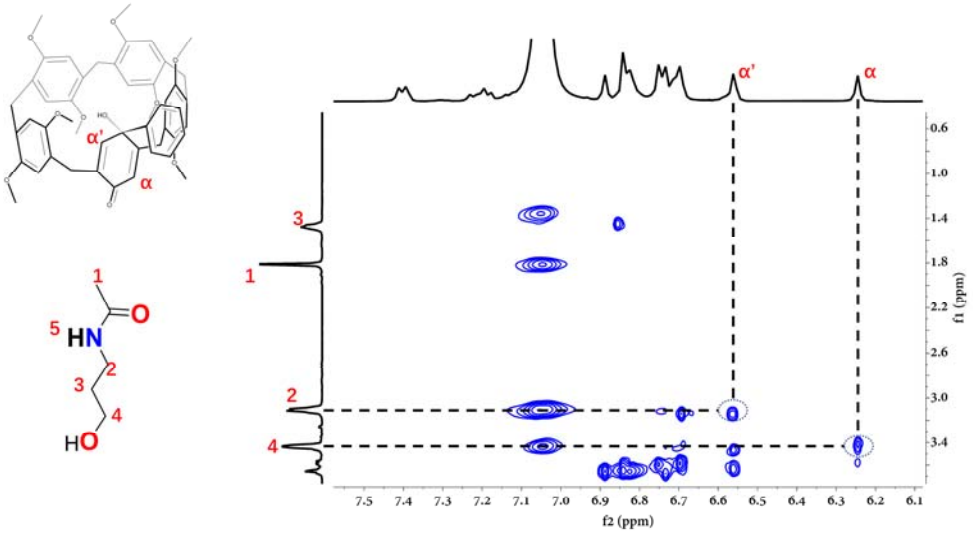

Figure S174. Partial 2D NOESY spectrum (400 MHz, $CDCl_3$, 298 K) of the mixture of **[P4-(OH)BPO]** (40 mM) and *N*-(3-hydroxypropyl)acetamide (**40**) (160 mM).

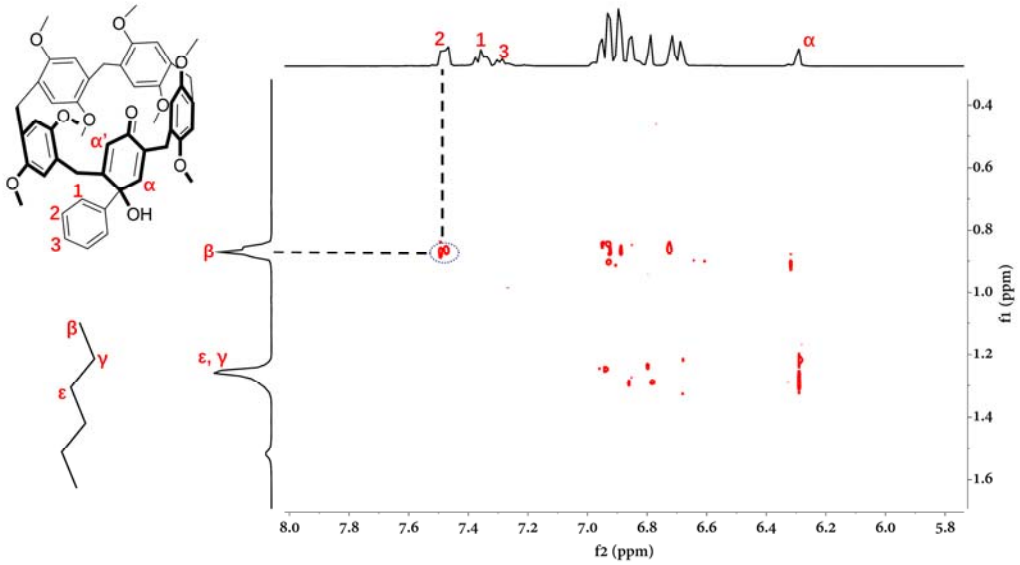

Figure S175. Partial 2D NOESY spectrum (400 MHz, $CDCl_3$, 298 K) of the mixture of **[P4-(OH)BPO]** (40 mM) and hexane (160 mM).

Single-Crystal X-ray Crystallography

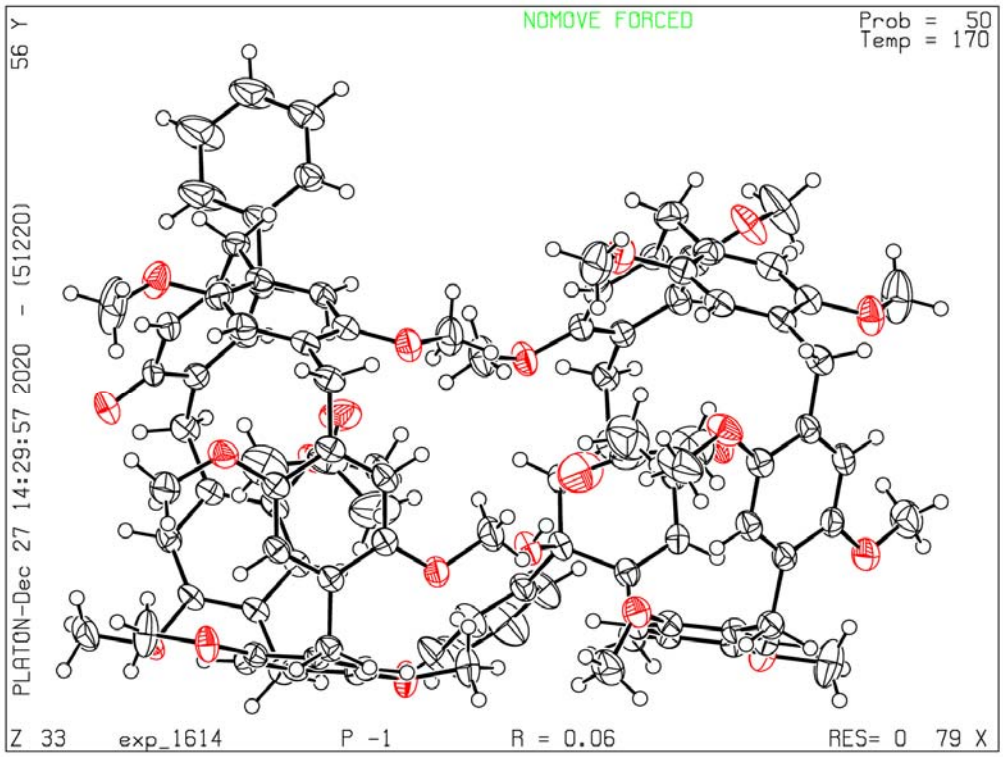

Crystallographic Data of acetone⊂*endo*-[P4-BPO(1-OH)]: $C_{52}H_{56}O_{11}$ (M =856.96 g/mol): triclinic, space group P-1 (no. 2), a = 12.6595(3) Å, b = 16.8962(5) Å, c = 23.3017(7) Å, α = 109.239(3)°, β = 91.141(2)°, γ = 99.679(2)°, V = 4623.6(2) Å^3, Z = 4, T = 169.99(10) K, μ(Cu Kα) = 0.697 mm^{-1}, *Dcalc* = 1.231 g/cm^3, 51235 reflections measured (7.106° ≤ 2Θ ≤ 134.158°), 16409 unique (R_{int} = 0.0476, R_{sigma} = 0.0494) which were used in all calculations. The final R_1 was 0.0588 (I > 2σ(I)) and wR_2 was 0.1668 (all data).

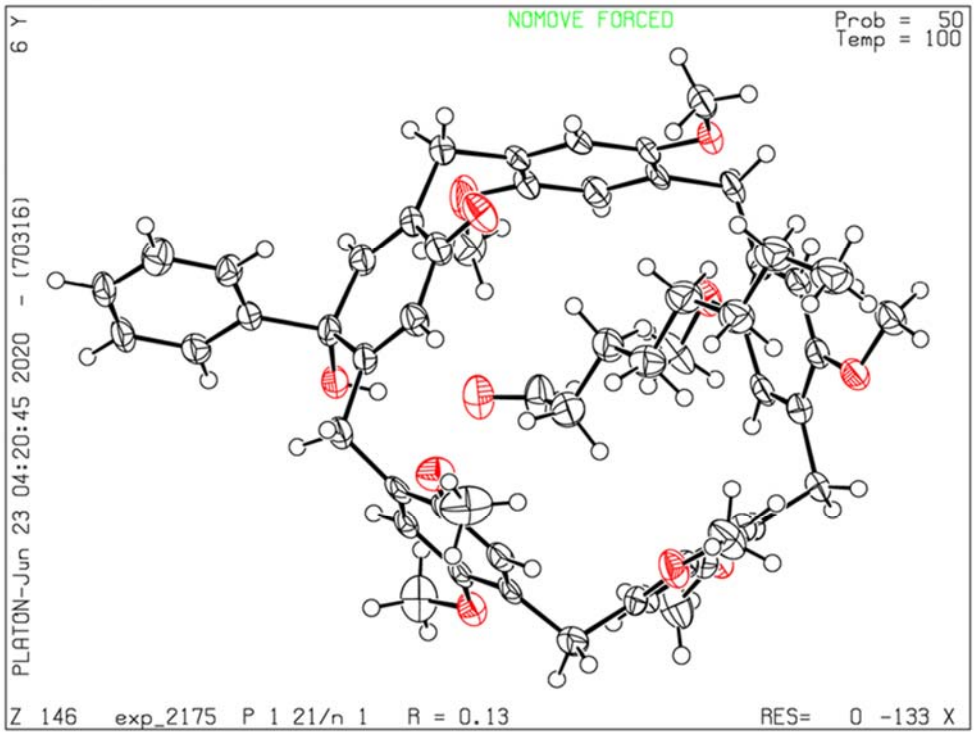

Crystallographic Data of 9⊂*endo*-[P4-(OH)BPO]: [C_{57} H_{66} O_{11}]; M_r = 927.09; T = 100.0 K; monoclinic; space group $P2_1/n$; a = 12.2551(4); b = 35.3374(12); c = 12.3763(5) Å; α =90; β = 112.092(4); γ =90; V = 4966.2(3) Å^3; Z = 4; ρcalcd = 1.240 g/cm^3; μ = 0.686 mm^{-1}; reflections collected 33633; unique reflections 9836; data/restraints/parameters 9836/0/623; *GOF* on F_2 1.077; *Rint* for independent data 0.0894; final R_1 = 0.1311, wR_2 = 0.3371; R indices (all data) R_1 =0.1473, wR_2 = 0.3453; largest diff. peak and hole: 0.63 and -0.38 eÅ^{-3}.

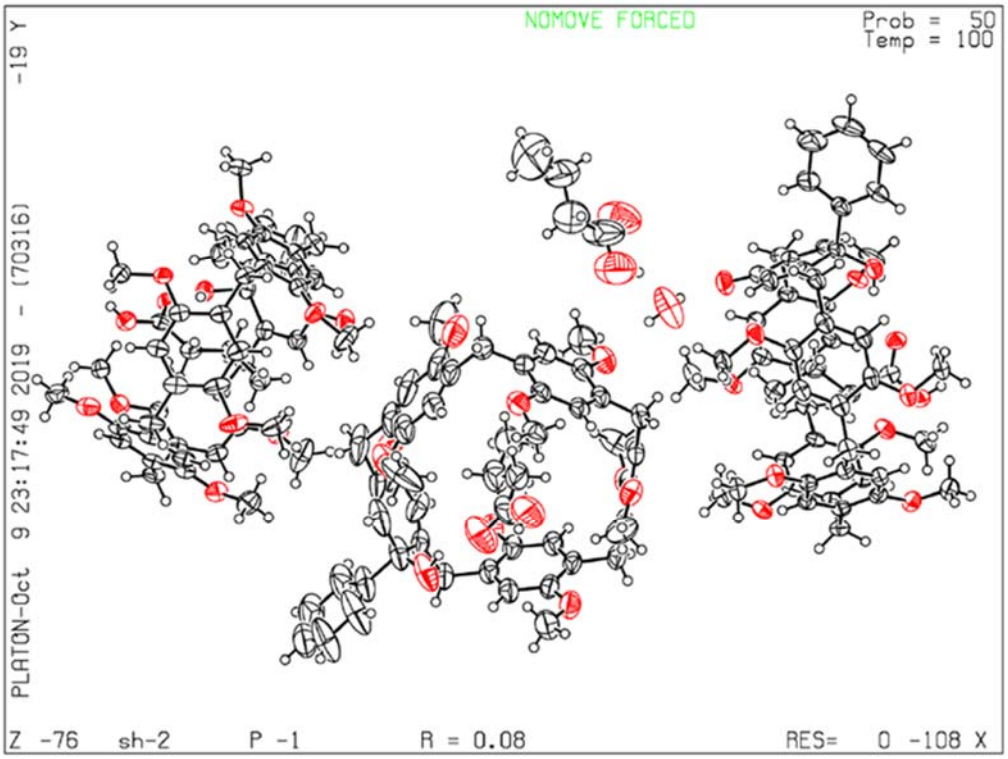

Crystallographic Data of 13⊂endo-[P4-BPO(1-OH)]: [C_{163} H_{184} NO_{39}]; *Mr* = 2767.09; T = 100.01(10) K; triclinic; space group P-1; *a* = 13.1627(4); *b* = 23.5857(5); *c* = 25.1617(8) Å; α =92.714(2); β = 94.925(3); γ =91.465(2); *V* = 7770.5(4) Å^3; Z = 2; ρcalcd = 1.183 g/cm^3; μ = 0.685mm^{-1}; reflections collected 57624; unique reflections 30492; data/restraints/parameters 30492/0/1857; *GOF* on F^2 1.038; *Rint* for independent data 0.0570; final R_1 = 0.0784, wR_2 = 0.2193; R indices (all data) R_1 =0.1187, wR_2 = 0.2546; largest diff. peak and hole: 0.48 and -0.70 eÅ^{-3}.

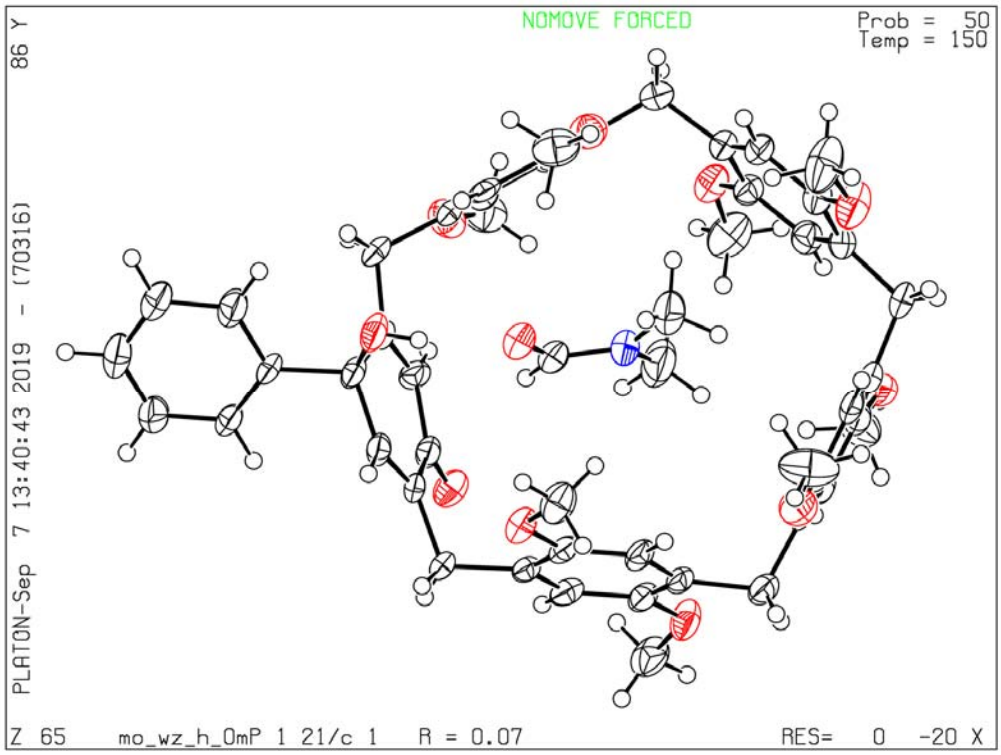

Crystallographic Data of 17⊂*endo*-[P4-BPO(1-OH)]: $C_{52}H_{57}NO_{11}$ (M =871.98 g/mol): monoclinic, space group $P2_1/c$ (no. 14), a = 14.722(2) Å, b = 13.987(2) Å, c = 22.898(3) Å, β = 96.609(4)°, V = 4683.6(12) Å^3, Z = 4, T = 150.01 K, μ(MoKα) = 0.086 mm^{-1}, *Dcalc* = 1.237 g/cm^3, 45103 reflections measured (4.276° ≤ 2Θ ≤ 41.846°), 4766 unique (R_{int} = 0.1087, R_{sigma} = 0.0523) which were used in all calculations. The final R_1 was 0.0683 (I > 2σ(I)) and wR_2 was 0.2285 (all data).

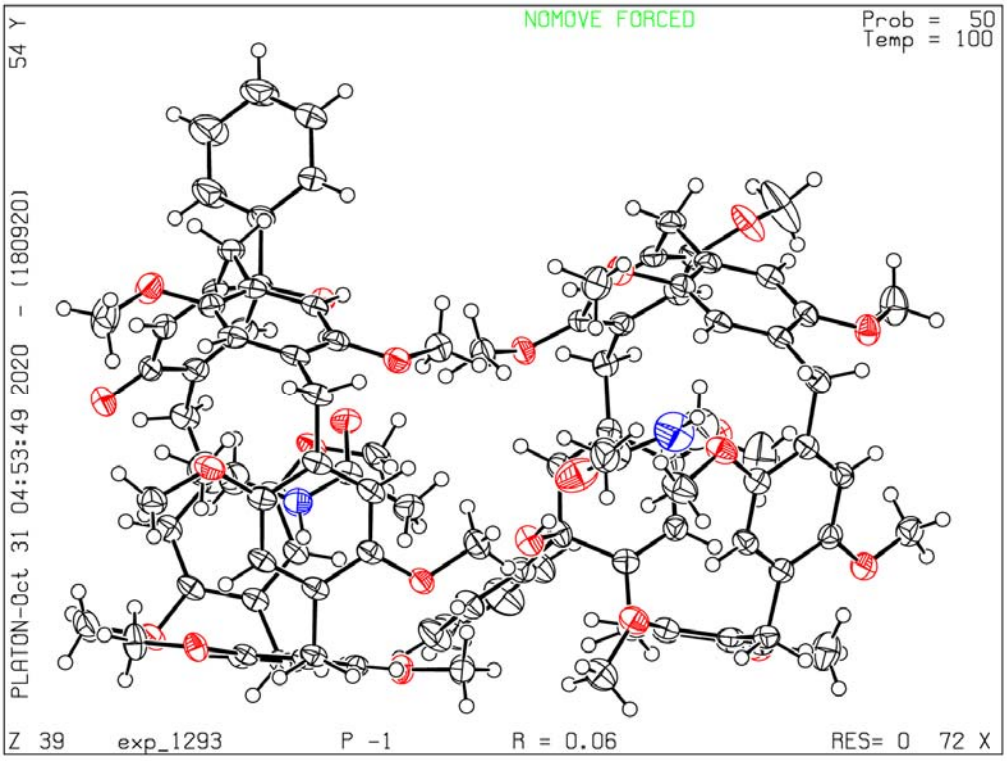

Crystallographic Data of 21⊂ *endo*-[P4-BPO(1-OH)]: $C_{59.125}H_{53.75}O_{5.375}N_{5.375}$ (M =925.57 g/mol): orthorhombic, space group $Pca2_1$ (no. 29), a = 22.9741(4) Å, b = 19.0211(6) Å, c = 23.0178(5) Å, V = 10058.6(4) Å^3, Z = 8, T = 100.00(13) K, μ(CuKα) = 0.629 mm^{-1}, *Dcalc* = 1.222 g/cm^3, 68268 reflections measured (4.646° ≤ 2Θ ≤ 134.158°), 17154 unique (R_{int} = 0.0768, R_{sigma} = 0.0560) which were used in all calculations. The final R_1 was 0.2440 (I > 2σ(I)) and wR_2 was 0.5872 (all data).

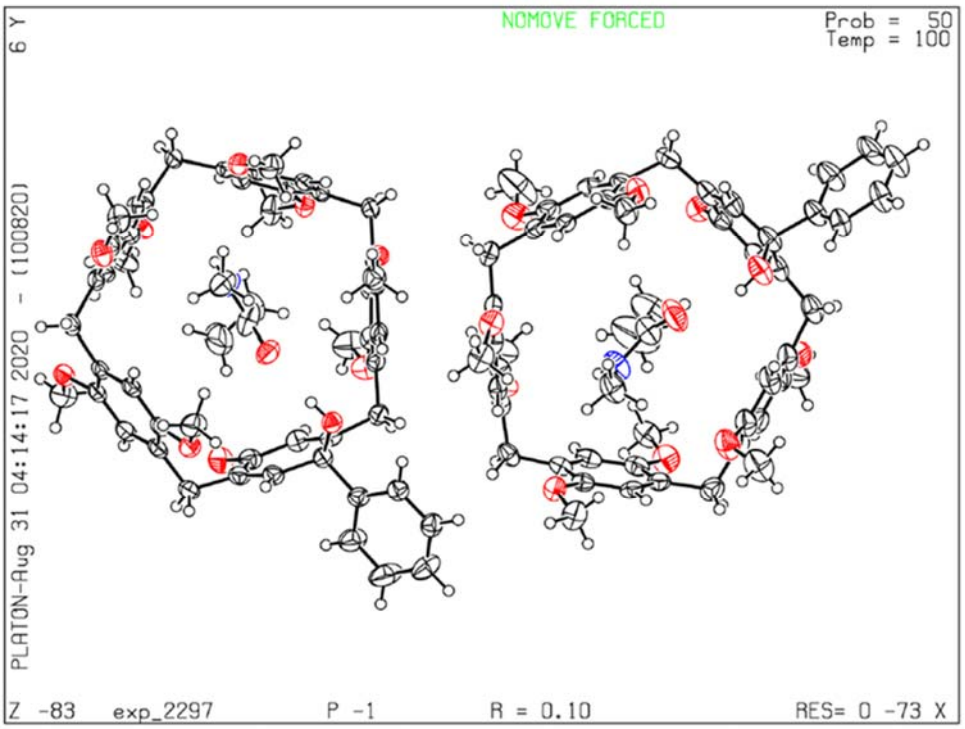

Crystallographic Data of 24⊂*endo*-[P4-BPO(1-OH)]: [C_{53} H_{59} N O_{11}]; M_r = 886.01; T = 100.01(13) K; triclinic; space group P-1; a = 12.6244(4); b = 17.1050(5); c = 23.3091(7) Å; α =109.895(3); β = 91.763(3); γ =98.274(3); V = 4966.5(3) Å^3; Z = 4; ρcalcd = 1.261 g/cm^3; μ = 0.713mm^{-1}; reflections collected 34743; unique reflections 18214; data/restraints/parameters 18214/2/1193; *GOF* on F_2 1.006; *Rint* for independent data 0.0680; final R_1 = 0.0977, wR_2 = 0.2449; R indices (all data) R_1 =0.1359, wR_2 = 0.2744; largest diff. peak and hole: 0.84 and -0.55 eÅ^{-3}.

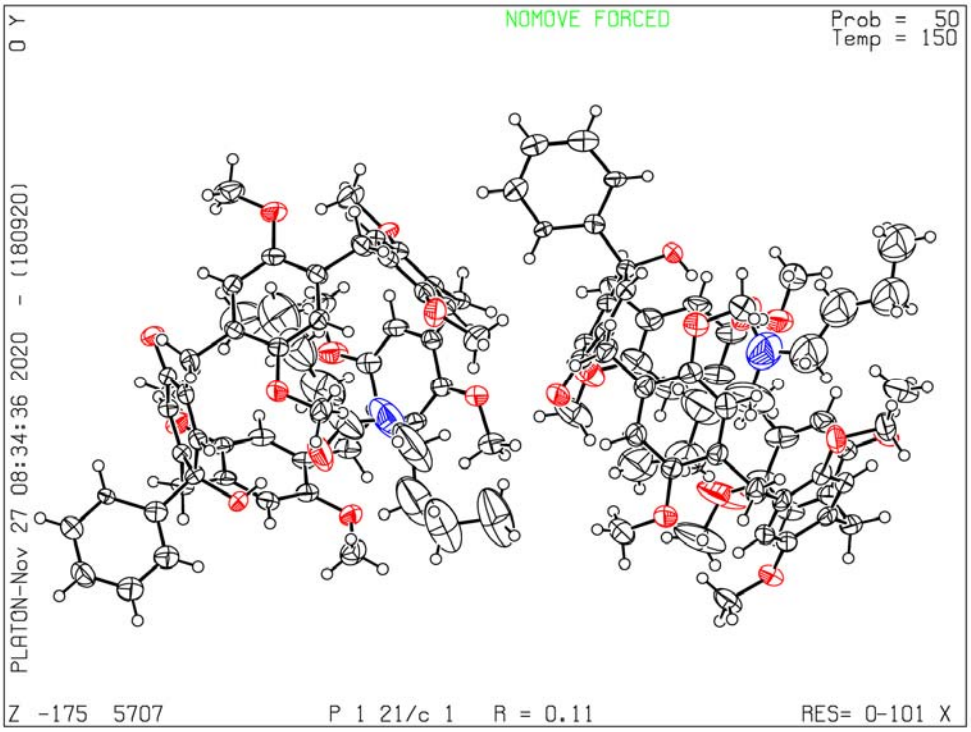

Crystallographic Data of 25⊂*endo*-[P4-BPO(1-OH)]: for $C_{57.5}H_{68}NO_{11}$ (M =949.12 g/mol): monoclinic, space group $P2_1/c$ (no. 14), a = 23.0837(2) Å, b = 19.0807(3) Å, c = 23.0142(3) Å, β = 90.2020(10)°, V = 10136.6(2) Å^3, Z = 8, T = 149.99(10) K, μ(Cu Kα) = 0.689 mm^{-1}, *Dcalc* = 1.244 g/cm^3, 19523 reflections measured (3.828° ≤ 2Θ ≤ 147.862°), 19523 unique (R_{int} = ?, R_{sigma} = 0.0341) which were used in all calculations. The final R_1 was 0.1125 (I > 2σ(I)) and wR_2 was 0.3108 (all data).

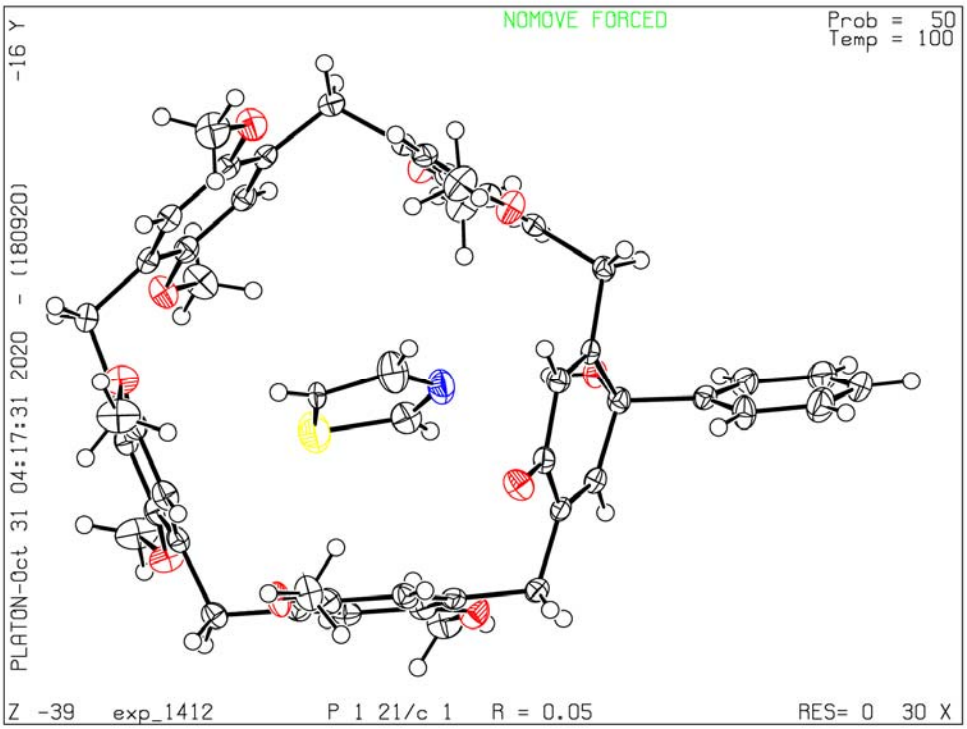

Crystallographic Data of 31⊂*endo*-[P4-BPO(1-OH)]: $C_{52}H_{53}NO_{10}S$ (M =884.01 g/mol): monoclinic, space group $P2_1/c$ (no. 14), a = 11.8319(2) Å, b = 41.9003(5) Å, c = 11.0969(2) Å, β = 112.302(2)°, V = 5089.88(16) Å^3, Z = 4, T = 100.01(10) K, μ(CuKα) = 1.013 mm^{-1}, *Dcalc* = 1.154 g/cm^3, 54175 reflections measured (8.348° ≤ 2Θ ≤ 134.16°), 9038 unique (R_{int} = 0.0438, R_{sigma} = 0.0284) which were used in all calculations. The final R_1 was 0.0514 (I > 2σ(I)) and wR_2 was 0.1363 (all data).

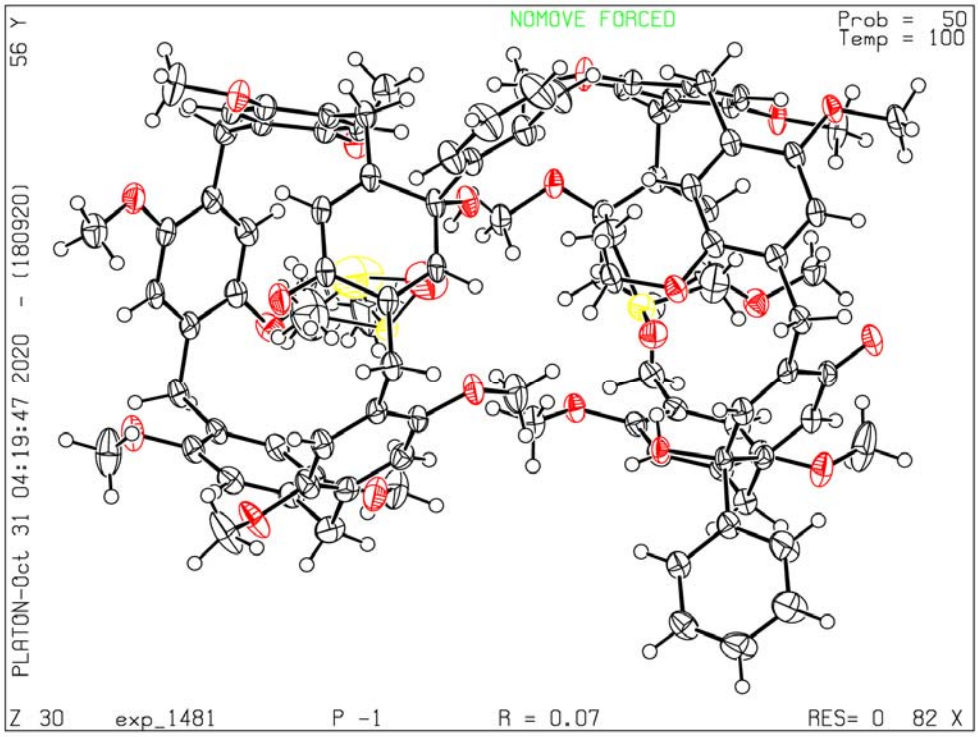

Crystallographic Data of 36⊂*endo*-[P4-BPO(1-OH)]: $C_{51}H_{56}O_{11}S$ (M =877.01 g/mol): triclinic, space group P-1 (no. 2), a = 12.5943(3) Å, b = 16.8101(4) Å, c = 23.4261(5) Å, α = 109.411(2)°, β = 91.212(2)°, γ = 99.439(2)°, V = 4599.05(19) Å^3, Z = 4, T = 99.99(11) K, μ(CuKα) = 1.125 mm^{-1}, *Dcalc* = 1.267 g/cm^3, 53526 reflections measured (7.138° ≤ 2Θ ≤ 134.148°), 16323 unique (R_{int} = 0.0918, R_{sigma} = 0.0801) which were used in all calculations. The final R_1 was 0.0682 (I > 2σ(I)) and wR_2 was 0.1947 (all data).

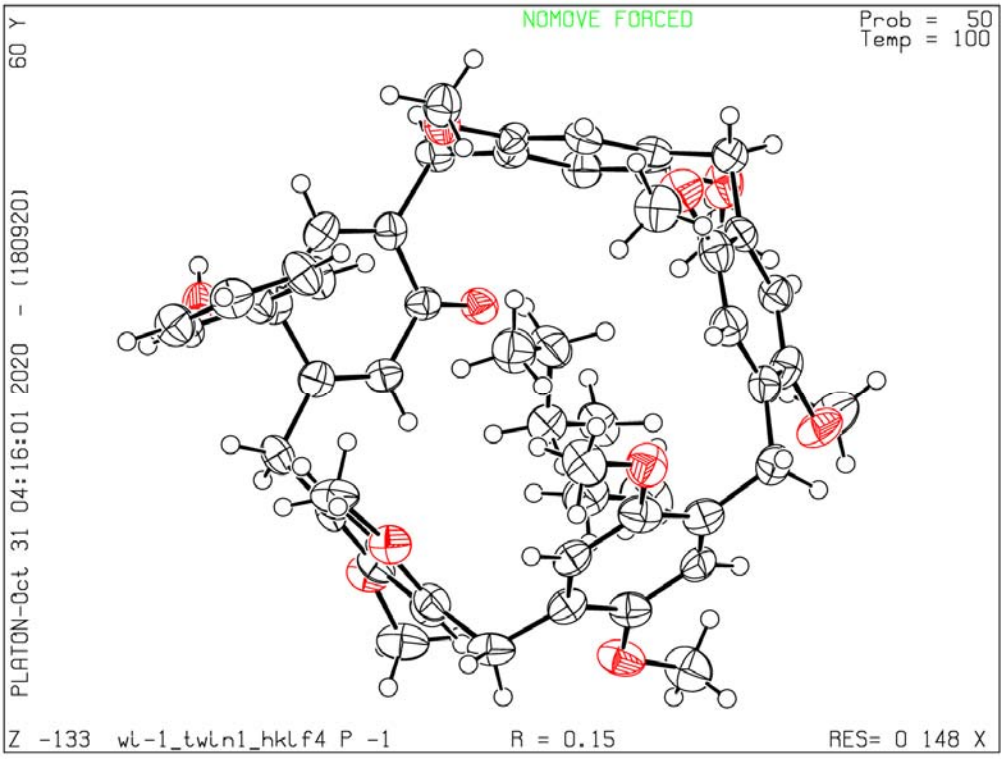

Crystallographic Data of hexane⊂exo-[P4-BPO(1-OH)]: $C_{55}H_{63}O_{10}$ (M =884.05 g/mol): triclinic, space group P-1 (no. 2), a = 10.4720(14) Å, b = 12.1028(17) Å, c = 21.674(3) Å, α = 75.542(12)°, β = 84.585(11)°, γ = 70.595(12)°, V = 2508.7(6) Å^3, Z = 2, T = 100.0(4) K, μ(Cu Kα) = 0.640 mm^{-1}, *Dcalc* = 1.170 g/cm^3, 14523 reflections measured (4.21° ≤ 2Θ ≤ 148.078°), 8617 unique (R_{int} = 0.1483, R_{sigma} = 0.1624) which were used in all calculations. The final R_1 was 0.1489 (I > 2σ(I)) and wR_2 was 0.4352 (all data).

Calculation of Mulliken Charges

The configurations of amides were optimized and Mulliken charges of atoms were calculated using Gaussian 09 at PM6D3 level.

Calculated Mulliken charges for the atoms in **21**

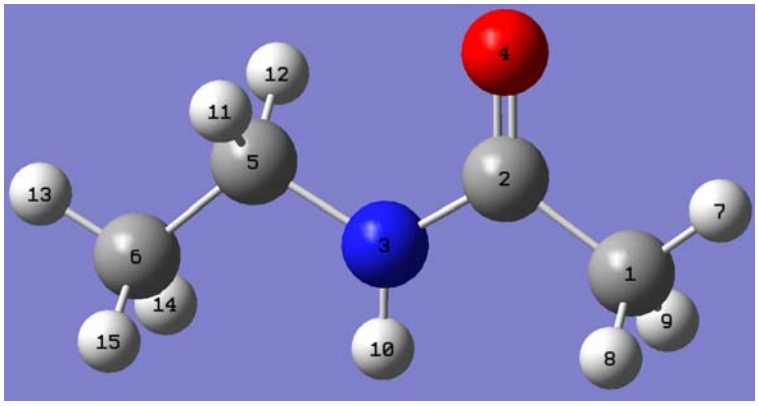

label	atom	Mulliken charge
1	C	**-0.617364**
2	C	0.640383
3	N	**-0.537076**
4	O	-0.558618
5	C	-0.031049
6	C	-0.505309
7	H	0.203227
8	H	0.186879
9	H	0.186885
10	H	0.269917
11	H	0.139389
12	H	0.139417
13	H	0.165025
14	H	0.159150
15	H	0.159142

Calculated Mulliken charges for the atoms in **24**

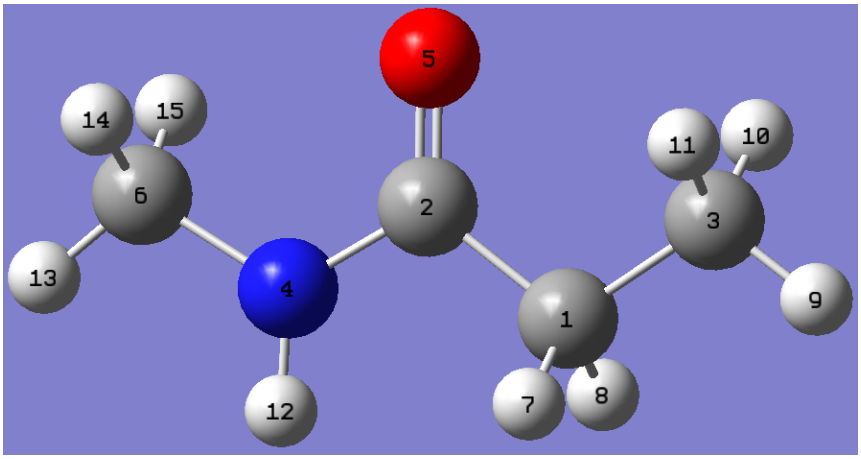

label	atom	Mulliken charge
1	C	**-0.374248**
2	C	0.602575
3	C	-0.419733
4	N	**-0.509102**
5	O	-0.543106
6	C	-0.266655
7	H	0.163304
8	H	0.163281
9	H	0.143461
10	H	0.161465
11	H	0.161484
12	H	0.264243
13	H	0.139101
14	H	0.156961
15	H	0.156970

Calculated Mulliken charges for the atoms in **25**

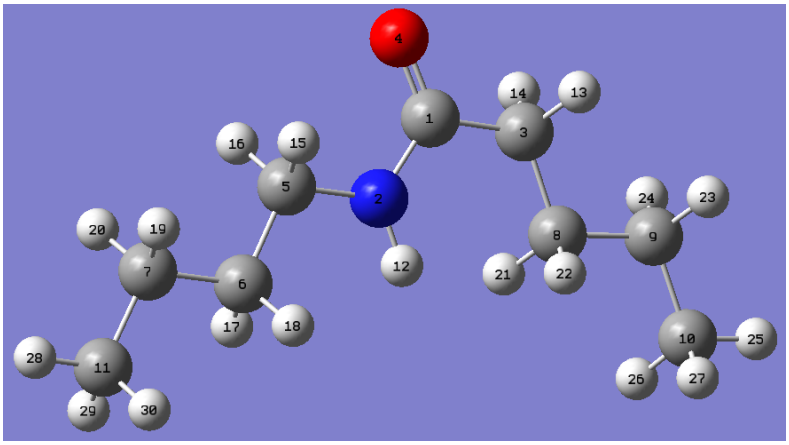

label	atom	Mulliken charge	label	atom	Mulliken charge
1	C	0.601771	16	H	0.144657
2	N	**-0.518556**	17	H	0.142606
3	C	**-0.417205**	18	H	0.142601
4	O	-0.572379	19	H	0.131052
5	C	-0.075983	20	H	0.131051
6	C	-0.308098	21	H	0.133263
7	C	-0.210534	22	H	0.133250
8	C	-0.239671	23	H	0.131007
9	C	-0.221022	24	H	0.131008
10	C	-0.465088	25	H	0.149009
11	C	-0.464434	26	H	0.148024
12	H	0.269452	27	H	0.148022
13	H	0.183265	28	H	0.148627
14	H	0.183244	29	H	0.148203
15	H	0.144655	30	H	0.148202

References:

S1. Xie, C.-D. et al. Synthesis of pillar[n]arene[5−n]quinines via partial oxidation of pillar[5]arene. *Chin. J. Chem*. **33**, 379-383 (2015).

S2. Ulatowski, F., Dąbrowa, K., Bałakier, T., Jurczak, J. Recognizing the limited applicability of Job plots in studying host–guest interactions in supramolecular chemistry

S3. Thordarson, P. Determining association constants from titration experiments in supramolecular chemistry. *Chem. Soc. Rev.* **40**, 1305–1323 (2011).

S4. Frisch M. J. *et al. Gaussian 16 Revision A 03* (Gaussian Inc., Wallingford, 2016).

S5. Lu, T. & Chen, F. Multiwfn: a multifunctional wavefunction analyzer. *J. Comput. Chem*. 33, 580–592 (2012)

S6. Smulders, M. M. J., Zarra, S. & Nitschke, J. R. Quantitative understanding of guest binding enables the design of complex host–guest behavior. *J. Am. Chem. Soc.* **135**, 7039–7046 (2013).

S7. Trott, O. & Olson, A. J. AutoDock Vina: improving the speed and accuracy of docking with a new scoring function, efficient optimization, and multithreading. *J. Comput. Chem*. **31**, 455–461 (2010)